Thèse présentée pour obtenir le grade de
Docteur de l'Université Louis Pasteur
Strasbourg I

Discipline : Chimie
Spécialité : Chimie informatique et théorique
par Chérif A. A. Ndoye

Electronic spectroscopy of small organic and organometallic molecules : electronic correlation, vibronic and spin-orbit couplings

Soutenance publique le 17 décembre 2008

Membres du jury

Co-directeur de Thèse : Mme Chantal Daniel, DR, Strasbourg
Co-directeur de Thèse : M. Alain Strich, Pr, Strasbourg
Rapporteur Interne : M. Roberto Marquardt, Pr, Strasbourg
Rapporteur Externe : M. Eric Henon, Pr, Reims
Rapporteur Externe : M. Claude Pouchan, Pr, Pau
Examinateur : M. Ajith Perera, Dr, Gainesville, USA

Remerciements/Aknowledgements

Je commencerai par remercier Chantal et Alain, mes co-directeurs de thèse. Je côtoie Chantal depuis mon stage de maîtrise et nous travaillons ensemble depuis le DEA. Quant à Alain il m'a tout simplement donné envie de faire de la chimie quantique avec ses cours que j'ai suivis depuis la licence. C'est dire le temps passé ensemble, merci pour votre enseignement, votre patience, votre soutien et d'avoir supporté mes états d'âme pendant tout ce temps.

This work would not be finished without Ajith Perera. I can only imagine the all work he went through so I can do mine, I'm deeply thankful to him. I would like to thank Dr. Bartlett for his support during my visits in QTP and for his patience and kindness during his class. Thanks to Marcel Nooijen for our discussion on vibronic coupling and for helping me run the program.

Merci aux membres du jury d'avoir accepté de juger mon travail et pour leurs commentaires qui ont participé à l'améliorer.

Un grand merci à tous les membres des labos du 4ème sud de l'institut Le Bel, plus particulièrement du ceux laboratoire de chimie quantique. Merci aux permanents pour leur accueil, aux thésards, postdocs et stagiaires pour tous les moments passés ensemble, au labo et en dehors. Un merci particulier va à David, Radovan et les deux Sébastien pour tous les petits tricks latex, python et autres qui m'ont beaucoup aidé tout au long de la thèse et pendant la rédaction. Merci à Etienne pour nos discussions sur le couplage vibronique, même si parfois j'en sortais encore plus confus, et pour son aide dans la préparation de la soutenance. Merci également à Emmanuel pour cette dernière partie. Et pour finir merci à FP mon compagnon de route depuis la licence.

I have a thought for all the QTP people. Particular thanks to Judy and Antoinette for the worm welcoming in Florida. Thanks to Andrew, Tom and Josh for the discussions and for just being so nice to me. I'm also thankful to Prakash and all the other members of Dr. Bartlett's group and all the basketball buddies.

Je remercie également le ministère de l'enseignement supérieur et de la recherche d'avoir financé cette thèse ainsi que la région Alsace pour son soutien financier lors de mes déplacements en Floride.

Last but not least, mes parents, mes frères et soeurs, wa ngueyène, wa ndoyène, sama gaa yi, Amath, ak ngi si dess, kou lim dioum ... sans vous j'en serais pas là aujourd'hui, je vous dois tout, MERCI ... tout simplement.

Contents

French Abstract

La prédiction de propriétés spectroscopiques moléculaires et l'interprétation de spectres expérimentaux nécessitent de faire appel à la théorie. Une première étape consiste à se limiter à la spectroscopie électronique dans l'approximation de Born-Oppenheimer ce qui consiste à considérer les noyaux de la molécule comme étant fixes et les états électroniques indépendants les uns des autres. L'objectif de cette thèse est d'étudier la structure électronique de petites molécules organiques et organométalliques dans l'approximation de Born-Oppenheimer dans un premier temps avant d'aller au delà en prenant en compte des effets tels que le couplage vibronique ou le couplage spin-orbite entre les états électroniques.

Chapitre 1: Aspects théoriques

Sont développées dans ce chapitre les méthodes utilisées pour obtenir les résultats présentés dans les chapitres ultérieurs. Une première partie est consacrée aux méthodes de structure électronique dans l'approximation de Born-Oppenheimer, elle est suivie d'une partie qui traite des effets de couplage vibronique et spin-orbite.

Chapitre 2: Structure électronique de MCH_2^+ (M=Fe, Co, Ni)

Les carbènes métalliques ont été identifiés comme produits intermédiaires dans certains processus catalytiques tels que la synthèse Fischer-Tropsch, mais leur réactivité, la nature de leurs liaisons, et leurs propriétés spectroscopiques sont loin d'être comprises et demeurent un domaine de recherche actif dans la chimie des métaux de transition. Parmi ces carbènes métalliques $FeCH_2^+$, $CoCH_2^+$ et $NiCH_2^+$ sont d'intérêt particulier et leur photo fragmentation a récemment été étudiée pour établir leur mé-

canisme de décomposition et estimer leurs énergies de dissociation [1]. Lorsqu'elles sont irradiées (entre 310 et 360 nm dans le cas de $FeCH_2^+$ et $CoCH_2^+$ et entre 360 et 410 nm dans le cas de $NiCH_2^+$) ces molécules donnent trois produits majeurs, M^+, MC^+ et MCH^+, la dissociation en M^+ et CH_2 étant le canal principal. Les études théoriques sur ces espèces, essentiellement limitées aux états fondamentaux, ont surtout porté sur leurs énergies de liaison et leurs structures d'équilibre plutôt que sur leur photochimie.

La structure électronique des complexes de métaux de transition est caractérisée par une forte densité d'états électroniques, certains pouvant être quasiment dégénérés, ainsi que par la présence d'états haut spin (triplets, quadruplets voire quintuplets), aussi le calcul de ces états n'est pas routinier et des approches non traditionnelles sont parfois nécessaires pour les traiter avec succès.

Dans ce travail nous exploitons la flexibilité de la méthode Coupled Cluster (CC) et de la méthode Equation Of Motion (EOM), son équivalent pour les états excités, pour une approche non conventionnelle dans le traitement des complexes de métaux de transition. Ainsi pour éviter les problèmes de contamination de spin dans la fonction d'onde nous utilisons une fonction de référence Kohn-Sham (KS) au lieu d'une fonction Hartree-Fock (HF). De plus dans la méthode CC la définition d'un espace actif n'est pas nécessaire ce qui permet d'éviter les problèmes tels que la discontinuité de l'énergie qui peut résulter d'un choix arbitraire de l'espace actif.

Chacun des trois carbènes MCH_2^+ est de symétrie C_{2v}. Une étude préliminaire a permis de déterminer la géométrie d'équilibre des trois carbènes métalliques étudiés, de calculer leurs énergies de dissociation qui sont en bon accord avec l'expérience et de caractériser l'état fondamental de chacun d'eux. $NiCH_2^+$ est ainsi caractérisé par un état fondamental $^2A_1$ séparé d'environ 30.0 kJ/mol du premier état excité $^2A_2$. $FeCH_2^+$ et $CoCH_2^+$ sont quant à eux caractérisés par un état fondamental quasi doublement dégénéré formé d'une composante $^4B_1$ et d'une composante $^4B_2$ dans le cas de $FeCH_2^+$ et d'une composante $^3A_2$ et d'une composante $^3A_1$ dans le cas de $CoCH_2^+$. Cette étude a également permis de calculer les premiers états électroniques excités.

La présence d'états de transfert de charge métal-$\pi^*_{MCH_2}$ avec des forces d'oscillateur significatives dans le domaine du proche UV-Visible dans les spectres théoriques de $FeCH_2^+$ et de $CoCH_2^+$ est sans doute à l'origine de la photo fragmentation de ces molécules observée après irradiation entre 310 et 360 nm. Forts de ses conclusions nous avons également calculé les courbes d'énergie potentielle à une dimension q=M^+-CH_2. Ces courbes d'énergie potentielle sont extrèmement compliquées et difficiles à exploiter pour une étude dynamique plus avancée.

Chapitre 3: Couplages vibroniques dans la spectroscopie électronique des fluoro-éthylènes.

Les halo-éthylènes ont largement été étudiés notamment à cause de leur toxicité. Cependant l'assignation de leurs spectres ainsi que la connaissance des propriétés de leurs états électroniques demeurent incomplètes. De nombreuses données expérimentales allant des spectres d'absorption aux résultats issus des études de photo dissociation sont disponibles principalement pour les fluoro-éthylènes. Elles montrent une constance dans l'énergie de l'orbitale moléculaire π de la liaison C=C alors que les liaisons σ sont stabilisées lorsqu'on passe de l'éthylène au tétrafluoro-éthylène. Les études de photo fragmentation ont quant à elles permis de mettre en évidence plusieurs canaux de dissociation comprenant la perte d'un atome d'hydrogène ou de fluor voire l'élimination d'une molécule de HF de H_2 ou de F_2. Les mécanismes supposés jusqu'ici sont purement spéculatifs voire inconnus.

A l'inverse peu d'études théoriques ont été menées sur les fluoro-éthylènes malgré l'aide précieuse qu'elles pourraient apporter dans la compréhension de leur spectroscopie. Une étude récente utilisant la méthode Symmetry-Adapted Cluster Configuration Interaction (SAC-CI) a porté sur la spectroscopie électronique des fluoro-éthylènes [2]. Elle a apporté de nouveaux éléments de réponse mais certaines énergies d'excitation restent à assigner. En outre cette étude se limite à la géométrie d'équilibre excluant ainsi les aspects liés aux effets de structure.

Dans le cadre de cette thèse nous proposons une étude plus détaillée de la spectro-

scopie électronique des fluoro-éthylènes notamment en prenant en compte les effets liés aux changements de structure. Pour ce faire nous faisons appel aux modes normaux de vibration pour extraire la partie des spectres due aux mouvements des noyaux mais aussi pour permettre aux états électroniques d'interagir entre eux et ainsi mettre en évidence les couplages vibroniques [3]. Nous avons pu obtenir des énergies d'excitation en meilleur accord avec l'expérience mais aussi montrer que certaines parties des spectres ne provenaient pas d'une absorption directe mais étaient dues à des couplages vibroniques entre états. L'analyse des surfaces d'énergie potentielle le long des coordonnées normales nous donne également un aperçu de la dynamique des noyaux.

Chapitre 4: Effets du couplage spin-orbite sur la spectroscopie électronique de H_2X (X=O,Te,Po).

Dans l'étude de la spectroscopie et la réactivité des complexes de métaux de transition il est parfois utile voire indispensable de prendre en compte les interactions spin-orbite. Il existe plusieurs méthodes permettant de traiter ces interactions et de rendre compte des effets de corrélation électronique, ce sont les méthodes SO-CI (Spin-Orbite Configuration Interaction).

Ayant une origine relativiste les interactions spin-orbite nécessitent, en toute rigueur, un traitement dans un formalisme à quatre ou deux composantes. Cependant dans l'étude de la réactivité des molécules il convient de distinguer les électrons de valence des électrons de coeur, ces derniers pouvant être considérés comme inertes. Le traitement complet de l'atome dans le formalisme à quatre ou à deux composantes n'est donc pas toujours justifié. De plus les effets relativistes sont plus importants dans le coeur, là où les électrons sont les plus rapides. Leur influence sur les orbitales de valence peut aujourd'hui être reproduite, sans trop perdre de précision, par des potentiels effectifs de coeur, soit via des potentiels AIMP (*abinitio* Model Potentiels) soit par des pseudopotentiels paramétrés.

La plupart des méthodes traitent ainsi les interactions spin-orbite dans un formal-

isme à une composante, soit avec tous les électrons si les atomes sont légers, soit avec des potentiels effectifs de coeur. Dans tous les cas il existe deux possibilités pour traiter la corrélation électronique et l'interaction spin-orbite. Soit on considère les deux dans la même étape de calcul, ce sont les méthodes à une étape, soit on traite la corrélation électronique le mieux possible dans une première étape en utilisant les méthodes corrélées usuelles avant de traiter l'interaction spin-orbite dans une étape ultime, ce sont les méthodes à deux étapes.

Les méthodes à une étape donnent des résultats de bonne qualité mais atteignent vite leurs limites notamment en terme de coût de calcul. Les méthodes à deux étapes qui traitent d'abord la corrélation électronique bénéficient quant à elles des progrès réalisés dans ce domaine, ce qui constitue d'ailleurs un de leurs principaux avantages.

Dans ce travail nous utilisons principalement des méthodes à deux étapes à savoir la méthode SO-RASSI [4] et la méthode EPCISO [5]. La première calcule l'interaction spin-orbite entre les états électroniques sur la base de leurs fonctions d'onde calculées au préalable au niveau RASSCF. La méthode EPCISO récemment développée présente l'avantage de n'utiliser qu'une fonction d'onde RASSCF pour calculer les premiers états électroniques excités ainsi que leur interaction spin-orbite. Dans le cas d'étude de l'eau et de ses homologues lourds (H_2Te et H_2Po) nous montrons que lorsque la fonction d'onde RASSCF utilisée est convenablement choisie des résultats comparables à ceux de la méthode SO-RASSI peuvent être obtenus, évitant ainsi de calculer la fonction d'onde de chacun des états.

Introduction

The purpose of this thesis is to open the route to new applications of coupled cluster theory, to validate the vibronic approach interfaced to ACES II [6] quantum chemical software on small organic molecules for which experimental spectra are known and to study the spin-orbit effects in the series H_2X (X=O, Te, Po).

Most of the quantum chemical calculations reported nowadays are based either on density functional theory (DFT) for electronic ground states properties in large organic/inorganic molecules or on CASSCF/MS-CASPT2 methods when possible. This method is the method of choice for transition metal complexes spectroscopy. In order to obtain better accuracy coupled cluster theory is an alternative. In our tentative to apply cluster expansion theory to transition metal complexes spectroscopy [7, 8] we aim in the present work at investigating the spectroscopy and the complicated mechanism of photofragmentation of MCH_2^+ (M=Ni, Fe,Co) by various coupled cluster methods.

The vibronic spectra of fluoroethylenes obtained by means of the module VIBRON [9] implemented and tested in ACES II within the present thesis, are compared to the experimental ones. The ultimate goal is to reproduce the experimental spectrum, analysis of the simulated spectrum will help us identify the root of each absorption, whether it is from specific excited states, normal modes, or vibronic coupling effects.

The electronic absorption spectra of H_2X (X=O, Te, Po) including spin-orbit (SO) corrections are compared and the use of two different approaches, EPCISO [10]

and SO-RASSI [4] is discussed in the perspective of future applications to large transition metal complexes.

The first chapter of the manuscript is devoted to a brief survey of the theoretical methods used in the present studies. The second chapter relates the study of the electronic structure of MCH_2^+ molecules whereas the third chapter is dedicated to the simulation of vibronic spectra of fluoroethylene molecules. The last chapter deals with the study of the spin-orbit effects on the spectroscopy of H_2X (X=O, Te, Po).

Chapter 1

Theoretical aspects

In this chapter a brief overview of the methods used for this work is presented. Particular attention is given to the coupled-cluster method which was used in most of the results presented in this work.

1.1 Molecular hamiltonian

Solving the Schrödinger equation is the first step on a quantum study of the properties of a molecule and its interaction with an external field. To do so one has to write down the molecular hamiltonian. For a system of N electrons located at $\{\boldsymbol{r}_i\}$ and M nuclei of mass m_A with atomic numbers Z_A and their location given by $\{\boldsymbol{R}_A\}$, the molecular hamiltonian is

$$\hat{H} = \hat{T}_{nuc} + \hat{T}_{el} + \hat{V} \tag{1.1}$$

where $\hat{T}_{nuc}$ is the kinetic energy operator for nuclei, $\hat{T}_{el}$ the kinetic energy operator for electrons and $\hat{V}$ the potential energy operator.

$$\hat{T}_{nuc} = -\sum_{A=1}^{M} \frac{1}{2m_A} \nabla^2(\boldsymbol{R}_A) \tag{1.2}$$

$$\hat{T}_{el} = -\frac{1}{2} \sum_{i=1}^{N} \nabla^2(\boldsymbol{r}_i) \tag{1.3}$$

in atomic units. $\nabla^2(\boldsymbol{x}_i) = \frac{\partial^2}{\partial x_i^2} + \frac{\partial^2}{\partial y_i^2} + \frac{\partial^2}{\partial z_i^2}$ in rectangular coordinates.

When limited to Coulombic interactions $\hat{V}$ consists of nucleus-electron attractions operator $\hat{V}_{ne}$, electron-electron repulsions operator $\hat{V}_{ee}$ and nucleus-nucleus repulsions operator $\hat{V}_{nn}$.

$$\hat{V} = \hat{V}_{ne} + \hat{V}_{ee} + \hat{V}_{nn} \tag{1.4}$$

with

$$\hat{V}_{ne} = -\sum_{i=1}^{N} \sum_{A=1}^{M} \frac{Z_A}{|\boldsymbol{r}_i - \boldsymbol{R}_A|} \tag{1.5}$$

$$\hat{V}_{ee} = \sum_{i=1}^{N} \sum_{j>i}^{N} \frac{1}{|\boldsymbol{r}_i - \boldsymbol{r}_j|} \tag{1.6}$$

$$\hat{V}_{nn} = \sum_{A=1}^{M} \sum_{B>A}^{M} \frac{Z_A Z_B}{|\boldsymbol{R}_A - \boldsymbol{R}_B|} \tag{1.7}$$

also in atomic units. Nucleus-electron attractions operator $\hat{V}_{ne}$ couples the nuclear and electronic motions and consequently complicates the treatment of electrons' and nuclei's dynamics at the same time. To overcome this difficulty electronic and nuclear coordinates are decoupled by invoking the well known Born-Oppenheimer approximation which consists of considering electrons to be moving in the field of fixed nuclei. This assumption arises from the fact that compared to electrons nuclei move slowly because of the large difference of mass. As a consequence, the kinetic

energy operator for nuclei $\hat{T}_{nuc}$ can be neglected and nucleus-nucleus repulsions operator $\hat{V}_{nn}$ becomes a constant. The electronic problem can then be solved separately by considering the remaining terms in the molecular hamiltonian, this defines the electronic hamiltonian

$$\hat{H}_{el} = \hat{T}_e + \hat{V}_{ee} + \hat{V}_{ne} + \hat{V}_{nn} \tag{1.8}$$

This operation can be repeated along different all nuclear coordinates to obtain series of points that will define potential energy surfaces. Solutions to the electronic problem (for the wavefunction and for the energy) will depend parametrically on the nuclear coordinates $\{\boldsymbol{R}_A\}$.

$$\hat{H}_{el}\Phi_{el}(\{\boldsymbol{r}_i\}, \{\boldsymbol{R}_A\}) = E_{el}(\{\boldsymbol{R}_A\})\Phi_{el}(\{\boldsymbol{r}_i\}, \{\boldsymbol{R}_A\}) \tag{1.9}$$

After solving the electronic energy, E_{el}, for a series of molecular geometries, nuclear dynamics can be investigated knowing that electronic information is included into potential energy surfaces.

In the next section (1.2) methods will be introduced for solving the electronic problem within the Born-Oppenheimer approximation. In section 1.3 the discussion will go beyond this approximation with the so-called vibronic and spin-orbit couplings.

1.2 Electronic problem in Born-Oppenheimer approximation

The electronic Schrödinger equation equation (1.9) can be solved exactly for only hydrogen atom or hydrogen-like ones. In this section approximate solutions are presented. The discussion begins with the well known Hartree-Fock approximation which gives a good starting point to the more precise methods such as Configuration Interaction (CI) or Coupled-Cluster (CC) methods. The CI method and its exact solution (Full CI) to the Schrödinger equation are presented. It is followed by the most important steps in the derivation of the CC equations with the inclusion of single and double excitations (CCSD) by Purvis and Bartlett [11]. The essence of the CC method is highlighted by showing how it gives a wavefunction closer to the exact one in comparison to truncated CI for example. The section ends with a brief presentation of multiconfigurational methods used in this work.

1.2.1 The Hartree-Fock approximation

A detailed overview of the Hartree-Fock method can be found in the excellent book of A. Szabo and N. S. Ostlund [12]. The basic principals of the method are given here. Starting with the electronic hamiltonian (1.8) and replacing the different terms by their expressions (1.3) and (1.5)-(1.7), it can be rewritten

$$\hat{H}_{el} = \underbrace{-\frac{1}{2}\sum_{i=1}^{N}\nabla^2(\boldsymbol{r}_i) - \sum_{i=1}^{N}\sum_{A=1}^{M}\frac{Z_A}{|\boldsymbol{r}_i - \boldsymbol{R}_A|}}_{\sum_i \hat{h}(i)} + \underbrace{\sum_{i=1}^{N}\sum_{j>i}^{N}\frac{1}{|\boldsymbol{r}_i - \boldsymbol{r}_j|}}_{\sum_{j>i}\hat{g}(i,j)} + \underbrace{\sum_{A=1}^{M}\sum_{B>A}^{M}\frac{Z_A Z_B}{|\boldsymbol{R}_A - \boldsymbol{R}_B|}}_{\hat{V}_{nn}} \tag{1.10}$$

Since this section only deals with the electronic problem, the subscript in $\hat{H}_{el}$ will be dropped for a more convenient form

$$\hat{H} = \sum_i \hat{h}(i) + \sum_{j>i}\hat{g}(i,j) + \hat{V}_{nn} \tag{1.11}$$

where $\hat{h}(i)$ and $\hat{g}(i,j)$ are the one-particle and two-particle operators of the electronic hamiltonian respectively.

The Hartree-Fock equations are obtained by minimizing the electronic energy

$$E = \langle \Psi | \hat{H} | \Psi \rangle \tag{1.12}$$

with respect to the spin orbitals ϕ_p used to expand the electronic wavefunction $|\Psi\rangle$ as the Slater determinant

$$|\Psi\rangle = |\phi_1 \phi_2 \cdots \phi_N\rangle \tag{1.13}$$

They are eigenvalue equations of the form

$$\hat{f}(i)\phi_p(i) = \varepsilon_p \phi_p(i) \tag{1.14}$$

where ε_p is the energy of the spin-orbital ϕ_p and $\hat{f}(i)$ the Fock operator

$$\hat{f}(i) = \hat{h}(i) + \hat{v}^{\mathrm{HF}}(i) \tag{1.15}$$

In a finite basis of size P > N, there are P such equations (1.14) which means that p can take the values $p = 1, 2, \cdots N, N+1, \cdots P$.
$\hat{v}^{\mathrm{HF}}(i)$ is the average potential experienced by the ith electron due to the presence of other electrons, it depends on their spin-orbitals which means that $\hat{f}$ depends on its eigenfunctions. A method called Self-Consistent-Field (SCF) is used to solve the Hartree-Fock equations. It starts with an initial guess of spin-orbitals $\{\phi_p\}$, calculates $\hat{v}^{\mathrm{HF}}$ from this starting guess and solves equation (1.14) for a new set of spin-orbitals. $\hat{v}^{\mathrm{HF}}$ is calculated with this new set of spin-orbitals and equation (1.14) is solved again. This procedure is repeated until the spin-orbitals used to expand the Fock operator are the same as its eigenfunctions, self-consistency is then reached.

Solving the Hartree-Fock equations provides a set of spin-orbitals ϕ_p. The N first spin-orbitals (with the lowest energy) are called the occupied or hole spin-orbitals, they are labeled $i, j, k, \cdots$, the remaining spin orbitals called virtual, unoccupied or particle spin-orbitals and are labeled $a, b, c, \cdots$. When the character of a spin-orbital is not specified (occupied or unoccupied), it is labeled $p, q, r, \cdots$. These spin-orbitals

will appear in the definition of the exact wavefunction which is the topic of the next section.

1.2.2 Exact wavefunction and Configuration Interaction (CI)

In the presentation of the CI and other methods discussed in this section it is convenient to work in the second quantization formalism, a summary of the notations and formulas used here can be found in Appendix 1.

The exact electronic wavefunction is the so-called Full Configuration Interaction (FCI) wavefunction. It has the following form

$$\Psi_{\mathrm{FCI}} = C_0\Phi_0 + \sum_{i,a} C_i^a \Phi_i^a + \sum_{\substack{i>j \\ a>b}} C_{ij}^{ab} \Phi_{ij}^{ab} + \cdots + \sum_{\substack{i>j>k\cdots \\ a>b>c\cdots}} C_{ijk\cdots}^{abc\cdots} \Phi_{ijk\cdots}^{abc\cdots} \tag{1.16}$$

where $\Phi_0 = |0\rangle$ is the Hartree-Fock SCF ground state wavefunction, it is the Slater determinant formed from the occupied spin-orbitals obtained by solving the Hartree-Fock equation. The Slater determinants $\Phi_{ijk\cdots}^{abc\cdots}$ are formed from the occupied spin-orbitals except $\phi_i, \phi_j, \phi_k, \cdots$ which have been replaced by $\phi_a, \phi_b, \phi_c, \cdots$ respectively. They are called excited determinants, they can be singly excited, meaning that one spin-orbital has been replaced, doubly excited, meaning that two spin-orbitals have been replaced and so on. $C_{ijk\cdots}^{abc\cdots}$ are the coefficients to solve for in order to obtain the exact wavefunction.

In order to compare the FCI wavefunction with the coupled-cluster one can write it as a function of Φ_0, for that we use second quantized operators and rewrite singly excited determinants as

$$\sum_{i,a} C_i^a \Phi_i^a = \hat{C}_1 \Phi_0 \tag{1.17}$$

where

$$\hat{C}_1 = \sum_{i,a} C_i^a \hat{a}^\dagger \hat{i}, \tag{1.18}$$

doubly excited determinants as

$$\sum_{\substack{i>j \\ a>b}} C_{ij}^{ab}\Phi_{ij}^{ab} = \hat{C}_2\Phi_0 \tag{1.19}$$

with

$$\hat{C}_2 = \sum_{\substack{i>j \\ a>b}} C_{ij}^{ab}\hat{a}^\dagger\hat{b}^\dagger\hat{j}\hat{i} \tag{1.20}$$

and more generally n-tuply excited determinants as

$$\sum_{\substack{i>j>k\cdots \\ a>b>c\cdots}} C_{ijk\cdots}^{abc\cdots}\Phi_{ijk\cdots}^{abc\cdots} = \hat{C}_n\Phi_0 \tag{1.21}$$

with

$$\hat{C}_n = \sum_{\substack{i>j>k\cdots \\ a>b>c\cdots}} C_{ijk\cdots}^{abc\cdots}\hat{a}^\dagger\hat{b}^\dagger\hat{c}^\dagger\cdots\hat{k}\hat{j}\hat{i}. \tag{1.22}$$

FCI wavefunction can then be written

$$\Psi_{\mathrm{FCI}} = (C_0 + \hat{C}_1 + \hat{C}_2 + \cdots + \hat{C}_n)\Phi_0 \tag{1.23}$$

The CI method is an application of the linear variational method where a linear combination of Φs is used as a trial function for the exact wavefunction and the matrix representation of the hamiltonian in the basis of these Φs, the FCI matrix, is formed and diagonalized in order to solve for its eigenfunctions. The FCI matrix has the following structure

$$\mathrm{H_{FCI}} = \begin{pmatrix} \langle 0|\hat{H}|0\rangle & & & & & \\ 0 & \langle S|\hat{H}|S\rangle & & & & \\ \langle D|\hat{H}|0\rangle & \langle D|\hat{H}|S\rangle & \langle D|\hat{H}|D\rangle & & & \\ 0 & \langle T|\hat{H}|S\rangle & \langle T|\hat{H}|D\rangle & \langle T|\hat{H}|T\rangle & & \\ 0 & 0 & \langle Q|\hat{H}|D\rangle & \langle Q|\hat{H}|T\rangle & \langle Q|\hat{H}|Q\rangle & \\ \vdots & \vdots & \vdots & \vdots & \vdots & \vdots \end{pmatrix} \tag{1.24}$$

where $|S\rangle$ represents the single excitation terms, $|D\rangle$ represents the double excitation terms, and so on. Vanishing terms are consequences of the Brillouin theorem and

Slater-Condon rules. Diagonalization of the CI matrix yields upper bound to the ground and excited states energies.

FCI is the exact solution to the electronic Schrödinger equation for a given basis set. When it is affordable it is a benchmark to which other electronic structure methods should be compared to. In practice the number of excited determinants grows very fast and only a reduced number of these determinants can be included in the wavefunction. Truncation has to be made at some excitation level, double for example to give the CI singles and doubles (CISD), the wavefunction then looks like

$$\Psi_{\text{CISD}} = (C_0 + \hat{C}_1 + \hat{C}_2)\Phi_0 \tag{1.25}$$

and the hamiltonian has the more tractable form

$$\text{H}_{\text{CISD}} = \begin{pmatrix} \langle 0|\hat{H}|0\rangle & & \\ 0 & \langle S|\hat{H}|S\rangle & \\ \langle D|\hat{H}|0\rangle & \langle D|\hat{H}|S\rangle & \langle D|\hat{H}|D\rangle \end{pmatrix} \tag{1.26}$$

The CC wavefunction is presented in the next section and compared to the one of truncated CI and FCI.

1.2.3 Coupled-Cluster equations

The starting point of CC method is the exponential ansatz, it consists in writing the CC wavefunction as

$$\begin{aligned} \Psi_{\text{CC}} &= e^{\hat{T}}\Phi_0 \\ &= (1 + \hat{T} + \frac{\hat{T}^2}{2} + \frac{\hat{T}^3}{3!} + \cdots)\Phi_0 \end{aligned} \tag{1.27}$$

where $\Phi_0 = |0\rangle$ is the reference function and $\hat{T}$ is an excitation operator composed of CI-like excitation operators,

$$\hat{T} = \hat{T}_1 + \hat{T}_2 + \cdots + \hat{T}_n \tag{1.28}$$

where $\hat{T}_1$ and $\hat{T}_2$ are given as

$$\begin{aligned} \hat{T}_1 &= \sum_{a,i} t_i^a \hat{a}^\dagger \hat{i}, \\ \hat{T}_2 &= \sum_{\substack{i>j \\ a>b}} t_{ij}^{ab} \hat{a}^\dagger \hat{b}^\dagger \hat{j}\hat{i} \end{aligned} \tag{1.29}$$

(1.30)

and more generally $\hat{T}_n$ as

$$\hat{T}_n = \sum_{\substack{i>j>k\cdots \\ a>b>c\cdots}} t_{ijk\cdots}^{abc\cdots} \hat{a}^\dagger \hat{b}^\dagger \hat{c}^\dagger \cdots \hat{k}\hat{j}\hat{i}. \tag{1.31}$$

$t_{ijk\cdots}^{abc\cdots}$ are called T_1, T_2, T_3 $\cdots$ amplitudes.

When $\hat{T}_n$ acts on the reference function it gives

$$\hat{T}_n \Phi_0 = \sum_{\substack{i>j>k\cdots \\ a>b>c\cdots}} t_{ijk\cdots}^{abc\cdots} \Phi_{ijk\cdots}^{abc\cdots}. \tag{1.32}$$

The Coupled-Cluster wavefunction can be explicitly written as

$$\begin{aligned} \Psi_{\mathrm{CC}} &= (1 + \hat{T}_1 + \hat{T}_2 + \cdots + \hat{T}_n \\ &\quad + \frac{(\hat{T}_1 + \hat{T}_2 + \cdots + \hat{T}_n)^2}{2} \\ &\quad + \frac{(\hat{T}_1 + \hat{T}_2 + \cdots + \hat{T}_n)^3}{3!} + \cdots)\Phi_0. \end{aligned} \tag{1.33}$$

Including only singly and doubly excited determinants into the wavefunction yields the CC singles and doubles (CCSD) wavefunction. $\hat{T}$ defined in (1.28) is truncated after $\hat{T}_2$ and is $\hat{T} = \hat{T}_1 + \hat{T}_2$.

Then

$$\begin{aligned} \Psi_{\mathrm{CCSD}} &= (1 + \hat{T}_1 + \hat{T}_2 + \frac{(\hat{T}_1 + \hat{T}_2)^2}{2} + \frac{(\hat{T}_1 + \hat{T}_2)^3}{3!} + \cdots)\Phi_0 \\ &= (1 + \underbrace{\hat{T}_1}_{\hat{C}_1} + \underbrace{\hat{T}_2 + \frac{\hat{T}_1^2}{2}}_{\in \hat{C}_2} + \underbrace{\frac{\hat{T}_1^3}{3!} + \hat{T}_1\hat{T}_2}_{\in \hat{C}_3} + \underbrace{\frac{\hat{T}_2^2}{2} + \frac{\hat{T}_1^2\hat{T}_2}{2}}_{\in \hat{C}_4} + \underbrace{\frac{\hat{T}_2^2\hat{T}_1}{2}}_{\in \hat{C}_5} + \underbrace{\frac{\hat{T}_2^3}{3!}}_{\in \hat{C}_6} + \cdots)\Phi_0 \end{aligned} \tag{1.34}$$

where the $\hat{C}_i$ are the same as in equations (1.23) and (1.25). The advantage of CC over CI at the same truncation level can be seen immediately. Even though $\hat{T}$ is only composed of $\hat{T}_1$ and $\hat{T}_2$ (singles and doubles), up to N-tuply excited determinants will be present in the coupled-cluster wavefunction. Some of the terms in equation (1.2.3) will vanish, however determinants present in the coupled-cluster wavefunction will always be of higher excitation order than CI determinants for the same truncation level.

To derive the coupled-cluster equations one can start with the Schrödinger equation

$$\hat{H}\Psi = E\Psi \tag{1.35}$$

The hamiltonian in its normal order form (defined in Appendix 2) is obtained by subtracting $\langle 0|\hat{H}|0\rangle\Psi$ from both sides

$$(\hat{H} - \langle 0|\hat{H}|0\rangle)\Psi = (E - \langle 0|\hat{H}|0\rangle)\Psi \tag{1.36}$$

and rewritten as

$$\hat{H}_N\Psi = \Delta E\Psi \tag{1.37}$$

where ΔE is the correlation energy in the Hartree-Fock case.
Replacing Ψ by the coupled-cluster wavefunction $\Psi_{CC} = e^{\hat{T}}|0\rangle$ and multiplying from the left by $e^{-\hat{T}}$ gives

$$\begin{aligned} e^{-\hat{T}}\hat{H}_N e^{\hat{T}}|0\rangle &= \Delta E|0\rangle \\ \hat{\mathcal{H}}|0\rangle &= \Delta E|0\rangle \end{aligned} \tag{1.38}$$

where $\hat{\mathcal{H}} = e^{-T}\hat{H}_N e^{T}$ is the similarity transformed hamiltonian.

$\hat{\mathcal{H}}$ can be considerably simplified by using **Baker-Campbell-Hausdorff expansion** (Appendix 3) to obtain

$$\hat{\mathcal{H}} = \hat{H}_N + [\hat{H}_N, \hat{T}] + \frac{1}{2}[[\hat{H}_N, \hat{T}], \hat{T}] + \frac{1}{3!}[[[\hat{H}_N, \hat{T}], \hat{T}], \hat{T}] + \frac{1}{4!}[[[[\hat{H}_N, \hat{T}], \hat{T}], \hat{T}], \hat{T}] \tag{1.39}$$

It has been shown that $\hat{\mathcal{H}}$ terminates after the fifth term using the **Generalized Wick's Theorem** (Appendix 4). When the latter is applied to the commutator between $\hat{H}_N$ and $\hat{T}$ it gives

$$[\hat{H}_N, \hat{T}] = \hat{H}_N\hat{T} - \hat{T}\hat{H}_N = \{\hat{H}_N\hat{T}\} + \{\hat{H}_N\hat{T}\} - \{\hat{T}\hat{H}_N\} - \{\hat{T}\hat{H}_N\} \tag{1.40}$$

where $\{\hat{H}_N\hat{T}\}$ ($\{\hat{T}\hat{H}_N\}$) is the sum of all normal products in which there are one or more contractions between the creation/annihilation operators in $\hat{H}_N$ and those in $\hat{T}$. Since $\hat{H}_N$ and $\hat{T}$ contain a pair number of operators, $\{\hat{H}_N\hat{T}\} = \{\hat{T}\hat{H}_N\}$ and

$$[\hat{H}_N, \hat{T}] = \{\hat{H}_N\hat{T}\} - \{\hat{T}\hat{H}_N\} \tag{1.41}$$

The only nonzero contractions are $\hat{i}^\dagger\hat{j} = \delta_{ij}$ and $\hat{a}\hat{b}^\dagger = \delta_{ab}$ (see equation (1.115) in Appendix 4). Since $\hat{T}$ contains only particle creation operators $\hat{a}^\dagger, \hat{b}^\dagger, \cdots$ and hole annihilation operators $\hat{i}, \hat{j}, \cdots$ no nonzero contraction can be obtained with a $\hat{T}$ on the left. The only surviving terms are those in which $\hat{H}_N$ is on the left and is connected by at least one contraction with each of the following $\hat{T}$ operators, they are called connected terms and the connection is symbolized by $\sqsupset\sqsubset$. Moreover, $\hat{H}_N$ contains at most four creation/annihilation operators so it can be contracted with at most four $\hat{T}$ operators, this is why Baker-Campbell-Hausdorff expansion terminates after the fifth term.

The final form of $\hat{\mathcal{H}}$ can then be written as

$$\begin{aligned}\hat{\mathcal{H}} &= \hat{H}_\mathrm{N} + \hat{H}_\mathrm{N}\hat{T} + \frac{1}{2}\hat{H}_\mathrm{N}\hat{T}\hat{T} + \frac{1}{3!}\hat{H}_\mathrm{N}\hat{T}\hat{T}\hat{T} + \frac{1}{4!}\hat{H}_\mathrm{N}\hat{T}\hat{T}\hat{T}\hat{T} \\ &= \left(\hat{H}_\mathrm{N}e^{\hat{T}}\right)_\mathrm{C}\end{aligned} \tag{1.42}$$

The C subscript indicates the restriction to connected terms.

Substituting $\hat{\mathcal{H}}$ into equation (1.38) and multiplying from the left by $\langle 0|$ one obtains the energy equation

$$\langle 0|\hat{H}_N e^{\hat{T}}|0\rangle_\mathrm{C} = \Delta E \tag{1.43}$$

or multiplying from the left with the excited determinants $\langle\Phi_{ij\cdots}^{ab\cdots}|$ one obtains the equations for the amplitudes

$$\langle\Phi_{ij\cdots}^{ab\cdots}|\hat{H}_N e^{\hat{T}}|0\rangle_\mathrm{C} = 0. \tag{1.44}$$

To derive CCSD equations we substitute $\hat{T}$ by $\hat{T}_1+\hat{T}_2$ in (1.43) and (1.44) keeping the surviving terms only. The latter can be identified using the fact that the hamiltonian is a two-particle operator which means that when acting on a determinant it can change its excitation order by two to the maximum. The result of the product of $\hat{H}_N$ by a cluster operator $\hat{T}_1$ or $\hat{T}_2$ or a disconnected cluster, $\hat{T}_1\hat{T}_2$ acting on the reference function on its right has to be of same excitation order as the determinant we use to project on the left. Energy and amplitude equations are then

$$\langle 0|\hat{H}_N(\hat{T}_2+\hat{T}_1+\frac{1}{2}\hat{T}_1^2)|0\rangle_{\mathrm{C}} = \Delta E \tag{1.45}$$

$$\langle \Phi_i^a|\hat{H}_N(1+\hat{T}_2+\hat{T}_1+\hat{T}_1\hat{T}_2+\frac{1}{2}\hat{T}_1^2+\frac{1}{3!}\hat{T}_1^3)|0\rangle_{\mathrm{C}} = 0 \tag{1.46}$$

$$\langle \Phi_{ij}^{ab}|\hat{H}_N(1+\hat{T}_2+\frac{1}{2}\hat{T}_2^2+\hat{T}_1+\hat{T}_1\hat{T}_2+\frac{1}{2}\hat{T}_1^2+\frac{1}{2}\hat{T}_1^2\hat{T}_2+\frac{1}{3!}\hat{T}_1^3+\frac{1}{4!}\hat{T}_1^4)|0\rangle_{\mathrm{C}} = 0 \tag{1.47}$$

To obtain programmable CCSD equations one can explicitly write all the terms in 1.45, 1.46 and 1.47 equations and algebraically derive the energy and the amplitude equations using the contraction rules, however this method can be quite tedious and prone to error. A more convenient method is the diagrammatic derivation. Diagrammatic notation was introduced to help identify the non-vanishing terms, it also brings out certain cancellations in these sums. Coupled-Cluster diagrams can be systematically produced and a procedure developed by Kucharski and Bartlett [13] ensures that only unique diagrams are obtained. Their interpretation will lead to the energy and amplitude equations.

Diagrammatically, the CCSD energy equation looks like

$\Delta E =$ 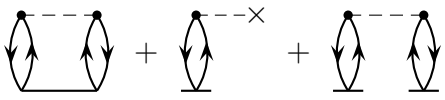 . (1.48)

The corresponding algebraic energy expression is

$$\Delta E = \frac{1}{4}\sum_{ijab}\langle ij\|ab\rangle t_{ij}^{ab} + \sum_{ia} f_{ia}t_i^a + \frac{1}{2}\sum_{ijab}\langle ij\|ab\rangle t_i^a t_j^b\,. \tag{1.49}$$

For more details a chapter on systematic derivation of the Coupled-Cluster equations can be found in reference [13] as well as complete amplitude equations up to CCSDTQ (Coupled-Cluster with single, double, triple and quadruple excitations).

For CCSD one obtains an equation for $\hat{T}_1$ amplitudes and another one for $\hat{T}_2$ amplitudes and, by an iterative procedure, solves for t_i^a for all i, a and t_{ij}^{ab} for all $i > j, a > b$. All elements needed to calculate the CCSD correlation energy (1.49) are then known.

Coupled-Cluster is the most accurate approximate *ab initio* method but it also has its disadvantages, one of them is the computational cost, in particular the amount of data to store and the number of computational steps. In general for a n-electron system and N functions there are $\sim n^l N^l$ amplitudes and an $\sim n^l N^{l+2}$ computational dependence for a given level of excitation l [14]. This makes the application of coupled-cluster method to large systems difficult, especially when high-order excitations are included. To overcome this difficulty a set of methods have been developed to approximate for example the inclusion of triples. Some of these methods like CCSDT-1 [15] and CCSDT-3 [16] are still iterative but they only include the lead terms in the CCSDT triples equations. Other methods like CCSD(T) [17, 18] and CCSD[T] [19] make a perturbative approximation of triple excitations.

Coupled-Cluster method, as described so far, is the so-called single-reference coupled-cluster and is adequate for electronic states dominated by a single reference which is the case for most molecules in their ground state and around their equilibrium geometry. The energy obtained can be used to estimate equilibrium structure, vibrational frequencies or other observable quantities. However to describe processes involving light absorption within the UV energy domain for example one has to extend coupled-cluster theory to excited states, this is done by the Equation Of Motion Coupled-Cluster (EOM-CC). Basic concepts of the EOM method are presented in the next section.

1.2.4 Equation Of Motion Coupled-Cluster

Starting with a coupled-cluster calculation as described in section 1.2.3 one applies a CI-like excitation operator

$$\hat{R}_k = r_0 + \sum_{i,a} r_i^a \{\hat{a}^\dagger \hat{i}\} + \sum_{i<j,\ a<b} r_{ij}^{ab} \{\hat{a}^\dagger \hat{i} \hat{b}^\dagger \hat{j}\} + \dots \tag{1.50}$$

on the initial state Ψ_0 to obtain the target state Ψ_k,

$$\Psi_k = \hat{R}_k \Psi_0 \,. \tag{1.51}$$

The energy of the target state is obtained through the energy difference between the initial state and the target state by simultaneously considering two Schrödinger equations, one for the initial state

$$\hat{H}_N \Psi_0 = \Delta E_0 \Psi_0 \tag{1.52}$$

and one for the target state

$$\begin{aligned} \hat{H}_N \Psi_k &= \Delta E_k \Psi_k \\ \hat{H}_N \hat{R}_k \Psi_0 &= \Delta E_k \hat{R}_k \Psi_0 \,. \end{aligned} \tag{1.53}$$

The energy difference between initial and target state $\omega_k = E_k - E_0$ is then

$$\omega_k = \Delta E_k - \Delta E_0 \tag{1.54}$$

since $\Delta E_0 = E_0 - E_{ref}$ and $\Delta E_k = E_k - E_{ref}$.
Left multiplying $\hat{R}_k$ both sides of the initial state equation (1.52) and subtracting it from the target state equation (1.53) one gets

$$\hat{H}_N \hat{R}_k |\Psi_0\rangle - \hat{R}_k \hat{H}_N |\Psi_0\rangle = (\Delta E_k - \Delta E_0) \hat{R}_k |\Psi_0\rangle \tag{1.55}$$

and, using $\Psi_0 = e^{\hat{T}}|0\rangle$, obtains

$$[\hat{H}_N, \hat{R}_k] e^{\hat{T}} |0\rangle = \omega_k \hat{R}_k e^{\hat{T}} |0\rangle \,. \tag{1.56}$$

Connected form of the EOM-CC equation, which eliminates common terms from the target state and initial state, is then obtained by multiplying from the left by

$e^{-\hat{T}}$ and, writing the commutator between $\hat{\mathcal{H}} = e^{-\hat{T}}\hat{H}_N e^{\hat{T}}$ and $\hat{R}_k$ as a connected product, one obtains the connected form of the EOM-CC equation

$$(\hat{\mathcal{H}}\hat{R}_k|0\rangle)_C = \omega_k \hat{R}_k|0\rangle \tag{1.57}$$

by applying the fact that $e^{-\hat{T}}$ and $\hat{R}_k$ commute.
Equation (1.57) is an eigenvalue equation and $\hat{H}$ and $\hat{\mathcal{H}}$ have the same spectrum regardless of the choice of $\hat{T}$, in that sense EOM is identical to FCI. As for $\hat{C}$ operator in CI, truncation has to be made in $\hat{R}_k$ expansion but EOM results are better than CI's in general because part of the correlation effects is folded in the transformed hamiltonian.

Another important feature of EOM method is that it is a multi-state scheme, diagonalization of the transformed hamiltonian yields several target states resulting in an improvement of the accuracy of the method because of error cancellation, it also simplifies the calculation of coupling elements, such as nonadiabatic or spin-orbit couplings, between target states.

Ionisation Potential (IP)/Electron Attachment (EA) EOM-CC

Since initial and target states need not to have the same number of electrons in the EOM-CC formalism this method can be applied to the treatment of ionization and electron attachment processes by using an $\hat{R}$ operator that reduces ($\hat{R}_{IP}$) or increases ($\hat{R}_{EA}$) the number of electrons.

$$\hat{R}_{IP} = \sum_i r_i \hat{i} + \sum_{b,\ j>i} r^b_{ji} \hat{b}^\dagger \hat{j}\hat{i} + \sum_{b>c,\ j>k>i} r^{bc}_{jki} \hat{b}^\dagger \hat{j}\hat{c}^\dagger \hat{k}\hat{i} + \dots \tag{1.58}$$

and

$$\hat{R}_{EA} = \sum_a r^a \hat{a}^\dagger + \sum_{a>b,\ j} r^{ba}_j \hat{b}^\dagger \hat{j}\hat{a}^\dagger + \dots . \tag{1.59}$$

The same treatment can be extended to double-ionization (DIP) or double electron attachment (DEA) processes by reducing or increasing the number of electrons by two instead of one.

Depending on the problem of interest IP and EA EOM-CC can be a more reasonable approach than EOM-CC. DIP method can be used to calculate Auger spectrum while DEA seems most useful to calculate excitation spectra of open-shell systems like carbon atom or oxygen molecule.
IP and EA methods are also one of the steps in the similarity-transformed EOM-CC (STEOM-CC) approach [20, 21] developed to overcome computational cost of EE-EOM-CC, this is the next topic.

Similarity Transformed EOM

EOM-CC is a very accurate and convenient method for treatment of exited, ionized and electron attached states. However it is computationally demanding since it requires solutions of both the ground state CCSD amplitudes equations (1.46, 1.47) and the EOM eigenvalue equation (1.57). The latter step consists in a diagonalization of a matrix of the rank of all single and double excitations and is the key of the problem to reduce the computational cost of the method.
The EOM hamiltonian is obtained through a similarity transformation $\hat{\mathcal{H}} = e^{-\hat{T}}\hat{H}_N e^{\hat{T}}$ of the normal ordered hamiltonian. The idea in STEOM is to perform another similarity transformation that yields a new hamiltonian

$$\hat{G} = e^{-\hat{S}}\hat{\mathcal{H}}e^{\hat{S}} \tag{1.60}$$

in which two-particle matrix elements that couple singly and doubly excited determinants are transformed to zero. All energies corresponding to singly excited states can then be obtained by diagonalizing $\hat{G}$ only in the space of single excitations.
It has been shown how such a transformation can be carried out [22] and elements of $\hat{G}$ that are required to vanish are g_{abej} and g_{mbij}. Subscript letters correspond to orbitals which are labeled as in subsection 1.2.1. The transformation can be obtained through $e^{\hat{S}}$ where

$$\hat{S} = \frac{1}{2}\sum_{a,b,e,j} s_{abej}\{\hat{a}^\dagger\hat{e}\hat{b}^\dagger\hat{j}\} + \frac{1}{2}\sum_{m,i,j,b} s_{mbij}\{\hat{m}^\dagger\hat{i}\hat{b}^\dagger\hat{j}\} \tag{1.61}$$

The first term in (1.61) corresponds to an EA process since two particles are created in a and b while only one is annihilated in j because e is unoccupied and no particle can be annihilated from it. Similarly the second term corresponds to an IP process since two particles are annihilated, from i and j, but only one is created, in b, because m is already occupied. Thus, EA and IP equations must be solved to obtain s_{abej} and s_{mbij} amplitudes respectively, however it is not necessary to include all EA's and IP's, a set of active orbitals can be chosen to be included in EA and IP process.

1.2.5 Multiconfigurational methods

In cases of degeneracy or near-degeneracy between electronic configurations, as in H_2 molecule at long internuclear distance, it's necessary to use multiconfigurational methods. Such methods exist in the coupled-cluster formalism but they have not reached the maturity of variational methods such as Multiconfigurational (MC) Self-Consistent Field (SCF) which are also used in this work, basic concepts of the method are presented next.

MCSCF method

Like the Full-CI wavefunction (eq. 1.23), the MCSCF wavefunction is constructed as a linear combination of several electronic configurations

$$\Psi_{\mathrm{MCSCF}} = \Phi_0 + \sum_{i,a} C_i^a \Phi_i^a + \sum_{\substack{i>j \\ a>b}} C_{ij}^{ab} \Phi_{ij}^{ab} + \cdots + \sum_{\substack{i>j>k\cdots \\ a>b>c\cdots}} C_{ijk\cdots}^{abc\cdots} \Phi_{ijk\cdots}^{abc\cdots} \,. \tag{1.62}$$

There are two major differences between CI and MCSCF methods. The first is that in MCSCF both CI coefficients $C_{ijk\cdots}^{abc\cdots}$ and molecular orbitals $\{\phi_i\}$ used to expand electronic configurations $\Phi_{ijk\cdots}^{abc\cdots}$ are optimized. The second difference is in the choice of the electronic configurations included in the wavefunction. While in truncated CI the criterion is the number of excitation, in MCSCF electronic configurations are chosen to correctly describe near-degeneracy effects. The main difficulty of the

method lies in that choice since it has to be made beforehand, therefore a knowledge of the electronic structure is needed. To overcome this difficulty Complete Active Space (CAS) method includes all electronic configurations generated from all possible excitations, under symmetry and spin constraints, within a so-called active space. In some cases the choice of this active space is rather obvious, in others some trial calculations are needed to find the best choice. The active space is defined by specifying the inactive orbitals that will remain doubly occupied, the active orbitals that can be unoccupied, singly or doubly occupied and the external or virtual orbitals that will remain unoccupied. When CAS is too big it can be divided into three active spaces in which the number of electrons can be restricted, this reduces the size of the problem.

The CASSCF method was developed to treat near-degeneracy effects, qualitatively it gives a reasonable answer but does not take into account dynamic correlation which is necessary to achieve accuracy. Nevertheless it gives a good starting point for applying second-order perturbation theory (PT2) such as in CASPT2 method.

CASPT2 method

In perturbation theory the total hamiltonian is partitioned into a zeroth order part $\hat{H}_0$, of which the eigenfunction and eigenvalue are known, and a perturbation term $\hat{V}$ that is small compared to $\hat{H}_0$. The smaller the perturbation is the closer the eigenfunction and eigenvalue of the total hamiltonian are to those of $\hat{H}_0$. The exact eigenfunctions and eigenvalues can be systematically approached by introducing an ordering parameter λ that will be set to 1 at the end.

The total hamiltonian can be written

$$\hat{H}_{el} = \hat{H}_0 + \lambda\hat{V} \tag{1.63}$$

and the wavefunction and energy are expanded in Taylor series of λ as

$$\begin{aligned} \Phi &= \Phi^{(0)} + \lambda\Phi^{(1)} + \lambda^2\Phi^{(2)} + \cdots \\ E &= E^{(0)} + \lambda E^{(1)} + \lambda^2 E^{(2)} + \cdots . \end{aligned} \tag{1.64}$$

Using (1.63) and (1.64) one can rewrite the Schrödinger equation and collect terms of the same order in λ to get

$$\begin{aligned} \hat{H}_0|\Phi^{(0)}\rangle &= E^{(0)}|\Phi^{(0)}\rangle \\ (\hat{H}_0 - E^{(0)})|\Phi^{(1)}\rangle &= (E^{(1)} - \hat{V})|\Phi^{(0)}\rangle \\ (\hat{H}_0 - E^{(0)})|\Phi^{(2)}\rangle &= (E^{(1)} - \hat{V})|\Phi^{(1)}\rangle + E^{(2)}|\Phi^{(0)}\rangle \end{aligned} \tag{1.65}$$

If the perturbed wavefunctions are assumed to be orthogonal to the zeroth order wavefunction, $\langle\Phi^{(0)}|\Phi^{(i)}\rangle = \delta_{0i}$, which means that $\langle\Phi|\Phi^{(i)}\rangle = 1$, perturbed energies can be expressed as

$$\begin{aligned} E^{(0)} &= \langle\Phi^{(0)}|\hat{H}_0|\Phi^{(0)}\rangle \\ E^{(1)} &= \langle\Phi^{(0)}|\hat{V}|\Phi^{(0)}\rangle \\ E^{(2)} &= \langle\Phi^{(0)}|\hat{V}|\Phi^{(1)}\rangle \end{aligned} \tag{1.66}$$

Expanding the first order wavefunction in configurations and inserting it into its equation in (1.65) yields, after some manipulations, a programmable expression of the second order perturbation energy

$$E^{(2)} = \frac{1}{4}\sum_{ijab}\frac{|\langle ij\|ab\rangle|^2}{\varepsilon_i + \varepsilon_j - \varepsilon_a - \varepsilon_b} \tag{1.67}$$

where $\langle ij\|ab\rangle$ is a two-electron integral and ε_i's are orbital energies. Higher order perturbation energies can also be obtained.

The CASPT2 method extends perturbation theory to the multiconfigurational case by partitioning the CI space into four subspaces: reference function, CAS, a subspace of single and double excitations with respect to CAS and the rest of CI space. The idea is to retrieve the second order perturbed energy of each of the configurations in the CAS through single and double excitations with respect to the CAS space.

1.3 Beyond Born-Oppenheimer approximation

In methods described so far, electronic states are not supposed to interact with each other in agreement with the Born-Oppenheimer approximation, however the latter breaks down when electronic states energies become too close. When such a situation is encountered the so-called non-adiabatic interactions between electronic states take place. In the following we will present two of them, namely vibronic and spin-orbit coupling, by describing their origin and how they can be treated.

1.3.1 Vibronic coupling

Excluding rotational and translational motions, a molecule can have up to 3N-6 (3N-5 for a linear molecule) nuclear degrees of freedom, N being the number of atoms, thus degeneracies between electronic states are very likely to occur as the nuclei move. In such cases vibronic coupling between states have to be considered, this is done by using a vibronic model that couples electronic states through vibrational normal modes [3].

Before going beyond Born-Oppenheimer approximation it is important to understand tis influence in molecular spectroscopy because. Although it shows limitations for some systems it does give very good results for others and remains a good starting point for when the non-Born-Oppenheimer effects have to be included. Up to now this approximation has been discussed qualitatively to explain the decoupling of the motion of the electrons from that of the nuclei, it is also central to the traditional approach of molecular spectroscopy, namely the Franck-Condon approach [23, 24]. As we have seen in section 1.1, after solving electronic Schrödinger equation 1.9, obtained by invoking the Born-Oppenheimer approximation, one gets the electronic wavefunction $\Phi_a(r, R)$ and the adiabatic potential energy surface $V_a(R)$ for each electronic state a

$$\hat{H}_{el}\Phi_a(r, R) = V_a(R)\Phi_a(r, R) \tag{1.68}$$

where shorthand notations r and R are used for electronic and nuclear coordinates respectively. In terms of wavefunction the decoupling of the electronic and the nuclear motions means that the molecular wavefunction can be written as a product of the electronic, $\Phi_a(r, R)$, and nuclear, $\chi_a(R)$, wavefunction

$$\Psi_{BO} = \chi_a(R)\Phi_a(r, R). \tag{1.69}$$

The Born-Oppenheimer approximation also implies that electronic states are not coupled to each other. This means that contribution from each state can be computed separately and the complete spectrum is simply the sum of the contributions of all electronic states.

Basically a molecule can interact with an electromagnetic field and absorb or release a photon of frequency ν only if it has, at least temporarily, a dipole oscillating at the same frequency. A dipole can be induced by a transition, when the latter occurs from an initial molecular state $|\Psi_I\rangle$ to a final one $|\Psi_F\rangle$, it can be expressed as

$$\mu_{FI} = \langle \Psi_F | \hat{\mu} | \Psi_I \rangle \tag{1.70}$$

where

$$\hat{\mu} = -\sum_{i=1}^{N} \boldsymbol{r}_i + \sum_{A=1}^{M} Z_A \boldsymbol{R}_A \tag{1.71}$$

is the dipole moment operator. The transition intensity is proportional to the square of transition dipole moment μ_{FI}. Combining (1.69), (1.70) and (1.71), it can be rewritten

$$\mu_{FI} = \left\langle \chi_F \Phi_F \left| -\sum_{i=1}^{N} \boldsymbol{r}_i + \sum_{A=1}^{M} Z_A \boldsymbol{R}_A \right| \chi_I \Phi_I \right\rangle \tag{1.72}$$

and factorised

$$\mu_{FI} = -\sum_{i=1}^{N} \langle \Phi_F | \boldsymbol{r}_i | \Phi_I \rangle \langle \chi_F | \chi_I \rangle + \sum_{A=1}^{M} Z_A \langle \Phi_F | \Phi_I \rangle \langle \chi_F | \boldsymbol{R}_A | \chi_I \rangle \tag{1.73}$$

The second term in equation 1.73 is equal to zero because $\langle \Phi_f | \Phi_i \rangle = 0$ since electronic

wavefunctions are orthogonal. Thus

$$\begin{aligned} \mu_{FI} &= -\sum_{i=1}^{N} \langle \Phi_F \left| \boldsymbol{r}_i \right| \Phi_I \rangle \langle \chi_F | \chi_I \rangle \\ &= \mu_{\Phi_F \Phi_i} S_{\chi_f \chi_I} \end{aligned} \tag{1.74}$$

where $\mu_{\Phi_F \Phi_I} = -\sum_{i=1}^{N} \langle \Phi_F \left| \boldsymbol{r}_i \right| \Phi_I \rangle$ is electronic transition dipole moment between initial and final states and $S_{\chi_F \chi_I} = \langle \chi_F | \chi_I \rangle$ is overlap between the vibrational state of the initial electronic state and the vibrational state of the final electronic state. Since the transition intensity is proportional to the square of transition dipole moment, absorption is proportional to $|S_{\chi_F \chi_I}|^2$ also called the Franck-Condon factor of the transition. Therefore, the more vibrational states of the initial and the final electronic states overlap, the stronger the intensity of the absorption will be.
Electronic transition dipole moments are provided by electronic structure calculation, what about nuclear wavefunctions ? The choice in this work is a set of harmonic-oscillator wavefunctions associated with each vibrational normal mode in the electronic ground state, they are also provided by electronic structure calculation.

As said before this picture of molecular spectroscopy does not hold anymore when electronic states energies become close, in such a situation they have to be coupled. Couplings between electronic states can be introduced in the wavefunction by writing it as a Born-Huang expansion [25] that makes a sum over all electronic states

$$\Psi_{BH} = \sum_{a} \chi_a(R) \Phi_a(r, R), \tag{1.75}$$

hence, even though Born-Oppenheimer approximation reaches its limits for some cases it remains the starting point for further improvements.
After the electronic problem is solved and the information about electrons is in some manner folded into the potentials $V_a(R)$ at each geometry R, the molecular hamiltonian can be built by adding the nuclear kinetic energy operator (excluding overall rotational and translational motion) to the electronic hamiltonian and rewrite

the total Schrödinger equation as

$$\sum_a \hat{H}_e(\chi_a\Phi_a) + \sum_a \underbrace{-\sum_A \frac{\hbar^2}{2m_A}\frac{\partial^2}{\partial R_A^2}}_{\hat{T}_{nuc}}(\chi_a\Phi_a) - \sum_a E(\chi_a\Phi_a) = 0 \tag{1.76}$$

where coordinates have been removed for clarity sake.

Multiplying from the left by Φ_b^* and integrating over the electronic coordinates leads to

$$\sum_a \left\langle \Phi_b \left| \hat{H}_e - \sum_A \frac{\hbar^2}{2m_A}\frac{\partial^2}{\partial R_A^2} \right| \chi_a\Phi_a \right\rangle = E\sum_a \chi_a \left\langle \Phi_b | \Phi_a \right\rangle . \tag{1.77}$$

Because the electronic states at fixed geometry are orthogonal, the sum on the right hand side of equation (1.77) collapses to χ_b. The derivation of the nuclear kinetic energy takes more steps. Let's first derive $\chi_a\Phi_a$ with respect to nuclear coordinates

$$\begin{aligned}
\frac{\partial}{\partial R_A}\chi_a\Phi_a &= \frac{\partial\chi_a}{\partial R_A}\Phi_a + \chi_a\frac{\partial\Phi_a}{\partial R_A} \\
\frac{\partial^2}{\partial {R_A}^2}\chi_a\Phi_a &= \frac{\partial^2\chi_a}{\partial {R_A}^2}\Phi_a + \frac{\partial\chi_a}{\partial R_A}\frac{\partial\Phi_a}{\partial R_A} + \frac{\partial\chi_a}{\partial R_A}\frac{\partial\Phi_a}{\partial R_A} + \chi_a\frac{\partial^2\Phi_a}{\partial {R_A}^2} \\
&= \frac{\partial^2\chi_a}{\partial {R_A}^2}\Phi_a + 2\frac{\partial\chi_a}{\partial R_A}\frac{\partial\Phi_a}{\partial R_A} + \chi_a\frac{\partial^2\Phi_a}{\partial {R_A}^2}
\end{aligned} \tag{1.78}$$

We can then write

$$\sum_a \left\langle \Phi_b \left| \frac{\hbar^2}{2m_A}\frac{\partial^2}{\partial {R_A}^2} \right| \chi_a\Phi_a \right\rangle = \sum_a \left[\frac{\hbar^2}{2m_A}\delta_{ab}\frac{\partial^2}{\partial {R_A}^2} + 2\left\langle \Phi_b \left| \frac{\hbar^2}{2m_A}\frac{\partial}{\partial R_A} \right| \Phi_a \right\rangle \frac{\partial}{\partial R_A} + \left\langle \Phi_b \left| \frac{\hbar^2}{2m_A}\frac{\partial^2}{\partial {R_A}^2} \right| \Phi_a \right\rangle \right] \chi_a \tag{1.79}$$

and finally the total Schrödinger equation is

$$\sum_a \left[\delta_{ab}(V_{ba} + \hat{T}_N) - \sum_A \frac{\hbar^2}{m_A}T'_{ba,A}\frac{\partial}{\partial R_A} - \sum_A \frac{\hbar^2}{2m_A}T''_{ba,A} \right] \chi_a = E\chi_b \tag{1.80}$$

where

$$\begin{aligned}
V_{ba} &= \left\langle \Phi_b \left| \hat{H}_e \right| \Phi_a \right\rangle \\
T'_{ba,A} &= \left\langle \Phi_b \left| \frac{\partial}{\partial R_A} \right| \Phi_a \right\rangle \\
T''_{ba,A} &= \left\langle \Phi_b \left| \frac{\partial^2}{\partial {R_A}^2} \right| \Phi_a \right\rangle .
\end{aligned} \tag{1.81}$$

V_{ba} is the potential energy matrix of the electronic states and $T'_{ab,A}$ and $T''_{ab,A}$ are the so-called kinetic coupling terms. The total Schrödinger equation can rewritten as

$$(V_b + \hat{T}_N - E)\chi_b = \frac{\hbar^2}{2m_A} \sum_a \sum_A \left[2T'_{ba,A} \frac{\partial}{\partial R_A} + T''_{ba,A} \right] \chi_a \tag{1.82}$$

where the full hamiltonian is identified as

$$\hat{H} = \hat{V}_b + \hat{T}_N - \hat{\Lambda} \tag{1.83}$$

where

$$\hat{\Lambda}_{ba} = \frac{\hbar^2}{2m_A} \sum_a \sum_A \left[2T'_{ba,A} \frac{\partial}{\partial R_A} + T''_{ba,A} \right] \chi_a \tag{1.84}$$

is the so-called non-adiabatic operator.

Adiabatic electronic states obtained by solving the Schrödinger equation under the Born-Oppenheimer approximation vary significantly around conical intersections. Such regions play an important role in the molecular dynamics, especially when vibronic couplings are taken into account, and their correct description is necessary. Unfortunately around those regions the energies of two different electronic states become very close which makes integrals such as $\langle \Phi_b \left| \partial / \partial R_A \right| \Phi_a \rangle$ diverge. This can be seen by using the Hellmann-Faynman theorem [26, 27] to rewrite these integrals as

$$T'_{ba,A} = \left\langle \Phi_b \left| \frac{\partial}{\partial R_A} \right| \Phi_a \right\rangle = \frac{\left\langle \Phi_b \left| \frac{\partial \hat{H}_{el}}{\partial R_A} \right| \Phi_a \right\rangle}{V_b(R) - V_a(R)}$$

thus

$$T'_{ba,A} \to \infty \quad \text{when} \quad V_b(R) \to V_a(R)$$

To overcome this difficulty one can move to the so-called diabatic basis $\{\phi_a\}$ to expand the wavefunction and the hamiltonian. Diabatic states are defined in such a way that they do not vary significantly along the nuclear coordinates, mathematically they are defined as states satisfying

$$\left\langle \phi_a \left| \frac{\partial}{\partial R_A} \right| \phi_b \right\rangle = 0 \qquad a \neq b \tag{1.85}$$

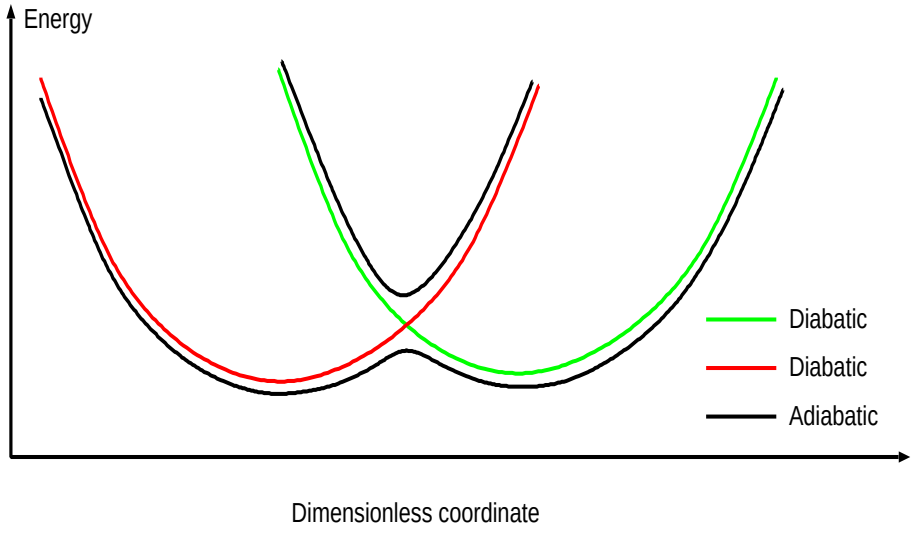

Figure 1.1: Potential energy surfaces in adiabatic and diabatic basis sets

and are obtained by a diabatization scheme that consists in finding the rotation matrix $\mathcal{R}(R)$ that will create them under this constraint. For a two-state system, in adiabatic basis the hamiltonian has the following form

$$\hat{H} = \hat{T}_N \cdot \mathbf{1} + \begin{bmatrix} V_a(R) - \hat{\Lambda}_{aa} & -\hat{\Lambda}_{ab} \\ -\hat{\Lambda}_{ba} & V_b(R) - \hat{\Lambda}_{bb} \end{bmatrix} \tag{1.86}$$

After $\mathcal{R}(R)$ has been found the hamiltonian can then be obtained in diabatic basis as

$$\hat{H} = \hat{T}_N \cdot \mathbf{1} + \mathcal{R}(R)^{-1} \cdot \begin{bmatrix} V_a(R) - \hat{\Lambda}_{aa} & -\hat{\Lambda}_{ab} \\ -\hat{\Lambda}_{ba} & V_b(R) - \hat{\Lambda}_{bb} \end{bmatrix} \cdot \mathcal{R}(R). \tag{1.87}$$

Thus calculating the kinetic coupling terms can be avoided by moving to a diabatic basis set. In that basis the couplings between electronic states are potential. The other advantage is that the elements V_{ab} (c.f. eq. 1.81) of the potential energy matrix vary smoothly with the nuclear coordinates as can be seen in figure 1.1. They can be expanded in a low-order accurate Taylor series, keeping in mind that each matrix element is a function of all the normal mode coordinates. For the two-state system

with electronic states a and b and m normal modes $i, j, ...$ the elements are given as

$$V_{ab}(R) = \delta_{ab}(V_0(R) + E_{ab}) + \sum_{i=1}^{m} E^i_{ab} R_i + \sum_{i,j=1}^{m} \frac{E^{ij}_{ab}}{2!} R_i R_j + \cdots \tag{1.88}$$

where $V_0(R)$ is the energy of the ground state at the geometry where the Taylor series expansion is made, generally at the ground state optimized geometry. E^i_{ab} and E^{ij}_{ab} are linear and quadratic coupling constants respectively, they connect electronic states through normal modes. Due to group symmetry constraints some couplings will vanish after integration over electronic coordinates. The product of the irreducible representations of electronic states by that of the normal mode has to belong to the completely symmetric representation.

For a two-state system (one symmetric, one asymmetric), two normal modes (one symmetric R_s, one asymmetric R_a) up to the quadratic term the vibronic hamiltonian is given as

$$\hat{H} = (\hat{T}_N + V_0(R)) \cdot \mathbf{1} + \begin{bmatrix} E_a + E^i_{aa} R_i + \frac{E^{ii}_{aa}}{2!} R_i R_i + \frac{E^{jj}_{aa}}{2!} R_j R_j & E^j_{ab} R_j + \frac{E^{ij}_{ab}}{2!} R_i R_j \\ E^j_{ba} R_j + \frac{E^{ij}_{ba}}{2!} R_i R_j & E_b + E^i_{bb} R_i + \frac{E^{ii}_{bb}}{2!} R_i R_i + \frac{E^{jj}_{bb}}{2!} R_j R_j \end{bmatrix} \tag{1.89}$$

The vibronic couplings in equation (1.89) are obtained through the following steps:

- Optimize the ground state geometry and obtain the force constant matrix and normal modes q_i of the ground state.
- Perform a calculation of the excited states at the ground state geometry and select the electronic states to be included in the vibronic model.
- Loop over a suitable set of small nuclear displacements along the normal modes $\Delta = R_i$ to extract linear or diagonal quadratic couplings, or $\Delta = R_i + R_j$ to extract off-diagonal quadratic coupling constants. At each slightly displaced geometry Δ the following steps are carried out:

- Calculate electronic energies $E_a(\Delta)$, transition moments $\mu_a(\Delta)$ (from the ground state), and adiabatic wavefunctions $\Psi_a(\Delta)$.

- Evaluate an approximate form for the overlap elements

$$S_{ab} = \langle \Psi_a(\Delta) | \Psi_b(0) \rangle \tag{1.90}$$

- Determine a unitary transformation of the adiabatic states, $\mathcal{R}_{ca}$, that minimizes the off-diagonal elements of the overlap matrix, *i.e.* that minimizes $\sum_{cb} |(1-\delta_{cb}) \sum_a \mathcal{R}_{ca} S_{ab}|$.

  The unitary transformation defines the diabatic states

$$\langle \phi_c(\Delta)| = \sum_a \mathcal{R}_{ca} \langle \phi_a(\Delta)| \tag{1.91}$$

- Transform the diagonal matrix of adiabatic total energies and the transition moments to the diabatic representation, to obtain

$$\tilde{E}_{cb}(\Delta) = \sum_a \mathcal{R}_{ca} E_a(\Delta) \mathcal{R}_{ab}, \qquad \tilde{\mu}_c(\Delta) = \sum_a \mathcal{R}_{ca} \mu_a(\Delta) \tag{1.92}$$

- Finally couplings are obtained by double-sided numerical differentiation, *e.g.* diagonal linear coupling constants in (1.89) are given by

$$E^i_{aa} = \frac{\tilde{E}_{aa}(R_i) - \tilde{E}_{aa}(-R_i)}{2R_i} \tag{1.93}$$

  and diagonal quadratic couplings by

$$E^{ii}_{aa} = \frac{\tilde{E}_{aa}(R_i) - 2\tilde{E}_{aa}(0) + \tilde{E}_{aa}(-R_i)}{R_i} \tag{1.94}$$

Once couplings have been obtained, the potential energy matrix (1.88) can be built up and diagonalized to get the adiabatic surfaces, the latter can provide great insight into the spectroscopy and the short-time dynamics of the studied systems. Diagonalizing the total vibronic hamiltonian (1.89) will yield vibronic eigenvalues that will ultimately appear as peaks in the simulated absorption spectrum.

1.3.2 Spin-orbit coupling

Origin of spin-orbit coupling

Spin-orbit coupling is another physical effect that can break down the Born-Oppenheimer approximation, its relativistic origin can be seen starting from the electronic hamiltonian (already seen in subsection 1.2.1) which has the general form

$$\hat{H} = \sum_i \hat{h}(i) + \sum_{j>i} \hat{g}(i,j) + \hat{V}_{nn}. \tag{1.95}$$

$\hat{h}(i)$ is the one-particle part and is composed of the kinetic energy operator of the electrons and nucleus-electron attractions operator, $\hat{g}(i,j)$ is the two-particle part and is only composed of electron-electron repulsions operator.
In relativistic theory $\hat{h}(i)$ is given by Dirac's hydrogen-like hamiltonian

$$\hat{h}_{Dirac}(i) = c\vec{\alpha_i} \cdot \vec{p}_i + (\beta_i - \mathbf{I}_4)mc^2 + \sum_A \hat{V}_{Ai} \tag{1.96}$$

where $\mathbf{I_4}$ is the 4×4 unit matrix and $\vec{p}_i = -i\vec{\nabla}_i$ the momentum vector of the electron i. β is the 4×4 Dirac matrix and $\vec{\alpha}$ is a vector of matrices, its three components $(\alpha_x, \alpha_y, \alpha_z)$ are expressed as a function of 2×2 Pauli matrices $\vec{\sigma}$. $\hat{V}_{Ai}$ is the interaction term with nucleus A.
This 4×4 matrix form of the hamiltonian implies a four component vector form for the wavefunction

$$|\Psi\rangle = \begin{pmatrix} \psi_\alpha^L \\ \psi_\beta^L \\ \psi_\alpha^S \\ \psi_\beta^S \end{pmatrix} \tag{1.97}$$

L and S represent large and small components of the wavefunction respectively while α and β are related to spin.
Solving Dirac equation for meaningful solutions for chemists leads to a decoupling of electronic and positronic degrees of freedom and to a two-component electronic

form. From that decoupling follows Pauli hamiltonian

$$\hat{h}_{Pauli} = \hat{h}_{nr} + \sum_{i}^{N} \hat{h}_{mv}(i) + \sum_{i}^{N} \hat{h}_{D}(i) + \sum_{i}^{N} \hat{h}_{SO}(i) \tag{1.98}$$

where $\hat{h}_{nr}$ is the non-relativistic hamiltonian, $\hat{h}_{mv}$ the mass correction operator and $\hat{h}_{D}$ the Darwin term. The forth term is the one we are interested in, it is the spin-orbit operator

$$\hat{h}_{SO} = \frac{\vec{\sigma}}{4m^2c^2} \cdot (\vec{\nabla} V(r) \times \vec{p}) \overset{V=-\frac{Z}{r}}{\longrightarrow} \frac{Z}{4m^2c^2r^3} \vec{\sigma} \cdot \vec{\mathrm{l}} \tag{1.99}$$

with $\vec{s} = \frac{\vec{\sigma}}{2}$.

Here we present Pauli hamiltonian just to show the spin-orbit interaction term in relativistic theory. In practice it can not be used for variational calculations but for a perturbative treatment and gives a good estimation of relativistic corrections to the energy up to transition metals of second and third rows of the periodic table. Other hamiltonian as Breit-Pauli's [28] or no-pair hamiltonian [29,30] are more often used for spin-orbit calculations.

Physical origin of spin-orbit coupling can be understood by moving to electron's coordinate system. In its coordinate system the electron "sees" the nucleus moving around him, this seeming motion of the nucleus creates a magnetic field that interacts with the intrinsic magnetic momentum of the electron namely the spin, leading to spin-orbit interaction.

In addition to spin-orbit coupling relativistic effects are also at the origin of other phenomena very important for the chemist and known as scalar relativistic effects. The latter mainly come from mass changing of the electron. In relativistic theory electron in motion has a mass $m = \gamma m_0$ where $\gamma = (1 - v^2/c^2)^{-1/2}$ is the Lorentz factor, c the speed of light, v the speed the electron and m_0 its mass when it is idle. When v is close to c the v^2/c^2 term is not negligible and the mass of the electron increases. Since Bohr radius is inversely proportional to the mass of the electron, this phenomenon manifests itself by a direct stabilization of orbitals close to the

nucleus, s and p orbitals especially, this stabilization induces, by a screening effect, an indirect destabilization of diffuse orbitals, especially d and f orbitals.

Treatment of spin-orbit coupling

Now that we have seen relativistic origin of spin-orbit coupling and its physical interpretation let's see how it is treated in practice. Two models are often used :

LS or Russell-Saunders coupling. It corresponds to a weak spin-orbit coupling for which the hamiltonian including electronic correlation and scalar relativistic but no spin-orbit (noso) effects $\hat{H}_{noso}$ commutes with the total angular momentum $\vec{L} = \sum_i \vec{l_i}$ and the total spin momentum $\vec{S} = \sum_i \vec{s_i}$ which are then good quantum numbers for eigenstates of $\hat{H}_{noso}$

$$\hat{H}_{noso}|LS\rangle = E_{LS}|LS\rangle \tag{1.100}$$

$|LS\rangle$ states are obtained by a correlated method, CI or CASSCF for example, and spin-orbit coupling is introduced as a perturbation and removes the degeneracy between LS states that split to J components with $|L - S| \leq J \leq L + S$.

jj or magnetic coupling. In this case spin-orbit coupling is not a perturbation anymore and is included in the hamiltonian from the beginning $\hat{H}_{so}$. Individual angular and spin momenta are not meaningful when taken separately, they strongly interact to give individual total momentum $\vec{j_i} = \vec{l_i} + \vec{s_i}$ which commutes with the hamiltonian and is a good quantum number for its eigenstates

$$\hat{H}_{so}|j\rangle = E_j|j\rangle \tag{1.101}$$

Interactions between individual total momenta define the total momentum $\vec{J} = \sum_i \vec{j_i}$.

How does one know which model to use ? In other words which of correlation or spin-orbit coupling effects are more important ? In general the more an atom is heavy the more spin-orbit coupling effects are important since they vary as Z^4, where Z is the atomic number. Rigorously they have to be treated in a four or

two component formalism with the jj coupling model and taking into account all electrons. However it is not always possible due to the size of the problem because, as we said previously, these effects are more important in heavy atoms which means a large number of electrons. For that reason four or two component methods quickly reach their limits. Moreover, working in a four or two component formalism implies changes in the nature of the hamiltonian which becomes complex making difficult the treatment of correlation effects.
Approximations can be made by separating core electrons from the valence ones more important for studying reactivity or valence spectroscopy. Effective core potentials (ECP) can then be used for core electrons but they have to reproduce correctly jj coupling effects of the core electrons and the influence of the relativistic effects on valence electrons. The latter can then be treated with the LS coupling model because they are slower then the electrons in the core.

The methods used in this work are based on the LS model. They treat electronic correlation and spin-orbit coupling using a set of orbitals obtained from a variational calculation in one component formalism. Two interactions can be treated in two manners. One can consider both in the same calculation step by doing a CI in the double symmetry group of the molecule, this is the so-called one-step method. The other possibility is to treat electronic correlation in a first step keeping LS coupling model and using habitual CI methods, spin-orbit coupling is then treated in a second step using LS states as a basis to expand spin-orbit states, this is the two-step method. In the following we will briefly talk about one-step methods before describing more in detail two-step methods since the methods we use belong to this category.

One-step methods

They treat correlation problem and spin-orbit coupling at the same time and for that reason they suffer from some problems. Spin-orbit coupling operator couples states of different spin which augments the size of the problem, moreover matrix

elements of the hamiltonian become complex which complicates the diagonalization process. Methods, such as a selection of states coupled by spin-orbit operator or transformation of the hamiltonian matrix, have been developed to overcome these problems with more or less success. Good results can be obtained at a reasonable price but one-step methods quickly reach their limits in general.

Two-step methods

Two-step methods first concentrate on electronic correlation problem before considering spin-orbit coupling in a final step. In that way they take profit of progresses made in the development of correlated methods like corrections of the non size-consistency problem coming from truncation in CI method.

In the first step CI is performed yielding $|\Psi_m\rangle$ states with energies E_m that are eigenvalues of the hamiltonian without spin-orbit $\hat{H}_{noso}$, each state $|\Psi_m\rangle$ is expanded in total space of determinants $\{\Phi_i\}$

$$|\Psi_m\rangle = \sum_i C_{im}|\Phi_i\rangle \tag{1.102}$$

Eigenfunctions corresponding to the roots of interest make the basis on which the matrix of the total hamiltonian $\hat{H}_{noso} + \hat{V}_{so}$ will be built and diagonalized.
$\{\Phi_i\}$ can be composed of thousands even millions of determinants and in some cases needs to be reduced to a model subspace which contains only determinants that contributes the most to the correlation energy. States $|\Psi'_m\rangle$ expanded in this new basis are, in a good approximation, considered as eigenfunctions of $\hat{H}_{noso}$ with eigenvalues E'_m different from E_m. The difference originates from the reduction of the basis. The correlation energy lost can be reintroduced in the model space with an effective hamiltonian

$$\hat{H}_{eff} = \hat{H}_{noso} + \sum_m (E_m - E'_m)|\Psi'_m\rangle\langle\Psi'_m| \tag{1.103}$$

The same technique can be used to improve the treatment of correlation effects by using energies provided by higher correlated method for E_m. CASPT2 energies for example will bring more dynamical correlation.

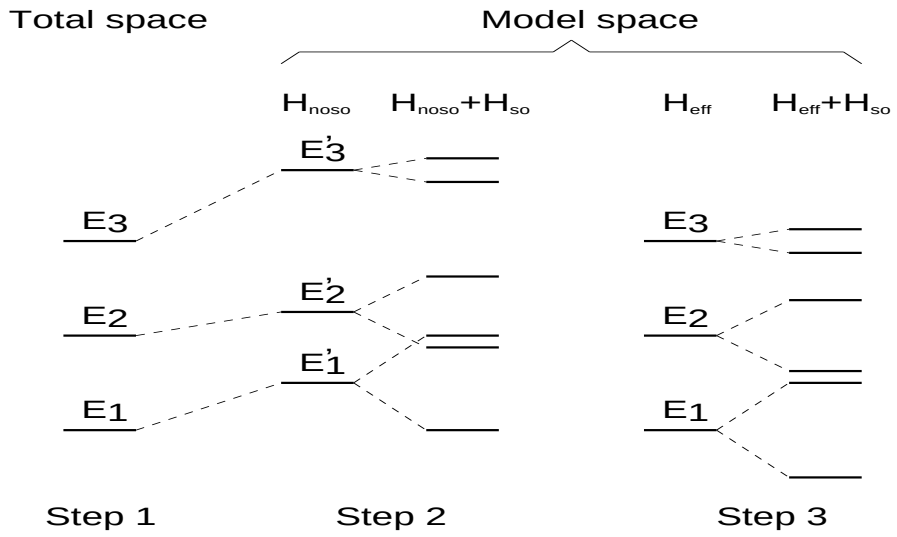

Figure 1.2: Effect of the effective hamiltonian on model space

Two-step methods as described so far are the contracted SO-CI methods because the total hamiltonian is built and diagonalised on the basis of $\{|\Psi_m\rangle\}$ states which means that C_{im} coefficients are not optimized, SO-RASSI method [4] used in this work belongs to this class of methods. They are not suited to describe the so-called spin-orbit polarisation effects that arise from the spin-orbit interaction between determinants.

To overcome this problem EPCISO method [10], also used in this work, builds and diagonalises the hamiltonian matrix on the basis of $\{|\Phi_i\rangle\}$ determinants. The large number of determinants enforces a selection to only include the ones needed to describe the states of interest and the ones contributing to spin-orbit polarisation. Effective hamiltonian technique can also be used to recover correlation energy lost by reducing the number of determinants.

In practice SO-RASSI and EPCISO methods have one major difference. SO-RASSI needs the wavefunctions, basically MCSCF wavefunctions, of all states for which one needs to compute the spin-orbit interaction while EPCISO has the advantage to start from a unique wavefunction and generates all $|\Phi_i\rangle$ determinants it needs to build the states of interest and compute their spin-orbit interaction.

Appendix

Appendix 1: Second quantized formulas

Here we summarize the second quantized notations and results we use in this chapter without proving them.

$\hat{p}^\dagger$ is the creation operator for a spin-orbital ϕ_p.

$\hat{p}$ is the annihilation operator for a spin-orbital ϕ_p.

When it's not specified whether the operator is a creation or an annihilation operator it's noted $\hat{p}'$.

A hole creation operator or a particle annihilation operator acting on the reference function gives zero

$$\hat{i}^\dagger|0\rangle = \hat{a}|0\rangle = 0 \tag{1.104}$$

Anti-commutation relations

The anticommutator of two operators $\hat{A}$ and $\hat{B}$ is defined as

$$\left[\hat{A}, \hat{B}\right]_+ = \hat{A}\hat{B} + \hat{B}\hat{A} \tag{1.105}$$

The anticommutator of second quantized operators are:

$$\begin{aligned} \left[\hat{p}, \hat{q}\right]_+ &= \hat{0} \\ \left[\hat{p}^\dagger, \hat{q}^\dagger\right]_+ &= \hat{0} \\ \left[\hat{p}^\dagger, \hat{q}\right]_+ &= \left[\hat{p}, \hat{q}^\dagger\right]_+ = \hat{\delta}_{pq} \end{aligned} \tag{1.106}$$

Second quantized form of the electronic hamiltonian

Electronic hamiltonian can be written in the second quantized form

$$\hat{H} = \sum_{p,q} h_{pq}\hat{p}^\dagger\hat{q} + \frac{1}{4}\sum_{p,q,r,s}\langle pq||rs\rangle\hat{p}^\dagger\hat{q}^\dagger\hat{s}\hat{r} \tag{1.107}$$

where

$$h_{pq} = \langle \phi_p | \hat{h} | \phi_q \rangle \tag{1.108}$$

and

$$\langle pq||rs\rangle = \int \phi_p^*(1)\phi_q^*(2) r_{12}^{-1}(1 - P_{12})\phi_r(1)\phi_s(2) d\tau_1 d\tau_2 \tag{1.109}$$

$r_{12} = |\boldsymbol{r}_1 - \boldsymbol{r}_2|$ and integration is over total coordinate (space and spin) τ_i of each electron. P_{12} is the operator exchanging electrons 1 and 2. For example $P_{12}\phi_r(1)\phi_s(2) = \phi_r(2)\phi_s(1)$

Appendix 2: Normal order form of the hamiltonian

Let's introduce some notations before we derive coupled-cluster working equations.

Normal order of a sequence of operators

To take advantage of the fact that $\hat{i}^\dagger|0\rangle = \hat{a}|0\rangle = 0$ normal order notation can be introduced. Normal order of a sequence of creation and annihilation operators $\hat{p}'\hat{q}'\hat{r}'\cdots$ ($N[\hat{p}'\hat{q}'\hat{r}'\cdots] = \{\hat{p}'\hat{q}'\hat{r}'\cdots\}$) is obtained by commuting operators to place all $\hat{i}^\dagger$ or $\hat{a}$ to the right of other operators. If $\hat{i}^\dagger$ and $\hat{a}$ are absent from the sequence of operators, $\{\hat{p}'\hat{q}'\hat{r}'\cdots\}|0\rangle = |\Phi_{ij\ldots}^{ab\cdots}\rangle$. In all cases

$$\langle 0|\{\hat{p}'\hat{q}'\hat{r}'\cdots\}|0\rangle = 0 \tag{1.110}$$

This result will simplify the computation of expectation values of a sequence of operators by helping identify the terms that vanish.

Normal order form of the hamiltonian

The normal order form of the hamiltonian is

$$\hat{H}_N = \hat{H} - \langle 0|\hat{H}|0\rangle = \sum_{p,q} h_{pq}\{\hat{p}^\dagger\hat{q}\} + \frac{1}{4}\sum_{p,q,r,s}\langle pq||rs\rangle\{\hat{p}^\dagger\hat{q}^\dagger\hat{s}\hat{r}\} \tag{1.111}$$

$$\hat{H}_N = \sum_{p,q} h_{pq}\{\hat{p}^\dagger\hat{q}\} + \frac{1}{4}\sum_{p,q,r,s}\langle pq||rs\rangle\{\hat{p}^\dagger\hat{q}^\dagger\hat{s}\hat{r}\} \tag{1.112}$$

Appendix 3: Baker-Campbell-Hausdorff expansion

$$
\begin{aligned}
e^{-\hat{B}}\hat{A}e^{\hat{B}} =& \big(1-\hat{B}+\frac{1}{2}\hat{B}^2-\frac{1}{3!}\hat{B}^3+\ldots\big)\hat{A}\big(1+\hat{B}+\frac{1}{2}\hat{B}^2+\frac{1}{3!}\hat{B}^3+\ldots\big) \\
=& \hat{A}+(\hat{A}\hat{B}-\hat{B}\hat{A})+\frac{1}{2}(\hat{A}\hat{B}^2-2\hat{B}\hat{A}\hat{B}+\hat{B}^2\hat{A}) \\
&+\frac{1}{3!}(\hat{A}\hat{B}^3-3\hat{B}\hat{A}\hat{B}^2+3\hat{B}^2\hat{A}\hat{B}-\hat{B}^3\hat{A})+\ldots \\
=& \hat{A}+[\hat{A},\hat{B}]+\frac{1}{2}\big\{(\hat{A}\hat{B}-\hat{B}\hat{A})\hat{B}-\hat{B}(\hat{A}\hat{B}-\hat{B}\hat{A})\big\} \\
&+\frac{1}{3!}\big\{[(\hat{A}\hat{B}-\hat{B}\hat{A})\hat{B}-\hat{B}(\hat{A}\hat{B}-\hat{B}\hat{A})]\hat{B} \\
&-\hat{B}[(\hat{A}\hat{B}-\hat{B}\hat{A})\hat{B}-\hat{B}(\hat{A}\hat{B}-\hat{B}\hat{A})]\big\}+\ldots \\
=& \hat{A}+[\hat{A},\hat{B}]+\frac{1}{2}[\,[\hat{A},\hat{B}],\hat{B}]+\frac{1}{3!}[\,[\,[\hat{A},\hat{B}],\hat{B}],\hat{B}]+\ldots\,.
\end{aligned}
\tag{1.113}
$$

Appendix 4: Generalized Wick's theorem

Before writing Generalized Wick's theorem let's define contraction between two creation/annihilation operators as

$$\hat{p}'\hat{q}' = \hat{p}'\hat{q}' - \{\hat{p}'\hat{q}'\} \tag{1.114}$$

For holes creation/annihilation operators possibilities are:

$$\begin{aligned}
\hat{i}^\dagger\hat{j}^\dagger &= \hat{i}^\dagger\hat{j}^\dagger - \hat{i}^\dagger\hat{j}^\dagger = 0 \\
\hat{i}\hat{j} &= \hat{i}\hat{j} - \hat{i}\hat{j} = 0 \\
\hat{i}\hat{j}^\dagger &= \hat{i}\hat{j}^\dagger - \hat{i}\hat{j}^\dagger = 0 \\
\hat{i}^\dagger\hat{j} &= \hat{i}^\dagger\hat{j} - (-\hat{j}\hat{i}^\dagger) = [\hat{i}^\dagger, \hat{j}]_+ = \delta_{ij}
\end{aligned} \tag{1.115}$$

while for particles creation/annihilation operators possibilities are:

$$\begin{aligned}
\hat{a}^\dagger\hat{b}^\dagger &= \hat{a}^\dagger\hat{b}^\dagger - \hat{a}^\dagger\hat{b}^\dagger = 0 \\
\hat{a}\hat{b} &= \hat{a}\hat{b} - \hat{a}\hat{b} = 0 \\
\hat{a}^\dagger\hat{b} &= \hat{a}^\dagger\hat{b} - \hat{a}^\dagger\hat{b} = 0 \\
\hat{a}\hat{b}^\dagger &= \hat{a}\hat{b}^\dagger - (-\hat{b}^\dagger\hat{a}) = [\hat{a}, \hat{b}^\dagger]_+ = \delta_{ab}
\end{aligned} \tag{1.116}$$

Generalized Wick's theorem can then be symbolically written

$$\begin{aligned}
\{\hat{p}'\hat{q}'\hat{r}'\}\{\hat{s}'\hat{t}'\}\{\hat{x}_u\hat{v}'\}\cdots \;=\; & \{\hat{p}'\hat{q}'\hat{r}'\cdots\} + \sum_{\substack{single\\contractions}} \overbrace{\{\hat{p}'\hat{q}'\hat{r}'\}\{\hat{s}'\hat{t}'\}}\{\hat{u}'\hat{v}'\}\cdots \\
& + \sum_{\substack{double\\contractions}} \overbrace{\{\hat{p}'\hat{q}'\hat{r}'\}\{\hat{s}'\hat{t}'\}\{\hat{u}'\hat{v}'\}}\cdots + \cdots \\
& + \sum_{\substack{full\\contracted\\products}} \overbrace{\{\hat{p}'\hat{q}'\hat{r}'\}\{\hat{s}'\hat{t}'\}\{\hat{u}'\hat{v}'\}}\cdots
\end{aligned} \tag{1.117}$$

The sums are over contractions of pairs of operators from different normal products of operators since contractions of pairs of operators within the same normal product of operators vanish. This can be seen from equation (1.114).

Chapter 2

Electronic structure and potential energy curves of MCH_2^+ (M=Fe, Co, Ni)

The metal carbenes have been identified as intermediates in several important catalytic processes, such as Fischer Tropsch synthesis. They also represent interesting transition metal complex prototypes and have been studied both experimentally and theoretically.

Theoretical studies have mainly focused on the nature of the metal-carbon bond. The latter can be purely covalent or purely dative depending on the metal center [31–40]. In contrast, little attention has been devoted to the spectroscopic properties. Metal carbenes are characterized by a high density of electronic states within a small energy window with several nearly degenerate states. The ground state of $FeCH_2^+$ is described by a pair of nearly degenerate $^4B_1$ and $^4B_2$ states with a $^4A_2$ state very close whereas the electronic ground state of $CoCH_2^+$ is described by two nearly degenerate $^3A_1$ and $^3A_2$ states and $NiCH_2^+$ by a $^2A_1$ state [41–43]. An accurate description of the structure and the energetics of the low-lying electronic states is required to clarify and determine the ground state of each complex and the nature of the metal-carbon

bond.

Recently, photofragment spectroscopy experiments have shown that the MCH_2^+ (M=Fe, Co, Ni) cations have three different dissociation channels [1]. The loss of CH_2 is the most favorable but the departure of H or H_2 was also reported. All these pieces information make metal carbenes an interesting set of small transition metal complexes with a few number of degrees of freedom to study the competition between dissociation channels. The size of the systems is reasonable and can be treated with highly correlated methods like coupled-cluster. The complexity of the electronic structure (open shell, nearly degenerate states, unsaturated valence shell of the metal) is a challenge to apply CC methods which have not yet been used so much for this kind of problems.

This chapter reviews the study of the electronic structure of MCH_2^+ (M=Fe, Co, Ni) complexes at the CCSD and EOM-CCSD level of theory with high quality basis sets. After focusing on the Franck-Condon region to determine the electronic ground state and the absorbing state(s), potential energy curves (PEC) are built along the relevant coordinates. Spin contamination issue occurring in these open shell systems is also discussed.

2.1 Electronic structure

The study of the electronic structure of metal carbenes is summarised in the following article.

Theoretical study of the electronic structure of MCH_2^+ (M=Fe,Co,Ni)

Sébastien VILLAUME, Alain STRICH, Chérif A. NDOYE, and Chantal DANIEL
Laboratoire de Chimie Quantique, UMR 7177, Institut de Chimie, Université Louis Pasteur/CNRS/ULP, 4 Rue Blaise Pascal, F-67000 Strasbourg, France

S. AJITH PERERA and Rodney J. BARTLETT
Quantum Theory Project, Department of Chemistry and Physics, University of Florida, P.O. Box 11 845, Gainesville, Florida 32611

Journal of Chemical Physics, 2007, vol. 126, numéro 154318, pages 1-9

Pages 53-59 :

2.2 Potential energy curves

Now that electronic states probably responsible of MCH_2^+ photo dissociation have been identified the next step is to calculate PES corresponding to these electronic states up to dissociation. The first thing is to identify relevant nuclear coordinates. Since MCH_2^+ photo dissociation yields primarily M^+ and CH_2, potential energy curves where calculated along the M-C bond elongation.

Coupled-Cluster method works well for most molecules around their equilibrium geometry but suffers from problems due to the single determinant reference function. RHF reference function does not describe correctly the asymptote for a closed-shell molecule while a ROHF one will meet similar problems for an open-shell molecule. The UHF gives the correct energy at dissociation limit but breaks the symmetry of the wave function.

In the present study calculated dissociation energies are in agreement with the experimental values. This suggests a correct treatment of the problem in hand by UKS-EOM-CCSD at equilibrium geometry and dissociation limit. Despite the well accepted fact that single reference methods are not always suitable to describe bond breaking reactions correctly the same method is used to calculate PES. This choice was motivated by different reasons. First off all coupled-cluster method and its excited state counterpart, equation of motion, are size-extensive which is a necessary feature for any method to treat bond breaking correctly at dissociation. They also have the advantage, over methods like CASSCF or CASPT2, to be not active space dependent. Using different active spaces at different geometries can result in discontinuities in potential energy curves. Coupled cluster method also has the advantage of being very versatile. Different kinds of wave functions, HF or KS, can be used as a reference function, that flexibility can be used to circumvent some difficulties. Using KS orbitals for example can considerably reduce spin contamination in the wave function as seen in section 2.1. Another feature of coupled-cluster method is to use a reference state, that is not necessarily the ground configuration state, with

a number of electrons different from that of the target state as in IP, DIP, EA or DEA-EOM. This last possibility makes EOM method even more flexible.
Moreover in the space created by $\hat{R}_k$ operator (equation 1.51) any determinant can have any weight it needs in the target state, for that reason EOM-CC can describe multi reference state within a single reference formalism. The reference state, however, is still described by a single reference coupled-cluster solution causing the problems mentioned earlier. However this issue might be avoided by the use of a high spin reference state which remains multiconfigurational in the bond breaking process as was suggested by Krylov *et al.* who motivated a new model EOM, spin-flip (SF) [44, 45], by this argument. Basically this method uses a high spin reference function and an excitation operator that conserves the total number of electrons but changes the number of α and β electrons to get a target state with a different spin multiplicity. In the present study we are dealing with high spin ground states, namely quartet, triplet and doublet states for $FeCH_2^+$, $CoCH_2^+$ and $NiCH_2^+$ respectively and the use of these high spin states as reference states could avoid the single reference problem.

PEC along metal carbon bond of studied molecules are calculated with the same methods and basis sets used in section 2 to calculate electronic excited states at equilibrium geometry. Wachters basis sets [46] augmented with f exponent were used for metal atoms while Dunning's correlation consistent triple zeta basis sets [47] was used for C and H atoms. Excited states were calculated at EOM-CCSD level of theory using a KS reference function to avoid the spin-contamination problem discussed in section 2. Figures 2.1, 2.2 and 2.3 show potential energy curves of calculated excited states along metal carbon bond for $FeCH_2^+$, $CoCH_2^+$ and $NiCH_2^+$ respectively. Only states that could be identified along the reaction pathway are represented. Strong mixing between other states generate incoherent behavior of PEC that become unworkable.

2.2.1 $FeCH_2^+$

Optimized bond length of 1.85 Å for Fe-C bond reported in section 2 is in perfect agreement with ground state potential energy curve of $FeCH_2^+$. The low lying electronic states of $FeCH_2^+$ are degenerate (a^4B_1, a^4A_2, b^4B_2,) and bound with respect to the Fe-CH_2 bond elongation as well as the a^4A_1 and b^4B_2 higher states. The absorbing state with most significant oscillator strength, namely the e^4B_2, calculated at 31180 cm^{-1} seems to dissociate. However the lack of points beyond 2.5 Å prevents further detailed analysis. At this point this state is the best candidate through which photodissociation of $FeCH_2^+$ could occur. c^4A_1 is the next most absorbing state calculated at 24870 cm^{-1} and seems to be slightly bound.

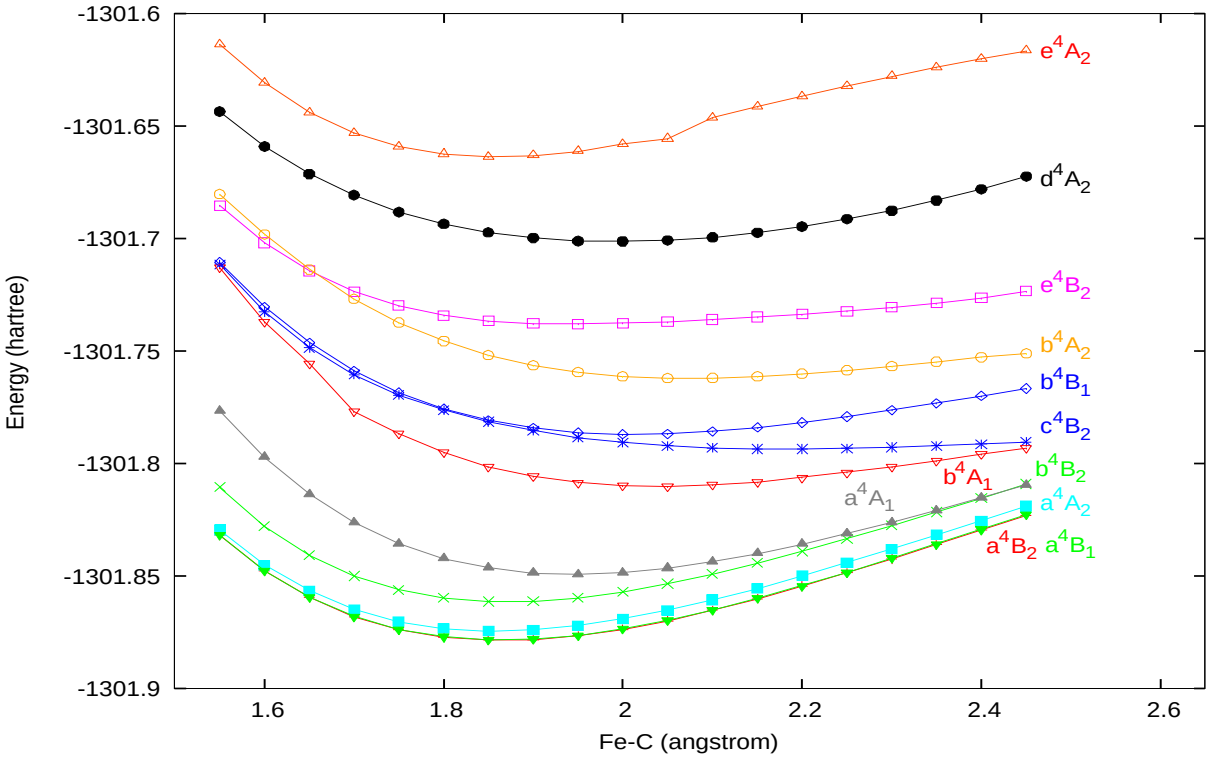

Figure 2.1: Potential energy curves of excited states of $FeCH_2^+$ along Fe-C bond.

2.2.2 $CoCH_2^+$

As reported in section 2, the ground state of $CoCH_2^+$ is described by two degenerate a^3A_2 and a^3A_1 states. Low lying excited states (a^3B_1 and a^3B_2) are very close

and become degenerate with the ground state as the Co-C bond is stretched and molecular orbitals collapse into d orbitals of Co^+ and CH_2 orbitals (SCHEME I in section 2). The minimum energy value agrees very well with the optimized Co-C bond length of 1.8 Å. d^3A_2 electronic state calculated at 31030 cm^{-1} with the main oscillator strength seems to be dissociative but here also the lack of points beyond 2.65 Å prevents further detailed analysis. c^3A_2 state calculated at 19020 cm^{-1} with significant oscillator strength is bound. The experimental irradiation between 27030 and 31250 cm^{-1} exceeds the transition energy of this state. According to these results, d^3A_2 state would be responsible of $CoCH_2^+$ photodissociation after irradiation in the energy window considered but more points beyond 2.65 Å are necessary to confirm this assumption.

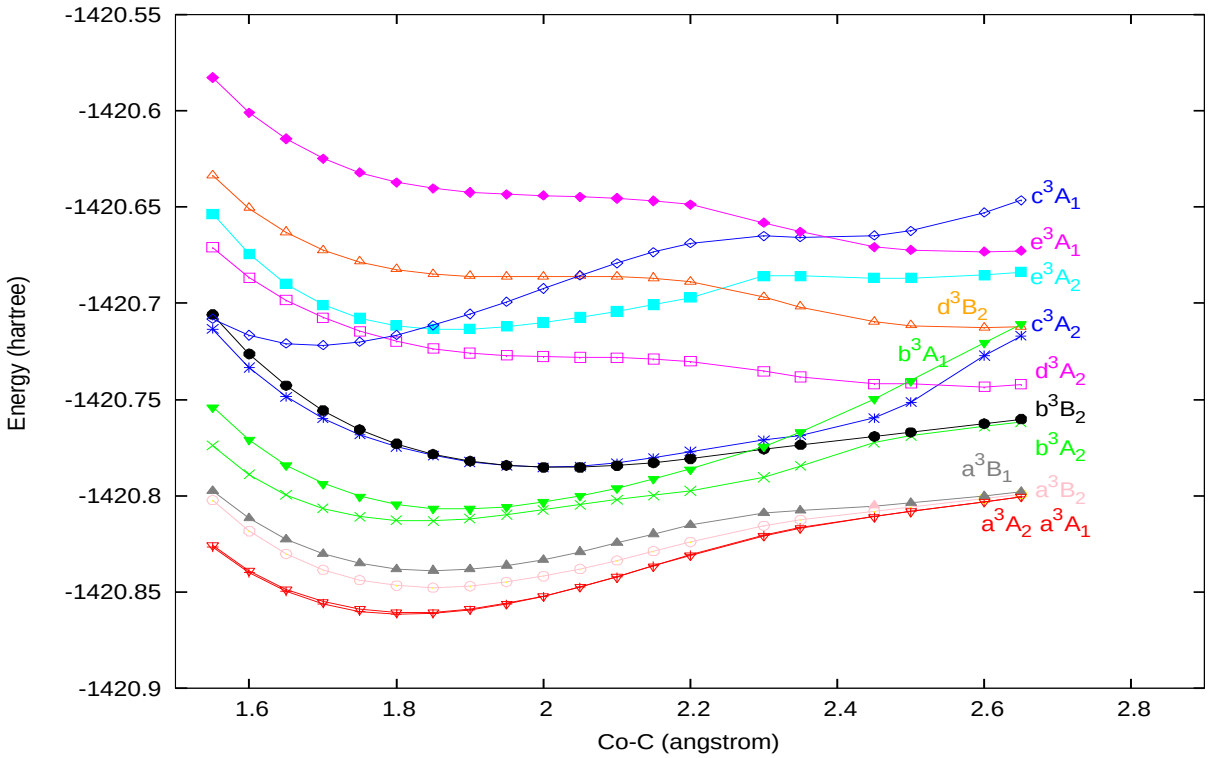

Figure 2.2: Potential energy curves of excited states of $CoCH_2^+$ along Co-C bond.

2.2.3 $NiCH_2^+$

In contrast to $FeCH_2^+$ and $CoCH_2^+$, $NiCH_2^+$ ground state is described by one well separated electronic state (a^2A_1) with a minimum at 1.8 Å in agreement with the optimized geometry of Ni-C bond length. Low lying excited states (a^2A_2, a^2B_2, b^2A_1) are close to the ground state and also bound. c^2A_1 state calculated at 17020 cm^{-1} with the most significant oscillator strength is bound. Many of $NiCH_2^+$ excited states seem to be dissociative up to 2.2 Å but non of them is assumed be a candidate for the photodissociation of the molecule since their oscillator strength is either very low or even zero. Notice however that d^2B_2 dissociative state could be of some interest since its oscillator strength (1.3×10^{-3}) is only one order of magnitude lower then the most absorbing state f^2A_1.

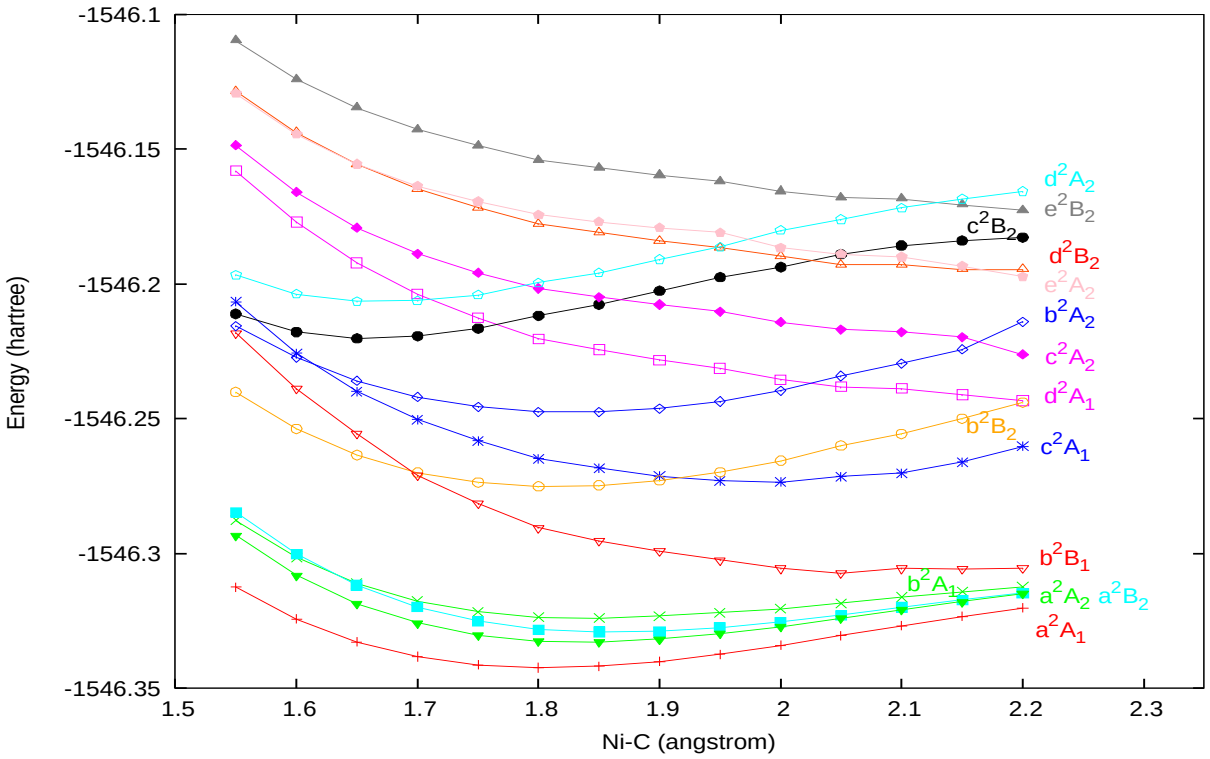

Figure 2.3: Potential energy curves of excited states of $NiCH_2^+$ along Co-C bond.

At this point only speculative conclusions can be made for MCH_2^+ PEC. For further analysis they must be obtained at least for all absorbing states and up to dissociation i.e. 3× equilibrium geometry. A solution must be found to the incoher-

ent behavior of strongly mixed states. It might imply using a multiconfigurational coupled-cluster methods, such as Fock-space coupled-cluster [48], most appropriate to handle such cases.

A particular issue has focussed our attention in the calculation of PEC. At dissociation limit one can expect the excited states of different fragments. In $CoCH_2^+$ case for instance the calculation at the asymptotic limit must yield triplet excited states of Co^+ and CH_2. A calculation at dissociation limit (6 Å) yields triplet states of Co^+ and a $^3B_1$ of CH_2 located at -1741 cm^{-1}. The ground state of Co^+ is a septuply degenerate ^3F, it is followed by a ^5F at about 4500 cm^{-1} and another ^3F at around 10000 cm^{-1} [49]. Our calculation of Co^+ excited states, starting from the closed-shell [Ar]$3d^{10}$ Co^- and using EOM-DIP method (section 1.2.4), did not yield the correct degeneracy of the ^3F ground state when using a KS reference function. A DIP calculation using a HF reference function perfectly reproduces the degeneracy of the ^3F state. The analysis reveals that atomic d orbitals are not degenerate in the KS reference function inducing lost of degeneracy of the ^3F ground state. The question whether the problem comes from the program or the method is not clarified yet.

2.3 Summary

In this work, coupled-cluster method was used to study electronic structure of transition metal carbene cations MCH_2^+ (M=Fe, Co, Ni). Both ground and excited states were investigated at equilibrium geometry to characterize the ground states of different molecules and identify their absorbing excited states. After these states were determined, PEC along the primary photodissociation pathway, namely the metal carbon bond, were calculated to identify excited states through which the photodissociation process occurs.

The electronic ground states of $FeCH_2^+$ and $CoCH_2^+$ are described by two nearly

degenerate states, $^4B_2/^4B_1$ and $^3A_2/^3A_1$, respectively while electronic ground state $NiCH_2^+$, $^2A_1$, is well separated from the other upper doublet states.

The lowest part of absorption spectra of $FeCH_2^+$, $CoCH_2^+$ and $NiCH_2^+$ is characterized by very low oscillator strengths and not expected to play a significant role in the electronic spectroscopy or in the photofragmentation of these molecules. Metal-$\pi^*_{MCH_2}$ charge transfer states with significant oscillator strengths in the visible/near-UV energy domain of the theoretical spectra of $FeCH_2^+$ and $CoCH_2^+$ are at the origin of the photofragmentation of these compounds observed after irradiation between 27800 and 32360 cm^{-1}. In contrast $NiCH_2^+$ does not show any significant absorption in this energy domain in agreement with the low cross section of photodissociation observed for this molecule.

Ground state PEC of studied molecules are in perfect agreement with optimized bond lengths of metal-carbon bonds. Low lying electronic states of three molecules are bound and become degenerate with the ground state as the metal-carbon bond is stretched. e^4B_2 state of $FeCH_2^+$ and d^3A_2 state of $CoCH_2^+$ have significant oscillator strengths and seem to be dissociative. They would be good candidates for photodissociation of these molecules but more points beyond 2.65 Å would be necessary to ascertain this point. PEC obtained for $NiCH_2^+$ correspond to states with low oscillator strengths that are not expected to play a role in the photodissociation process.

It is important to stress that all electronic states could not be represented all along the studied dissociation pathway. Some states present a strong mixing character resulting in an incoherent behavior. A correct treatment of absorbing states at least up to dissociation is necessary to study metal carbene cations photodissociaton. A multiconfigurational method such as Fock-space coupled-cluster would be more appropriate for treating strongly mixed states.

This preliminary study aiming of describing the photofragmentaion of small metal carbenes ($MCH2^+$, M=Fe, Co, Ni) reveals the complexity of their electronic

structure, in particular a high density of states in a small energy range leading to intricate PEC. It also shows that single reference EOM-CC is perhaps not the best suited method to investigate PEC of studied molecules. Nevertheless the study helped to identify electronic states probably responsible for the photodissociation of small metal carbenes. Further investigations will be devoted to the calculation of PEC of all electronic states along the metal carbon bond and up to dissociation. Other methods could be checked to study the crossing regions characterized by strong mixing between electronic states. Distortion along other molecular coordinates like H-C-H angle and other dissociation pathways will also be considered.

Chapter 3

Vibronic spectra of fluoroethylenes

3.1 Molecular systems

The spectroscopy of haloethylenes has been widely studied experimentally for many reasons including the fact that some of them are toxic pollutants. Studies reported on absorption, photo electron, electron-impact excitation and electron energy loss spectra of fluoroethylenes [50–54]. The absorption spectra are roughly characterized by an easily identified broad $\pi \rightarrow \pi^*$ band . This diffuse band and has some indication of vibrational fine structure but this is difficult to ascertain since the band is overlapped by numerous Rydberg bands.
Tentatives of assignment and reassignment have been made with some controversies and in some cases these assignments are only speculative. High-level theory was used only recently to help assigning the transitions and understand the spectroscopy of the complete series of fluoroethylenes [55]. In some cases agreement with experimental results is good and reasons including structural changes where suggested to interpret some features of the experimental spectra.

Photodissociation studies [56–64] found different dissociation channels for different fluoroethylenes. Depending on the case, irradiation of fluoroethylenes yields H and F atoms, HF, H_2 and F_2 molecules or C=C bond breaking but the mech-

anisms that might involve triplet states of such photolysis are not clearly known. Photoisomerizations have also been evidenced [65].

Theoretical study of the electronic spectra of fluoroethylene is the first step to understand their spectroscopy and photochemistry. Except for few number of them [66] only vertical excitation energies were reported so far and vibrational effects were not taken into account.

In this work we aim to go one step further by doing a detailed study of electronic absorption spectra of the whole series of fluoroethylenes. For that propose we try to reproduce absorption spectra and identify interesting aspects arising from controversies in interpretation or through the computational process. This includes identifying the origin of the spectroscopic contributions, whether they are from specific excited electronic states, vibrational modes, or vibronic coupling effects.

3.2 Computational details

Absorption spectrum simulation goes through the following steps

i Geometry optimization

ii Vibrational normal modes calculation

iii Single-Point STEOM calculation to select electronic states to be included in the vibronic Hamiltonian

iv Vibronic Hamiltonian calculation

v Potential energy surfaces generation. They can be used as a check to make sure that the vibronic coupling constants are physically meaningful (upside-down surfaces for example are an indication of an unphysical result)

vi Franck-Condon or Vibronic spectrum simulation

All electronic structure calculations were performed with ACES II quantum chemical program package [6] using polarized basis set (PBS) from Sadlej [67]. Ground state optimized geometries (i) and normal mode frequencies (ii) have been calculated at the CCSD [11] level of theory. Excited states energies and their transition moments (iii) are calculated with the STEOM-CCSD [20, 21] method. Potential energy surfaces and simulated spectra are obtained with the program VIBRON [9].

The absorption spectra of fluoroethylenes are characterized by a broad $\pi \rightarrow \pi^*$ band and a series of Rydberg states that become very dense after 9 eV. These states can be accessed only by using a very large basis set which is not the case in this work for computational reasons. Obtaining vibronic coupling Hamiltonian requires calculation of all excited states at all distorted geometries, depending on the couplings to be calculated the number of geometries can grow very fast e.g. for a calculation of linear and diagonal quadratic vibronic coupling constants, 25 single-point calculations will be necessary while up to 103 single-point calculations are needed to obtain cubic and quartic coupling constants in addition to linear and diagonal quadratic. For that reason we limit our selves to the first part of the spectrum, up to 9 eV, above that value the spectrum is essentially composed of Rydberg states that are usually easier to assign anyway.

Symmetries of studied molecules and the size of the active space in the STEOM calculation are summarized in table 3.1. Active space is chosen in such a way the percentage of singles in excited states (IP, EA and EE) is above 90, experience has shown that below that value results are poor and not very stable [68]. Active space is specified by giving an energy threshold above which all occupied orbitals are included (IP-low) and another energy threshold below which all virtual orbitals are also included (EA-high). The corresponding number of orbitals is given and IP-low and EA-high are in brackets.

The most time consuming step is the determination of quanta distribution in the spectrum simulation, ideally one would simply include all possible electronic states

and assign large quanta distributions to all normal modes but due to computational limitation it is not possible to proceed that way. One solution is to break the absorption spectrum into different regions based on spectral features or characters (Valence or Rydberg) of the calculated excited state.

Molecule	Symmetry	Orbitals in STEOM active space	
		Occupied (IP low eV)	Virtual (EA high eV)
monofluoroethylene	C_s	5 (-19.5)	22 (9.0)
cis-difluoroethylene	C_{2v}	6 (-20.0)	24 (10.0)
trans-difluoroethylene	C_{2h}	8 (-21.5)	24 (9.5)
1,1-difluoroethylene	C_{2v}	8 (-23.0)	25 (10.2)
trifluoroethylene	C_s	7 (-20.5)	22 (8.8)
tetrafluoroethylene	D_{2h}	6 (-19.8)	28 (10.2)

Table 3.1: Symmetry of molecular systems and details of active space used in the STEOM calculation.

3.3 Results and discussion

The most complete and recent theoretical study of the absorption spectra of fluoroethylenes was done by Arulmozhiraja *et al.* [55]. They investigated electronic structure of these molecules using SAC-CI singles and doubles method [69] with Dunnings's valence triple-zeta basis set and experimental geometries except for trifluoroethylene for which they used a DFT/B3LYP/aug-cc-pVTZ optimized geometry since the experimental geometry seems inaccurate.

Except for one or two fluoroethylenes the excitation energies they obtained agree well with the experiment. Thus the results obtained in this work will be compared to their results, relative energies may be compared despite the fact that different bases are used. To gauge the accuracy of the two theoretical methods, calculated values will be compared to the values found in the literature.

3.3.1 Optimized geometries and vibrational normal modes

Optimized geometries are reported in table 3.2 along with experimental geometries that could be found in the literature.

Parameter	monofluoroethylene	Cis-difluorethylene	trans-difluorethylene
r(C=C)	1.337 (1.333)[a]	1.339 (1.324)[b]	1.338 (1.316)[c]
r(C-H)	1.097 (1.087)	1.093 (1.080)	1.094 (1.080)
r(C-F)	1.350 (1.343)	1.342 (1.337)	1.348 (1.352)
$\angle$(H-C=C)	121.1 (120.3)	122.5 (121.2)	125.0 (126.3)
$\angle$(F-C=C)	121.0 (121.6)	122.3 (122.9)	119.9 (119.2)
	1,1-difluorethylene	trifluorethylene	tetrafluorethylene
r(C=C)	1.331 (1.340)[d]	1.335	1.333
r(C-H)	1.090 (1.091)	1.090	
r(C-F)	1.324 (1.315)	1.322	1.319
$\angle$(H-C=C)	119.2 (119.0)	122.9	
$\angle$(F-C=C)	125.2 (124.7)	120.2	123.3

[a]Reference [70]
[b]Reference [71]
[c]Reference [72]
[d]Reference [73]

Table 3.2: Optimized and experimental (in parenthesis) geometries for fluoroethylenes. Bond lengths are given in Å and angles in degrees.

Calculated geometries agree very well with the experimental ones. Normal modes frequencies calculated at these geometries also agree with experimental values we could found in the literature. They are given in the appendix at the end of this chapter with a description of vibrations.

3.3.2 Electronic excited states

Vertical excitation energies

Calculated vertical excitation energies and oscillator strengths of singlet states included in vibronic model Hamiltonians are reported in tables 3.3 and 3.4 for the whole series of fluoroethylenes along with experimental and SAC-CI values.

All states are excitations from π orbital including the main $\pi \rightarrow \pi^*$ excitation. The latter mentioned is preceded and followed by the first member of different Rydberg series. Vertical excitation energies are calculated to gauge the accuracy of the method for states that will be included in the vibronic model. For now, suffice it to say that STEOM energies agree very well with available experimental values, even better than SAC-CI's. Higher excited states, mainly Rydberg states, can not be reliably accessed considering the size of the basis set used, diffuse basis functions would be necessary for that purpose.

state	STEOM				SAC-CI[a]			Expt.[b]
	Nature		$\Delta E(eV)$	f	Nature	$\Delta E(eV)$	f	
				monofluoroethylene				
aA"	$2a'' \rightarrow 11a'$	0.628	7.12	0.0548	$\pi \rightarrow 3s$	7.11	0.0549	6.98
	$2a'' \rightarrow 19a'$	-0.195						
	$2a'' \rightarrow 20a'$	-0.158						
bA'	$2a'' \rightarrow 3a''$	0.462	7.56	0.3124	$\pi \rightarrow \pi^*$	7.68	0.3240	7.45
	$2a'' \rightarrow 4a''$	-0.357						
	$2a'' \rightarrow 6a''$	-0.326						
bA"	$2a'' \rightarrow 12a'$	0.610	7.77	0.0043	$\pi \rightarrow 3p\sigma_x$	7.75	0.0037	
	$2a'' \rightarrow 18a'$	0.210						
cA"	$2a'' \rightarrow 13a'$	0.481	8.00	0.0003	$\pi \rightarrow 3p\sigma_y$	7.96	0.0027	
	$2a'' \rightarrow 14a'$	0.341						
dA"	$2a'' \rightarrow 13a'$	0.392	8.54	0.0000	$\pi \rightarrow 3d\sigma$	8.50	0.0016	8.59
	$2a'' \rightarrow 14a'$	-0.278						
	$2a'' \rightarrow 15a'$	-0.290						
	$2a'' \rightarrow 23a'$	0.218						
cA'	$2a'' \rightarrow 3a''$	0.459	8.56	0.0191	$\pi \rightarrow 3d\pi$	8.92	0.0146	
	$2a'' \rightarrow 4a''$	0.509						
				cis-difluoroethylene				
aB_2	$2b_2 \rightarrow 8a_1$	0.487	6.60	0.0267	$\pi \rightarrow 3s$	6.68	0.0380	6.49
	$2b_2 \rightarrow 9a_1$	0.284						
	$2b_2 \rightarrow 12a_1$	-0.313						
bB_2	$2b_2 \rightarrow 8a_1$	-0.400	7.25	0.0076	$\pi \rightarrow 3p\sigma_z/\sigma^*$	7.37	0.0027	
	$2b_2 \rightarrow 9a_1$	0.480						
	$2b_2 \rightarrow 14a_1$	0.200						
aB_1	$2b_2 \rightarrow 2a_2$	0.525	7.84	0.3437	$\pi \rightarrow \pi^*$	8.12	0.3825	7.82
	$2b_2 \rightarrow 3a_2$	-0.437						
aA_2	$2b_2 \rightarrow 7b_1$	0.633	7.93	0.0000	$\pi \rightarrow 3p\sigma_y$	8.02		
	$2b_2 \rightarrow 10b_1$	-0.228						
bA_1	$2b_2 \rightarrow 3b_2$	0.689	8.26	0.0207	$\pi \rightarrow 3p\pi$	8.09	0.0111	7.82
				trans-difluoroethylene				
aB_g	$2a_u \rightarrow 8b_u$	0.452	6.84	0.0000	$\pi \rightarrow \sigma^*/3p\sigma_x$	7.02		
	$2a_u \rightarrow 11b_u$	-0.400						
	$2a_u \rightarrow 15b_u$	0.231						
aA_u	$2a_u \rightarrow 8a_g$	0.643	7.20	0.0377	$\pi \rightarrow 3s$	7.40	0.0438	6.99
	$2a_u \rightarrow 12a_g$	-0.262						
aB_u	$2a_u \rightarrow 2b_g$	0.557	7.46	0.2787	$\pi \rightarrow \pi^*$	7.79	0.3197	7.45
	$2a_u \rightarrow 3b_g$	-0.302						
	$2a_u \rightarrow 4b_g$	0.261						
bB_g	$2a_u \rightarrow 7b_u$	0.593	7.56	0.0000	$\pi \rightarrow 3p\sigma_y$	7.77		
	$2a_u \rightarrow 9b_u$	0.256						
bA_g	$2a_u \rightarrow 3a_u$	0.689	8.26	0.0000	$\pi \rightarrow 3p\pi$	8.17		8.25

[a] Reference [55]
[b] Reference [50]

Table 3.3: Calculated and experimental excitation energies (in eV) for monofluoroethylene, cis- and trans-difluoroethylene. The oscillator strength f are also given.

Potential energy curves

After electronic states to be included in the simulation have been chosen and the vibronic Hamiltonian calculated, the potential energy curves can be generated along each normal mode. They can be used as a check of the vibronic Hamiltonian. In fluoroethylene for example linear and quadratic vibronic coupling constant were calculated. Potential energy curves along modes 10, 11 and 12. These modes are non-symmetric out-of-plane modes corresponding roughly to out-of-plane displacements of the hydrogen atoms. They exhibit unphysical shape as shown in figure 3.1. Excited states energy is plotted along non-symmetric modes with zero being the ground state geometry. Vibronic quadratic coupling constants along these out-of-plane modes are known to be hard to obtain, their close inspection reveals their abnormally high values compared to vibronic coupling constants in other modes. To walk around this problem we decided to only include linear vibronic couplings in these problematic modes. Potential energy curves obtained with this new vibronic Hamiltonian model are more physically meaningful, they are also shown in figure 3.1. We have the same problem with cis-difluoroethylene hydrogens out of plan bending modes (6, 7 and 12), only linear coupling constants are included in those modes. For other systems quadratic coupling constants yield unphysical potential energy curves so we decided to include linear couplings only in the vibronic Hamiltonian. Ultimately absorption spectrum simulation will give us an indication of how correct the approximation we make is.

Potential energy curves are obtained by diagonalizing the potential energy matrix containing vibronic coupling constants. Therefore coupling constants determine the shapes of potential energy curves. Interactions between deferent excited states can be seen with a quick look at potential energy curves. Notice for example the slight "double well" shape of states aA" and cA" and the "steep well" shape of state cA' along mode 12 in figure 3.1 in the linear model. Vibronic coupling forces interacting states to bend, creating a "double well" lower surface (aA" and cA") and a "steep well"

state	STEOM				SAC-CI[a]			Expt.[b]
	Nature		$\Delta E(eV)$	f	Nature	$\Delta E(eV)$	f	
				1,1-difluoroethylene				
aB_1	$2b_1 \rightarrow 9a_1$	0.600	7.00	0.0459	$\pi \rightarrow 3s$	7.05	0.0580	6.74
	$2b_1 \rightarrow 14a_1$	-0.293						
bA_1	$2b_1 \rightarrow 3b_1$	0.544	7.53	0.2876	$\pi \rightarrow \pi^*/3p\pi$	7.74	0.2470	7.51
	$2b_1 \rightarrow 5b_1$	-0.358						
aA_2	$2b_1 \rightarrow 6b_2$	0.613	8.09	0.0000	$\pi \rightarrow 3p\sigma_y$	8.02		
	$2b_1 \rightarrow 8b_2$	-0.285						
bB_1	$2b_1 \rightarrow 9a_1$	-0.216	8.11	0.0003	$\pi \rightarrow 3p\sigma_z$	8.06	0.0009	
	$2b_1 \rightarrow 10a_1$	0.602						
	$2b_1 \rightarrow 15a_1$	0.205						
bA_2	$2b_1 \rightarrow 7b_2$	0.528	8.69	0.0000	$\pi \rightarrow 3d\sigma/\sigma^*$	8.58		
	$2b_1 \rightarrow 10b_2$	0.362						
cA_1	$2b_1 \rightarrow 3b_1$	0.390	8.93	0.0684	$\pi \rightarrow 3p/\pi^*/3d\pi$	8.58	0.1588	7.91
	$2b_1 \rightarrow 4b_1$	0.499						
	$2b_1 \rightarrow 5b_1$	0.278						
cB_1	$2b_1 \rightarrow 11a_1$	0.575	9.13	0.0020	$\pi \rightarrow 3d\sigma$	8.84	0.0023	
	$2b_1 \rightarrow 12a_1$	0.260						
	$2b_1 \rightarrow 17a_1$	-0.255						
				trifluoroethylene				
aA"	$4a'' \rightarrow 17a'$	0.455	6.59	0.0186	$\pi \rightarrow 3s$	6.65	0.0287	6.50
	$4a'' \rightarrow 19a'$	0.302						
	$4a'' \rightarrow 24a'$	0.282						
bA"	$4a'' \rightarrow 17a'$	0.371	7.13	0.0123	$\pi \rightarrow 3p\sigma_y/3s/\sigma^*$	7.23	0.0120	7.1[c]
	$4a'' \rightarrow 18a'$	0.314						
	$4a'' \rightarrow 19a'$	-0.259						
	$4a'' \rightarrow 26a'$	0.242						
bA'	$4a'' \rightarrow 5a''$	0.532	7.75	0.2241	$\pi \rightarrow 3p\pi + \pi \rightarrow \pi^*$	7.79	0.1151	7.75
	$4a'' \rightarrow 6a''$	-0.244						
	$4a'' \rightarrow 7a''$	-0.224						
	$4a'' \rightarrow 8a''$	-0.299						
cA"	$4a'' \rightarrow 17a'$	-0.219	7.81	0.0009	$\pi \rightarrow 3p\sigma_x$	7.86	0.0028	7.97
	$4a'' \rightarrow 18a'$	0.461						
	$4a'' \rightarrow 19a'$	0.375						
cA'	$4a'' \rightarrow 5a''$	0.438	8.51	0.1180	$\pi \rightarrow \pi^* + \pi \rightarrow 3p\pi/3d\pi$	8.43	0.2117	7.75
	$4a'' \rightarrow 6a''$	0.375						
	$4a'' \rightarrow 7a''$	0.259						
	$4a'' \rightarrow 8a''$	0.275						
dA"	$4a'' \rightarrow 18a'$	0.317	8.84	0.0087	$\pi \rightarrow 3d\sigma$	8.79	0.0286	
	$4a'' \rightarrow 19a'$	-0.231						
	$4a'' \rightarrow 20a'$	-0.287						
	$4a'' \rightarrow 21a'$	-0.277						
	$4a'' \rightarrow 29a'$	0.247						
				tetrafluoroethylene				
aB_{1u}	$2b_{1u} \rightarrow 7a_g$	0.629	6.66	0.0246	$\pi \rightarrow 3s/\sigma^*$	7.09	0.0381	6.37
	$2b_{1u} \rightarrow 9a_g$	-0.178						
	$2b_{1u} \rightarrow 10a_g$	-0.248						
aB_{3g}	$2b_{1u} \rightarrow 5b_{2u}$	0.410	6.90	0.0000	$\pi \rightarrow \sigma^*$	7.01		
	$2b_{1u} \rightarrow 7b_{2u}$	0.510						
	$2b_{1u} \rightarrow 8b_{2u}$	0.216						
aB_{2g}	$2b_{1u} \rightarrow 6b_{3u}$	0.592	7.83	0.0000	$\pi \rightarrow 3p\sigma_z$	8.24		8.01
	$2b_{1u} \rightarrow 8b_{3u}$	-0.324						
bA_g	$2b_{1u} \rightarrow 3b_{1u}$	0.692	8.13	0.0000	$\pi \rightarrow 3p\pi$	8.24		
aB_{3u}	$2b_{1u} \rightarrow 2b_{2g}$	0.231	8.70	0.4407	$\pi \rightarrow \pi^*$	9.41	0.5108	8.89
	$2b_{1u} \rightarrow 3b_{2g}$	0.653						

[a]Reference [55], [b]Reference [50], [c]Reference [52]

Table 3.4: Calculated and experimental excitation energies (in eV) for electronic excited states included in the vibronic model Hamiltonian of 1,1-difluoroethylene, trifluoroethylene and tetrafluorethylene. The oscillator strength f are also given.

upper surface (cA'). Examination of vibronic coupling constants confirms strong coupling between both aA" and cA" with cA' along mode 12. A glance through potential energy curves can give a rough idea of important vibrational modes.

3.3.3 Absorption spectra

Absorption spectra of the whole series of fluoroethylenes were simulated with both Franck-Condon (FC) and vibronic coupling methods. All electronic states reported in tables 3.3 and 3.4 were included in the simulations. In experimental spectra taken from reference [50], R, R' and R" Rydberg states correspond to excitations from π orbital to ns, np and nd (where n is the principal quantum number) orbitals respectively. FC overlap factors (section 1.3.1) that appear as peaks in the simulated spectra are calculated until they sum up to threshold value of 0.99. Different trial simulations have to be made to establish a vibronic simulation strategy. Individual peaks are convoluted with Lorentzians to create line spectra, they are reported in figures 3.2, 3.3 and 3.4 along with experimental spectra.

Simulated spectra do not perfectly reproduce experimental spectra but many pieces of information can be gained from them. In all spectra the overall shape and the position of the broad $\pi \rightarrow \pi^*$ are reproduced.
In monofluoroethylene and cis-difluoroethylene, individual FC spectra show that only the first member of the first Rydberg series, namely aA" and aB_2 respectively, has significant intensities. Other Rydberg states have very small or zero intensities in agreement with transition moments reported in table 3.3.
Trans-difluoroethylene presents an interesting case of vibronic coupling. The long progression starting around 50000 cm^{-1} and present in both experimental and vibronic spectra but not in the FC spectrum is probably a vibronic coupling effect. aB_g states lying in that region with a vertical excitation energy of 55000 cm^{-1} and zero transition moment is probably absorbing through vibronic coupling with ab-

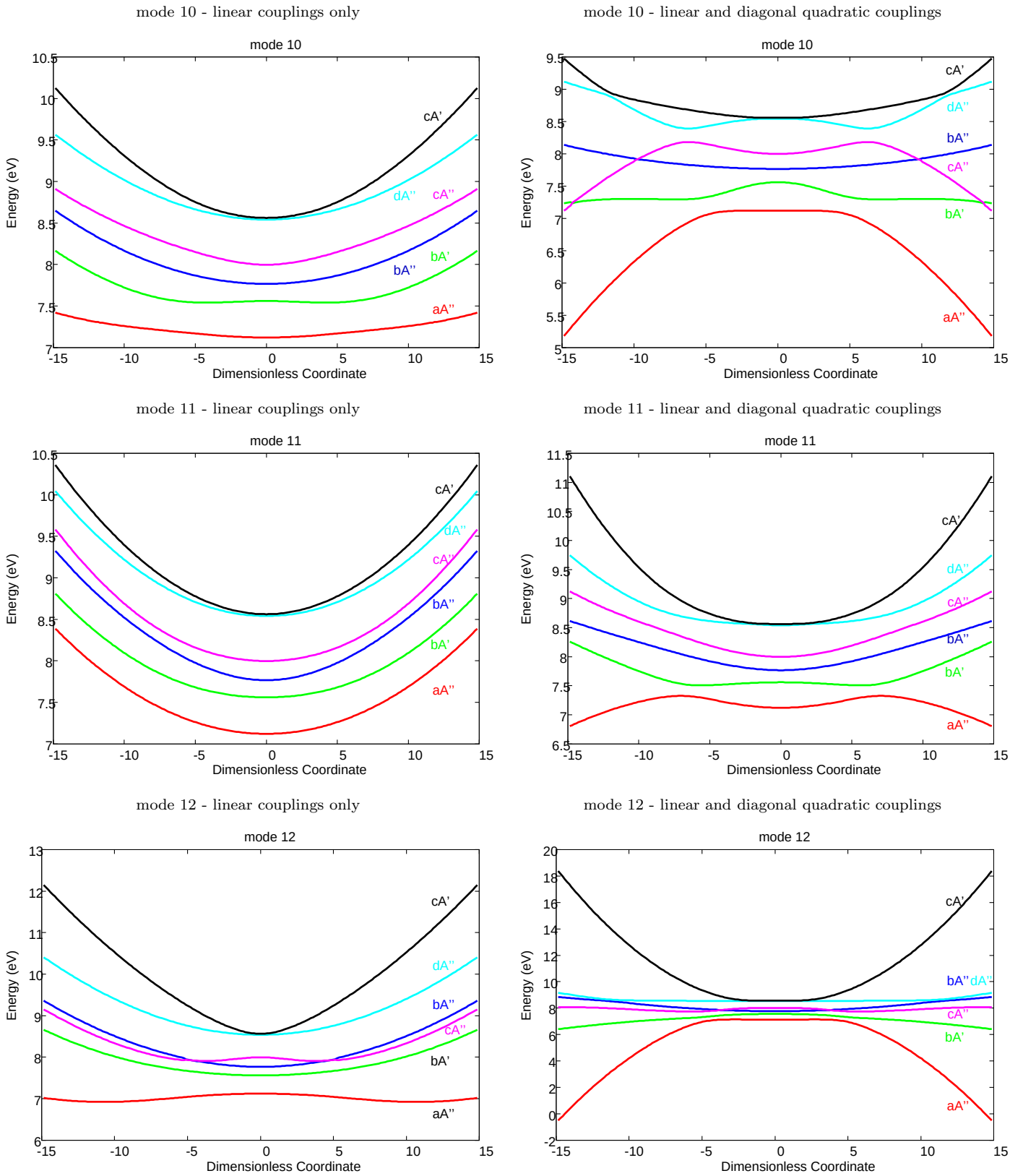

Figure 3.1: Electronic excited states included in the vibronic model of monofluoroethylene along modes 10, 11 and 12 (described in the appendix). In the left panels only vibronic linear couplings are included while linear and diagonal quadratic couplings are included in the right panels.

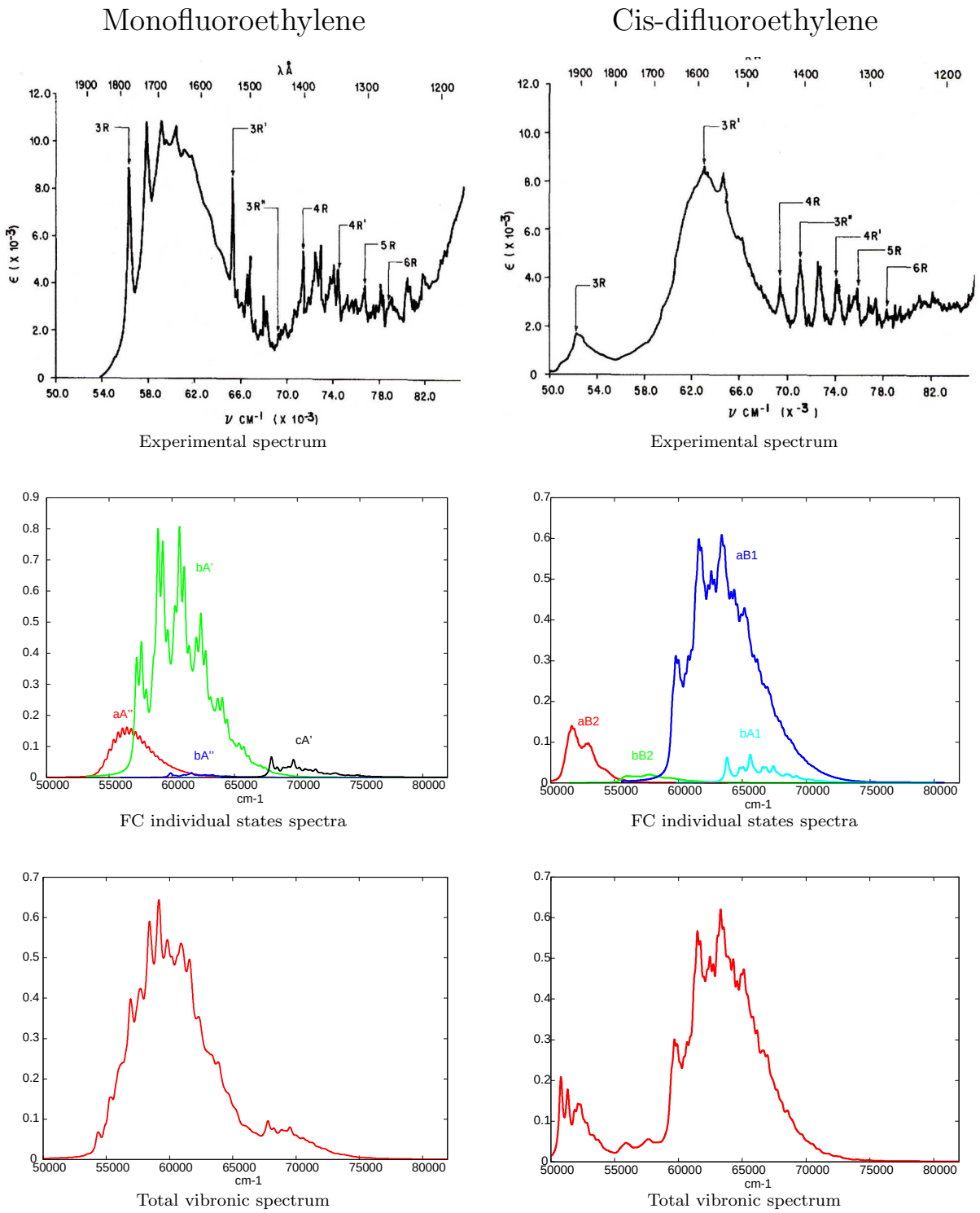

Figure 3.2: Experimental (top panels, reference [50]), FC individual states (middle panels) and total vibronic (bottom panels) absorption spectra of monofluoroethylene (on the left) and cis-difluoroethylene (on the right).

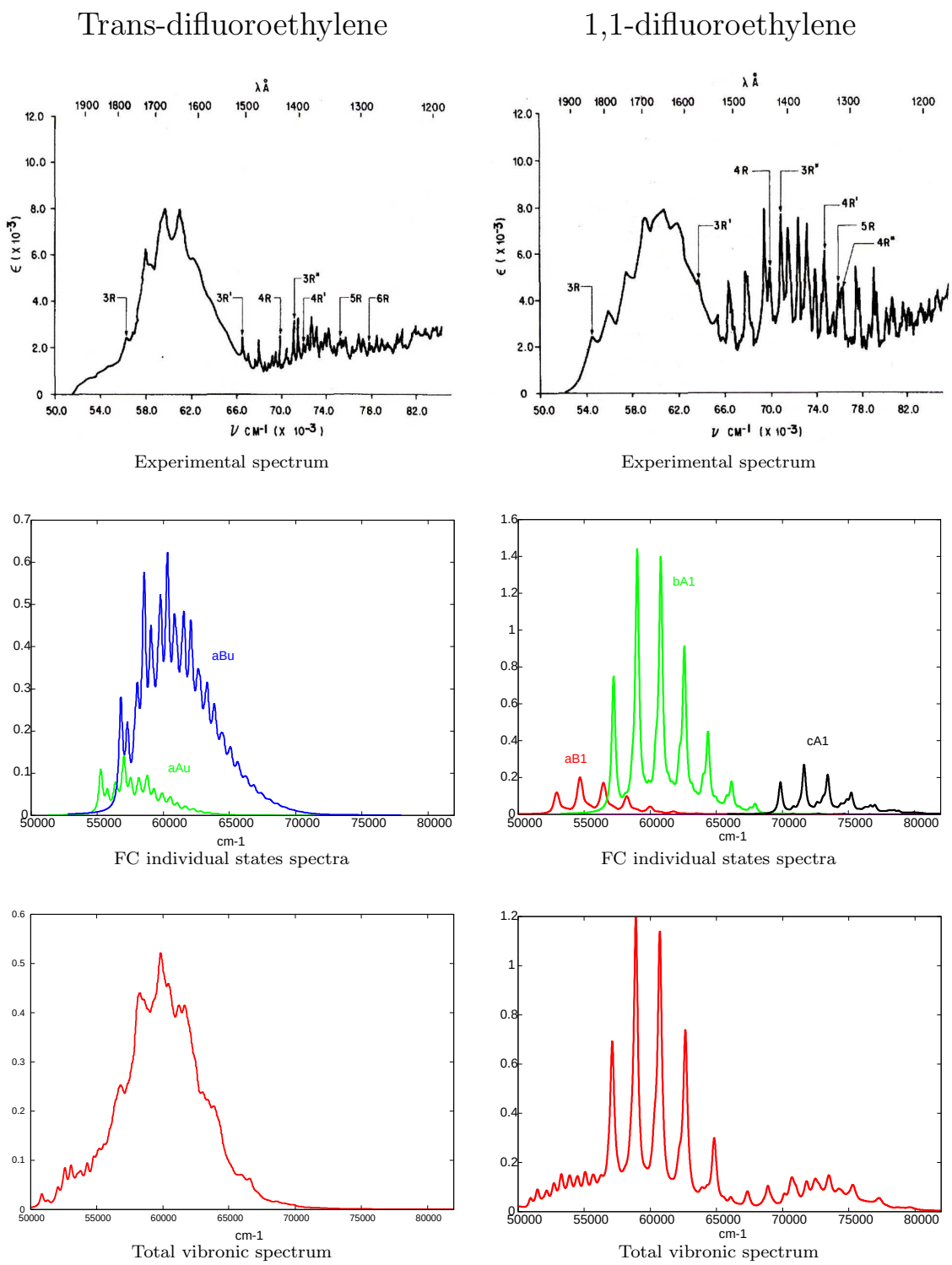

Figure 3.3: Experimental (top panels, reference [50]), FC individual states (middle panels) and total vibronic (bottom panels) absorption spectra of trans-difluoroethylene (on the left) and 1,1-difluoroethylene (on the right).

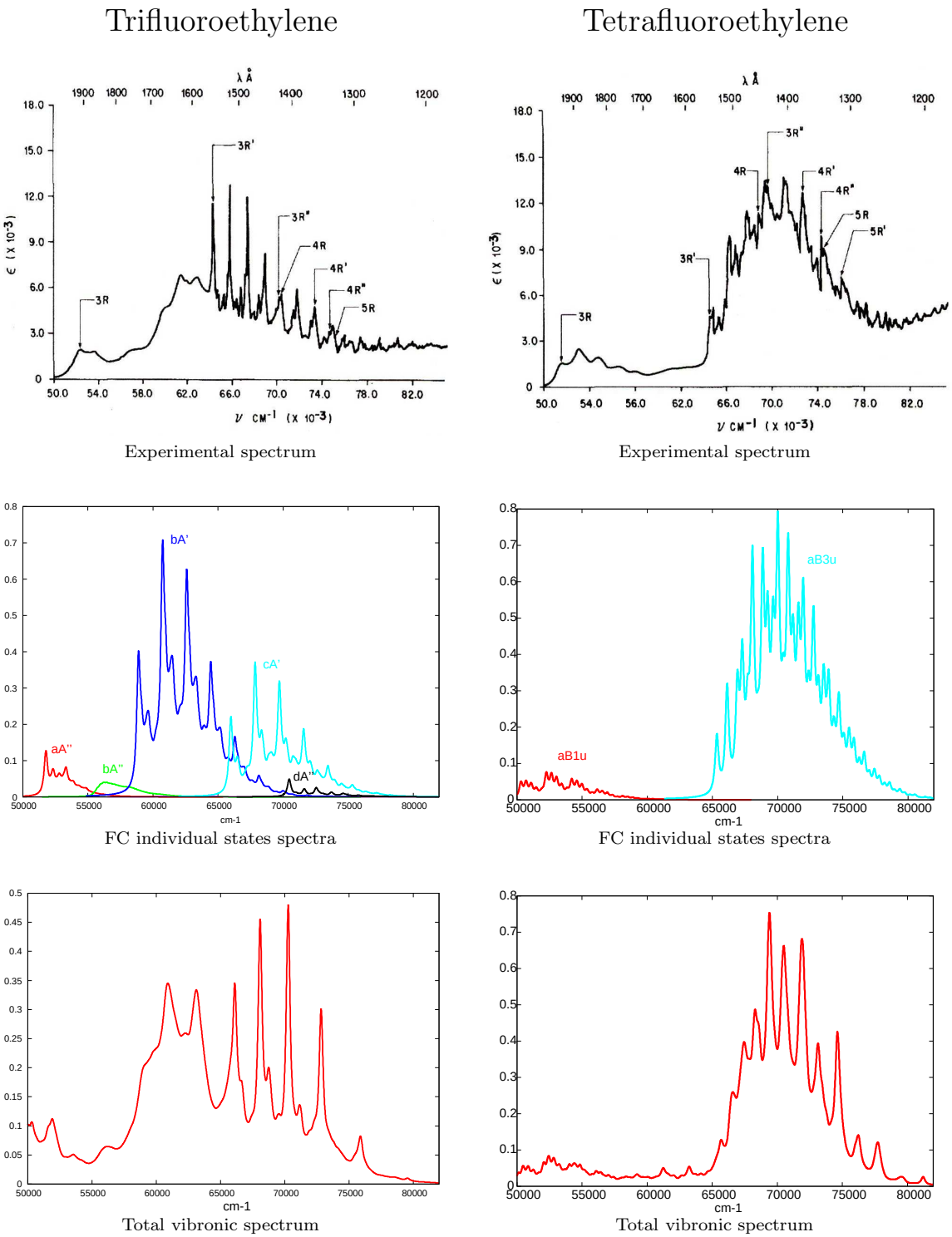

Figure 3.4: Experimental (top panels), FC individual states (middle panels) and total vibronic (bottom panels) absorption spectra of trifluoroethylene (on the left) and tetrafluoroethylene (on the right).

sorbing states.
FC and vibronic spectra of 1,1-difluoroethylene are not very different from each other, they don't reproduce the overall experimental spectrum but the vibrational progress seems to be well simulated.
The closer to experience calculated spectrum is vibronic spectrum of trifluoroethylene. Comparison with FC shows that vibronic coupling effects mainly mitigate the intensity and the vibrational progression in the valence (bA') state.
There is no evident vibronic coupling effect in the spectrum of tetrafluoroethylene since the FC simulation is very close to the experience but this has to be ascertained by an improved vibronic spectrum.

Even though it provides a good insight in the absorption spectroscopy of fluoroethylenes, vibronic simulations did not yield satisfactory results. To improve the agreement with experience a new two-step strategy was adopted. As the states couple to each other weak transitions can be become stronger. In the first step, vertical transitions moments are recalculated using the vibronic model. A regular FC calculation is performed in the second step using recalculated transitions moments. The $\pi \rightarrow \pi^*$ valence state is simulated with a structure-less broad smooth feature.

Starting with vinyl fluoride, figure 3.5 shows, on the left panel, absorption spectra of individual states, except the valence state bA', using transition moments and excitations energies obtained from STEOM calculation. One the right panel of the same figure are shown absorption spectra of the same states simulated using new transition moments and excitations energies. It can be seen that weak transitions become stronger when vibronic couplings are included, especially for bA", cA" and dA" states.

The overall simulated spectrum is shown in figure 3.6 from 54000 to 70000 cm^{-1} along with the experimental spectrum and the individual contributions of electronic states. The simulated spectrum is shifted by 1500 cm^{-1} to match the experimental one and the intensity of the first Rydberg state (aA") is scaled by 1/2.

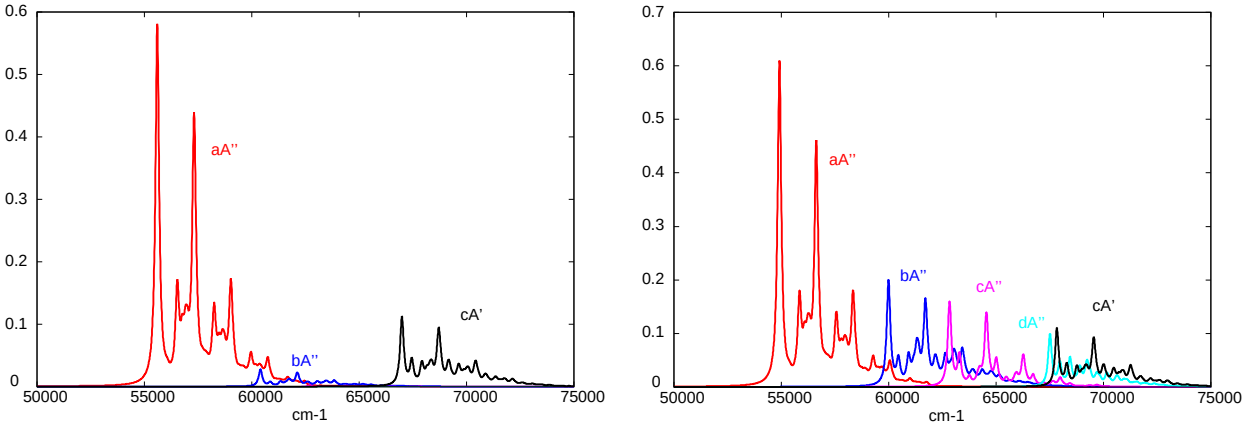

Figure 3.5: Absorption spectra for vinyl fluoride states (except bA') using STEOM excitation energies and transition moments (on the left) and using excitation energies and transition moments recalculated with the vibronic model (on the right).

The improvement upon first simulated spectrum of monofluoroethylene 3.2 is flagrant. Rydberg states (aA" and cA") are at the origin of the vibrational progression in the spectrum, their sharp features is well reproduced. Other simulations need to be performed for further analysis but one can state that this new strategy is more suited for simulating absorption spectra of fluoroethylenes. It will be used to simulate absorption spectra of other fluoroethylenes.

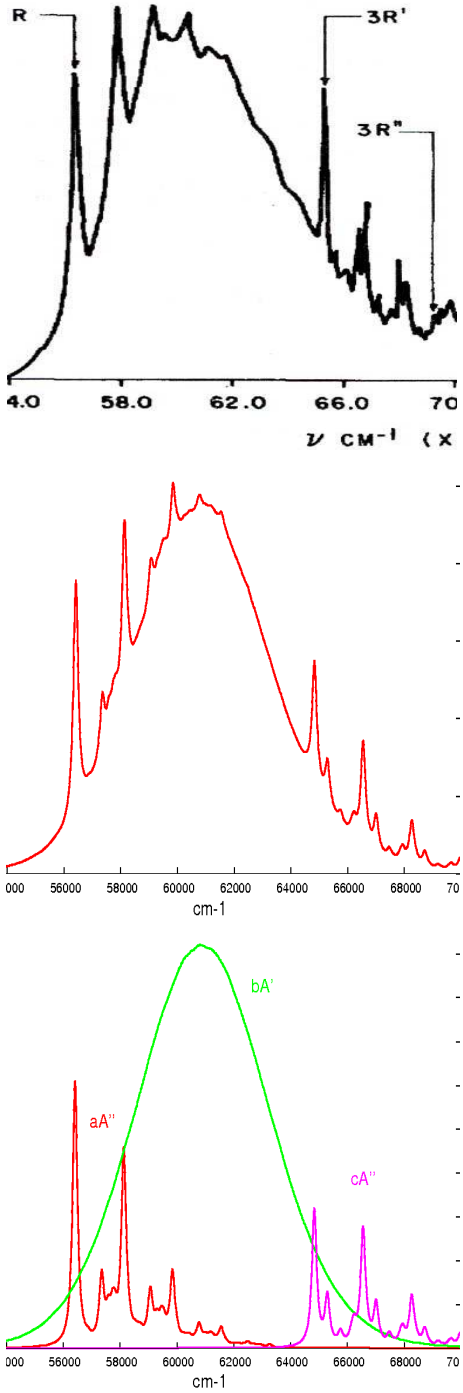

Figure 3.6: Experimental (top panel) and simulated (middle and bottom panels) absorption spectra for vinyl fluoride.

3.4 Summary

Absorption spectra of fluorotethylenes were investigated using FC and vibronic coupling methods. In the vibronic method a model Hamiltonian is calculated through the following steps:
The ground state geometry is optimized and frequencies of vibrational normal modes calculated at the obtained geometry. Excited states are calculated at the same geometry and a selection of states to be included in the vibronic model is made. Calculation of parameters that enter the vibronic Hamiltonian includes excited states calculations at displaced geometries around the equilibrium. Potential energy curves can be obtained from the vibronic Hamiltonian. Their analysis will help design a vibronic model. Finally vibronic spectra can be simulated and compared to FC and experimental ones.

Ground state optimized geometry, and frequencies of the vibrational normal modes are obtained at CCSD level of theory, they are in good agreement with available experimental values. Excited states energies obtained at EOM-CCSD level of theory are also in accord with experiment, even better than recent SAC-CI results. Vibronic couplings calculations reveal that obtaining quadratic coupling constants for fluoroethylenes is not a trivial task. Except for monofluoroethylene and cis-difluoroethylene, for which quadratic constants were included for selected normal modes, vibronic model is limited to linear coupling constants. However this simple model shows that vibronic coupling effects can be significant and must be considered to correctly describe the absorption spectroscopy of fluoroethylenes. Simulations do not reproduce perfectly the experimental spectra but reveal evidence of vibronic coupling effects. The absorption of Rydberg states of monofluoroethylene could be reproduced only with the inclusion of vibronic coupling effects. The long progression starting around 50000 cm^{-1} in the absorption spectrum of trans-difluoroethylene is another vibronic coupling effect. Vibronic coupling effects mitigate the intensity and the vibrational progression of the $\pi \rightarrow \pi^*$ (bA') valence state of trifluoroethylene.

There is no major difference in FC and vibronic spectra of other fluoroethylenes. Vibronic simulations have to be improved. A new strategy that consists in recalculating transition moments with the vibronic model and performing a regular FC simulation with the obtained values was adopted. It has been applied to the monofluoroethylene case and shows great improvement. Basically the new methodology does in two steps what vibronic simulation does in one and results from both methods should not be so different. This suggests us some investigations in the vibronic coupling simulations that are being carried out. For the moment following simulations will be made adopting the new strategy. Calculation of vibronic coupling constants has to be improved to obtain higher order constants, that will allow us to reach high quality simulations and also have access to high order effects such as Dushinsky [74, 75] or anharmonicity effects.

After a good agreement with experiment is achieved, teasing the simulated spectra apart and identifying the root of spectroscopic contributions, whether it is from specific excited states, normal modes, or vibronic coupling effects, will give us great insight into the absorption spectroscopy of the studied molecules.

3.5 Appendix

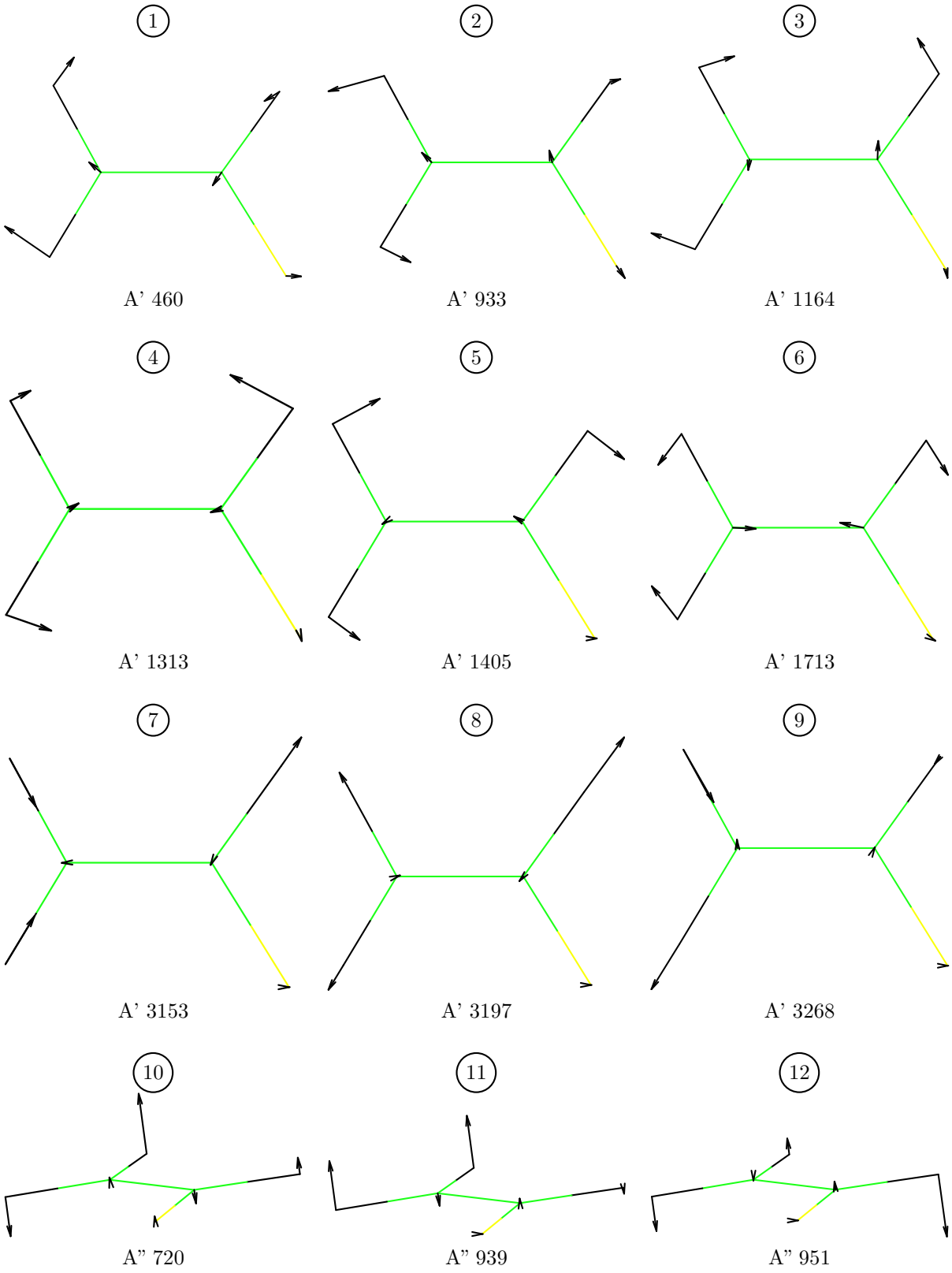

Figure 3.7: Calculated frequencies for the vibrational normal modes of monofluoroethylene at CCSD level of theory.

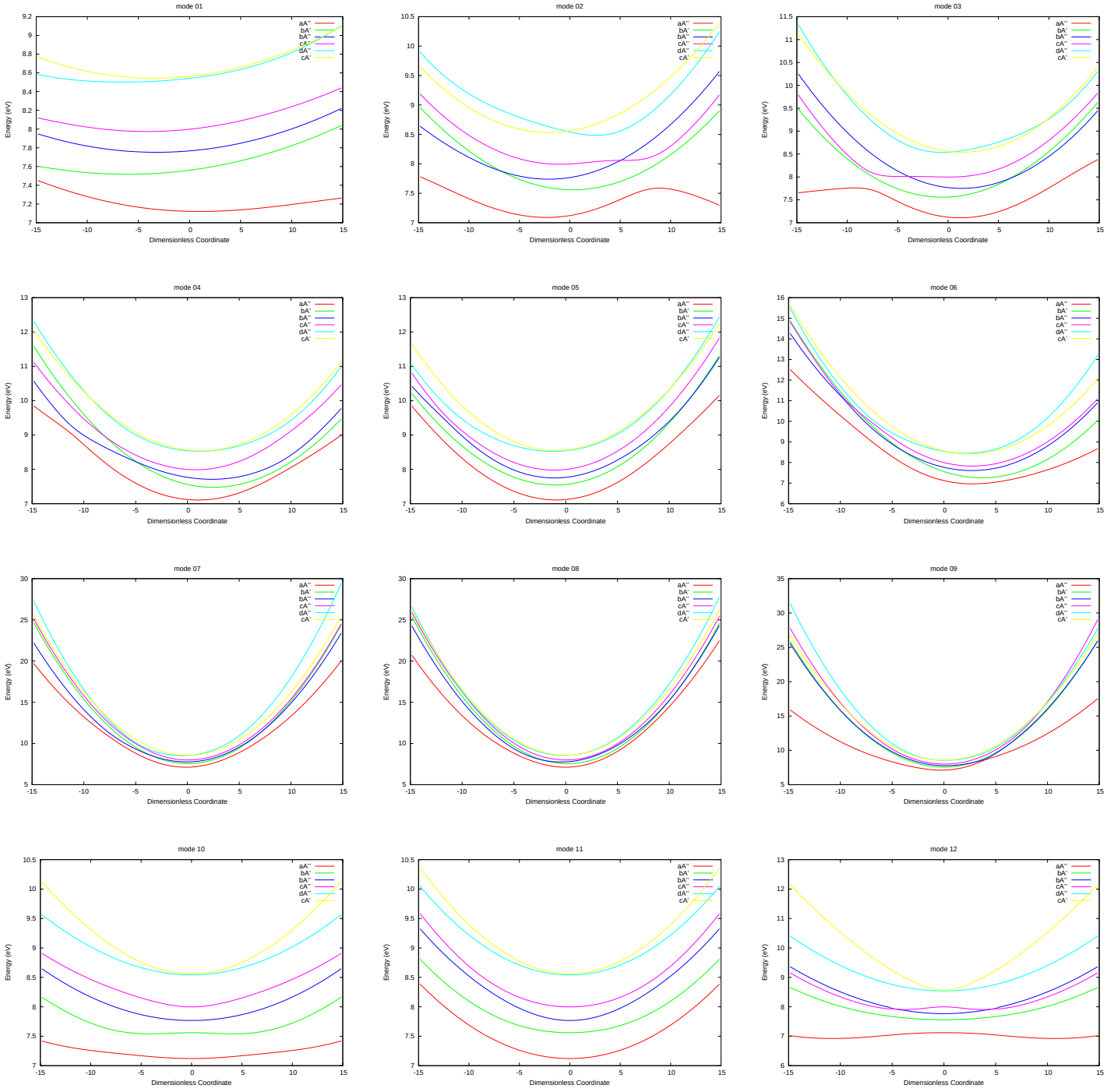

Figure 3.8: Potential energy curves of the excited states of monofluoroethylene along vibrational normal modes represented in figure 3.7. Linear and diagonal quadratic couplings are included along modes 1 to 9 and linear couplings only are included along mode 10 to 12.

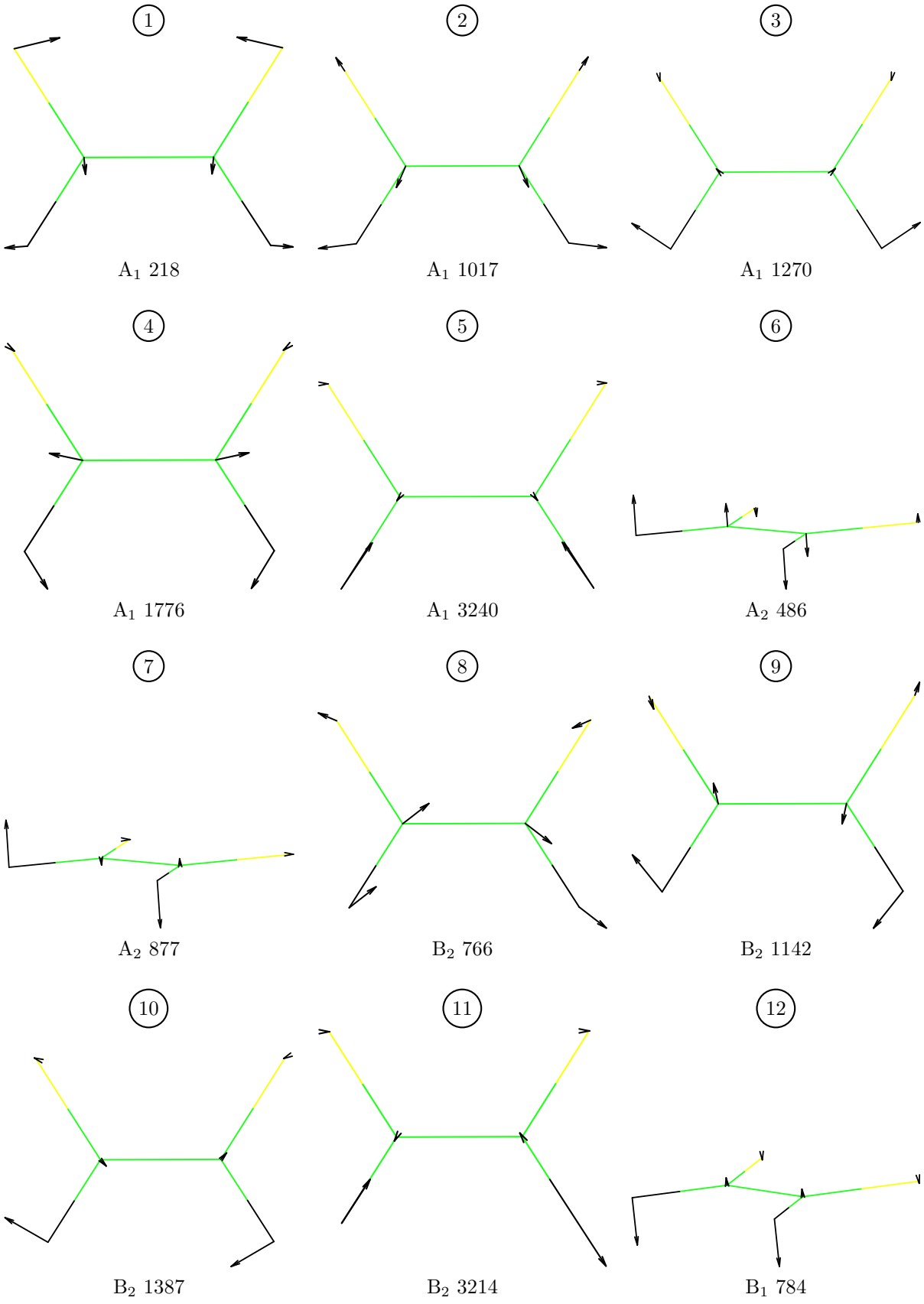

Figure 3.9: Calculated frequencies for the vibrational normal modes of cis-difluoroethylene at CCSD level of theory.

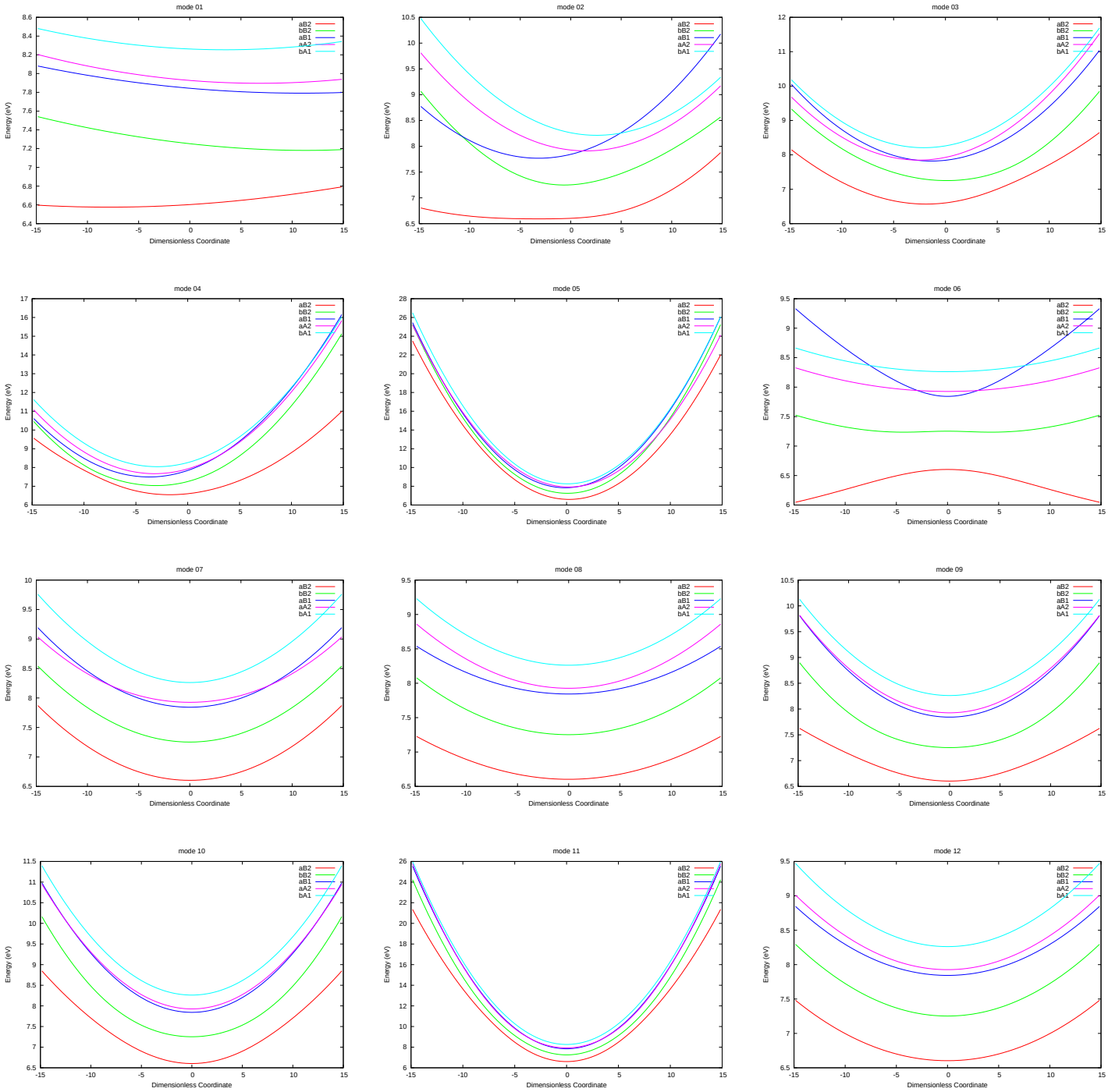

Figure 3.10: Potential energy curves of the excited states of cis-difluoroethylene along vibrational normal modes represented in figure 3.9. Linear couplings are included along modes 6, 7 and 12 while linear and diagonal quadratic couplings are included along the remaining modes.

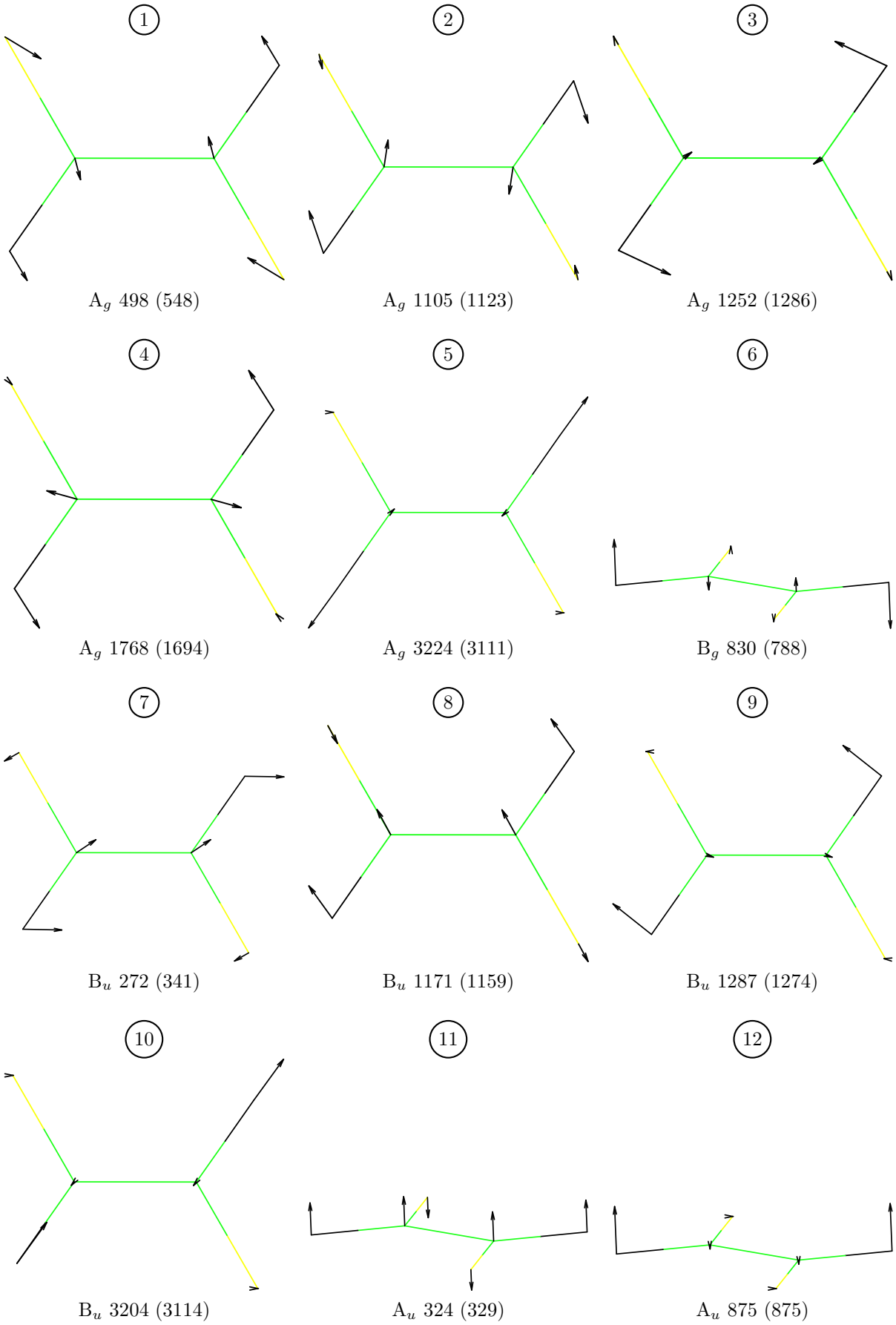

Figure 3.11: Calculated (and experimental [76] in parenthesis) frequencies for the vibrational normal modes of trans-difluoroethylene at CCSD level ot theory.

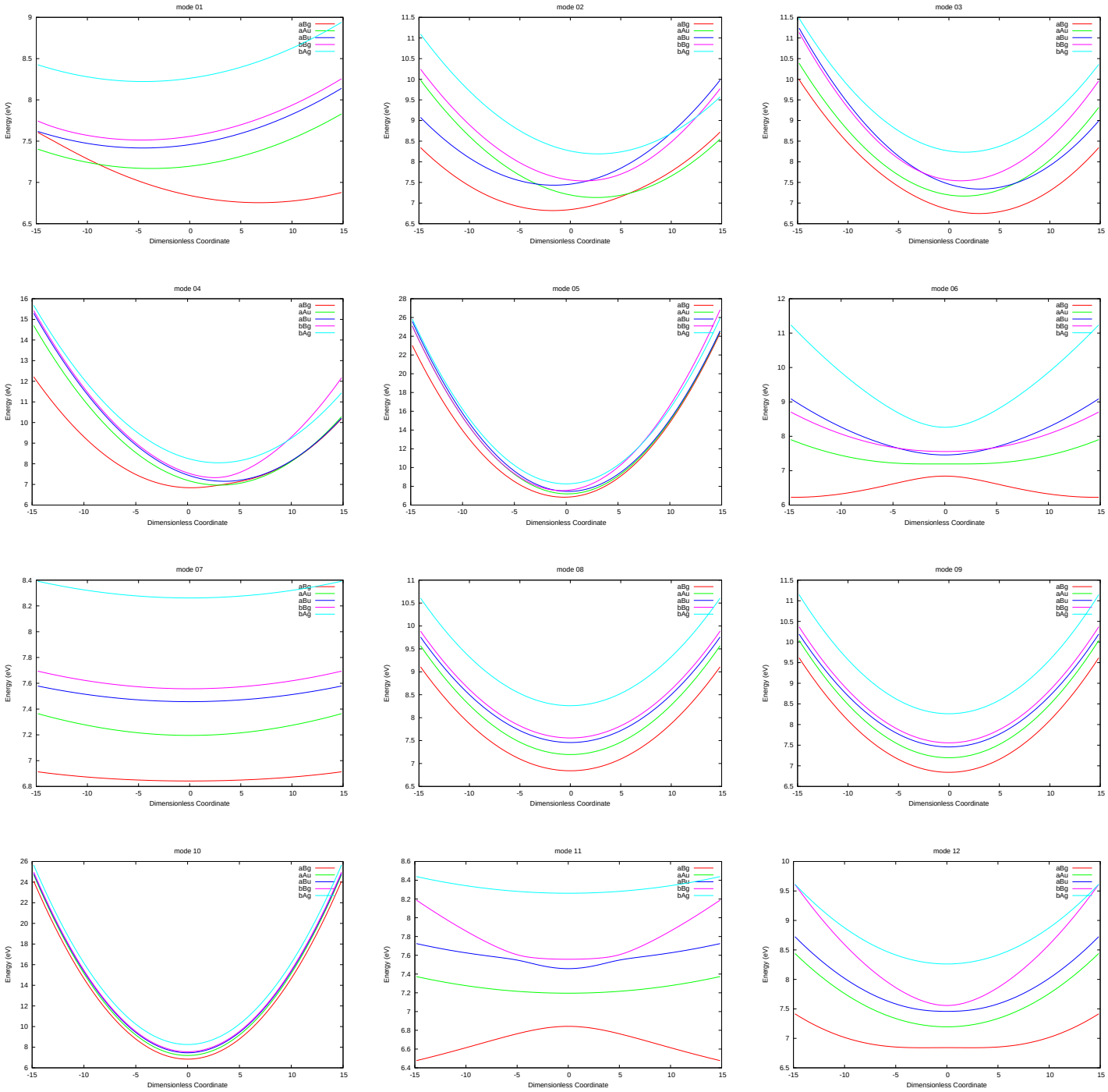

Figure 3.12: Potential energy curves of the excited states of trans-difluoroethylene along vibrational normal modes represented in figure 3.11 including linear couplings only.

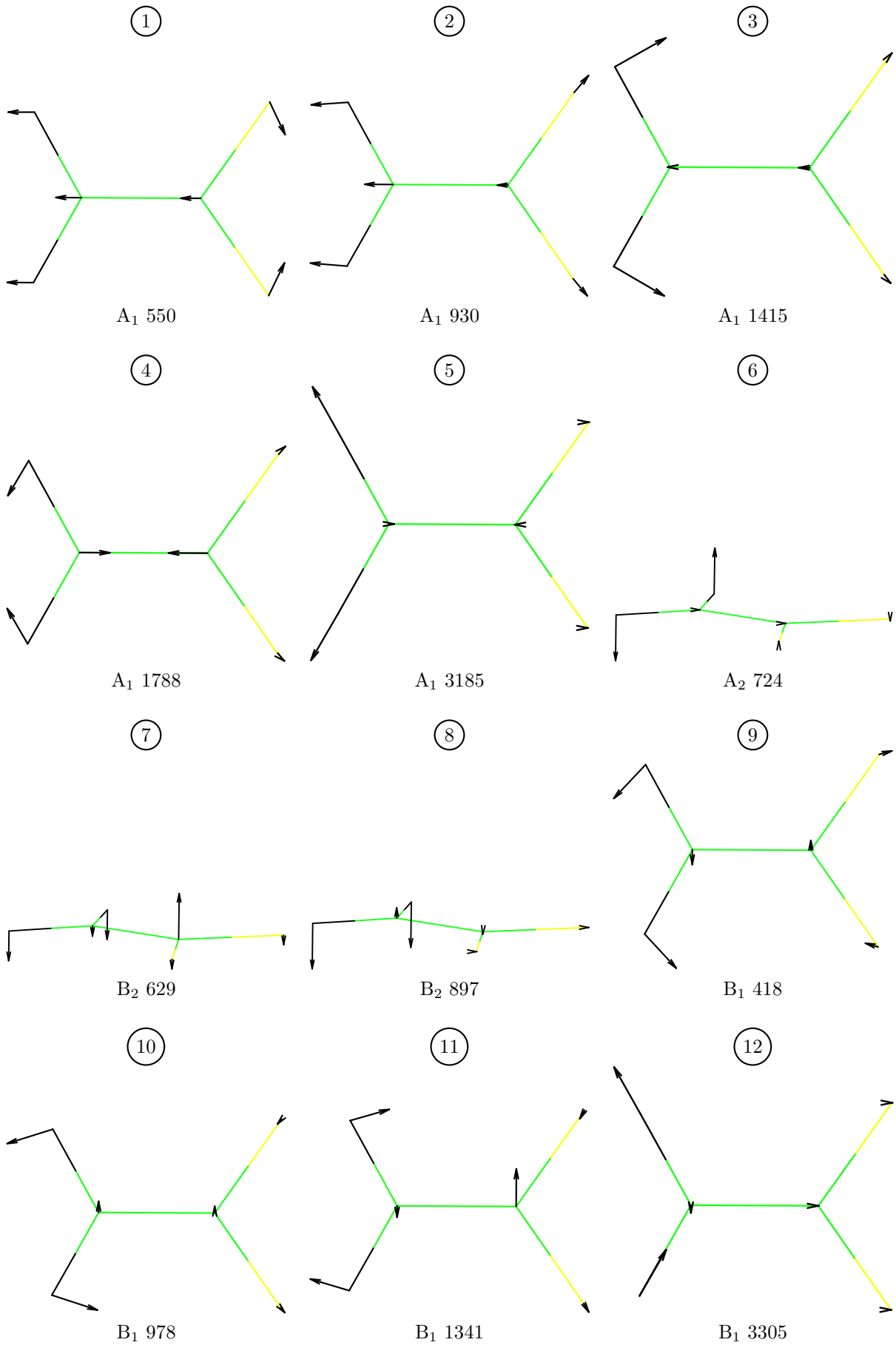

Figure 3.13: Calculated frequencies for the vibrational normal modes of 1,1-difluoroethylene at CCSD level of theory.

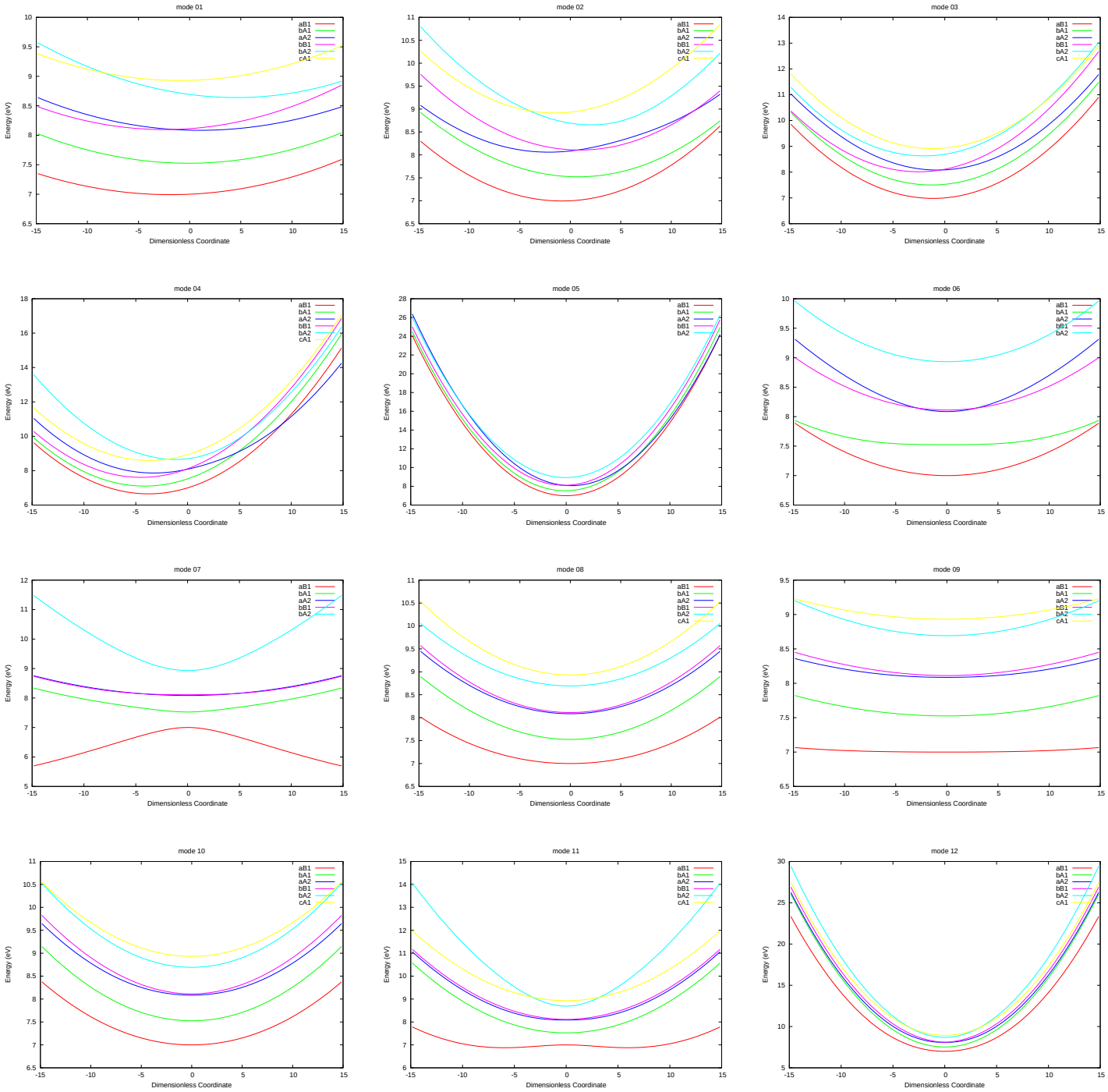

Figure 3.14: Potential energy curves of the excited states of 1,1-difluoroethylene along vibrational normal modes represented in figure 3.13 including linear couplings only.

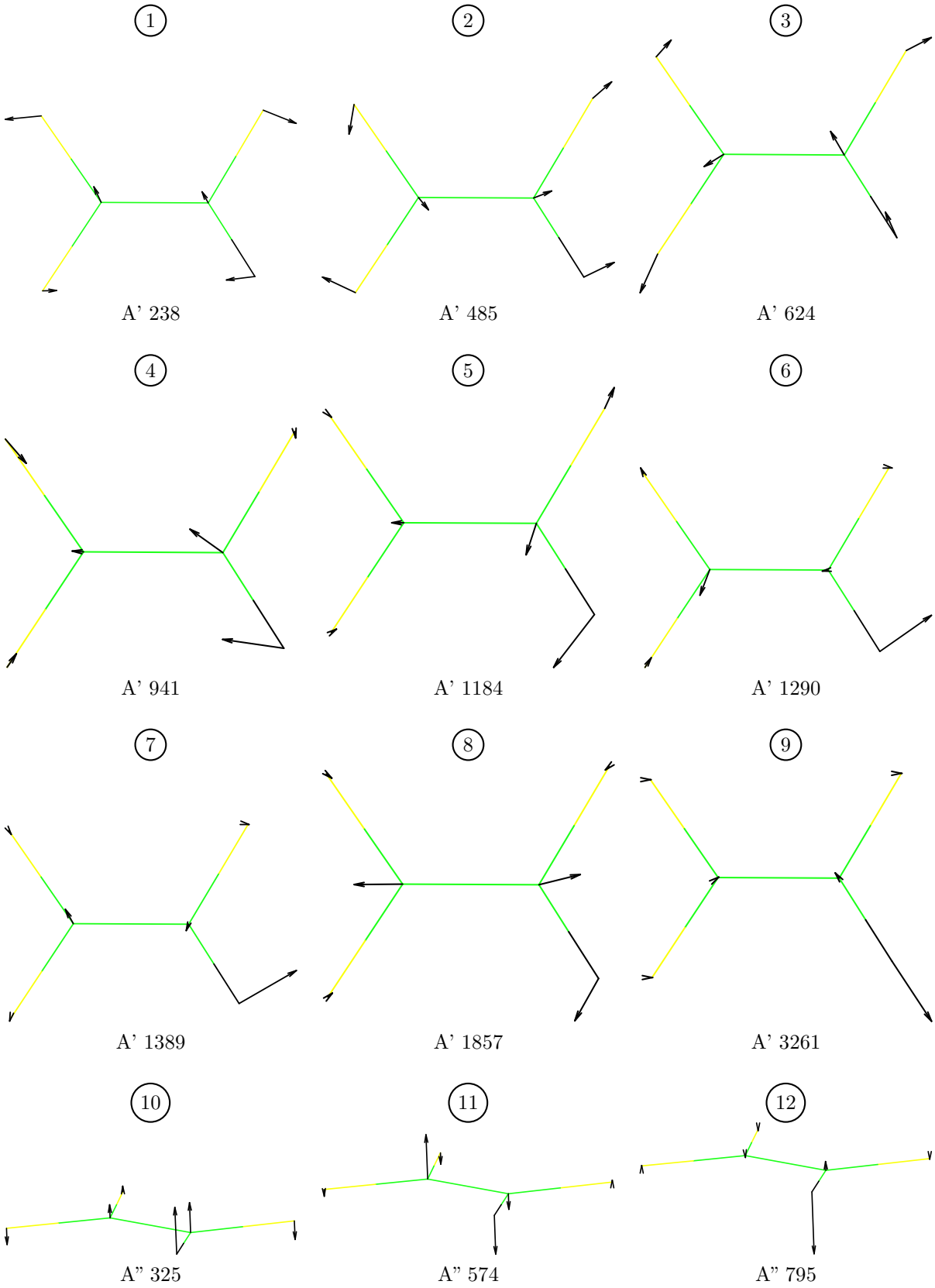

Figure 3.15: Calculated frequencies for the vibrational normal modes of tri-fluoroethylene at CCSD level of theory.

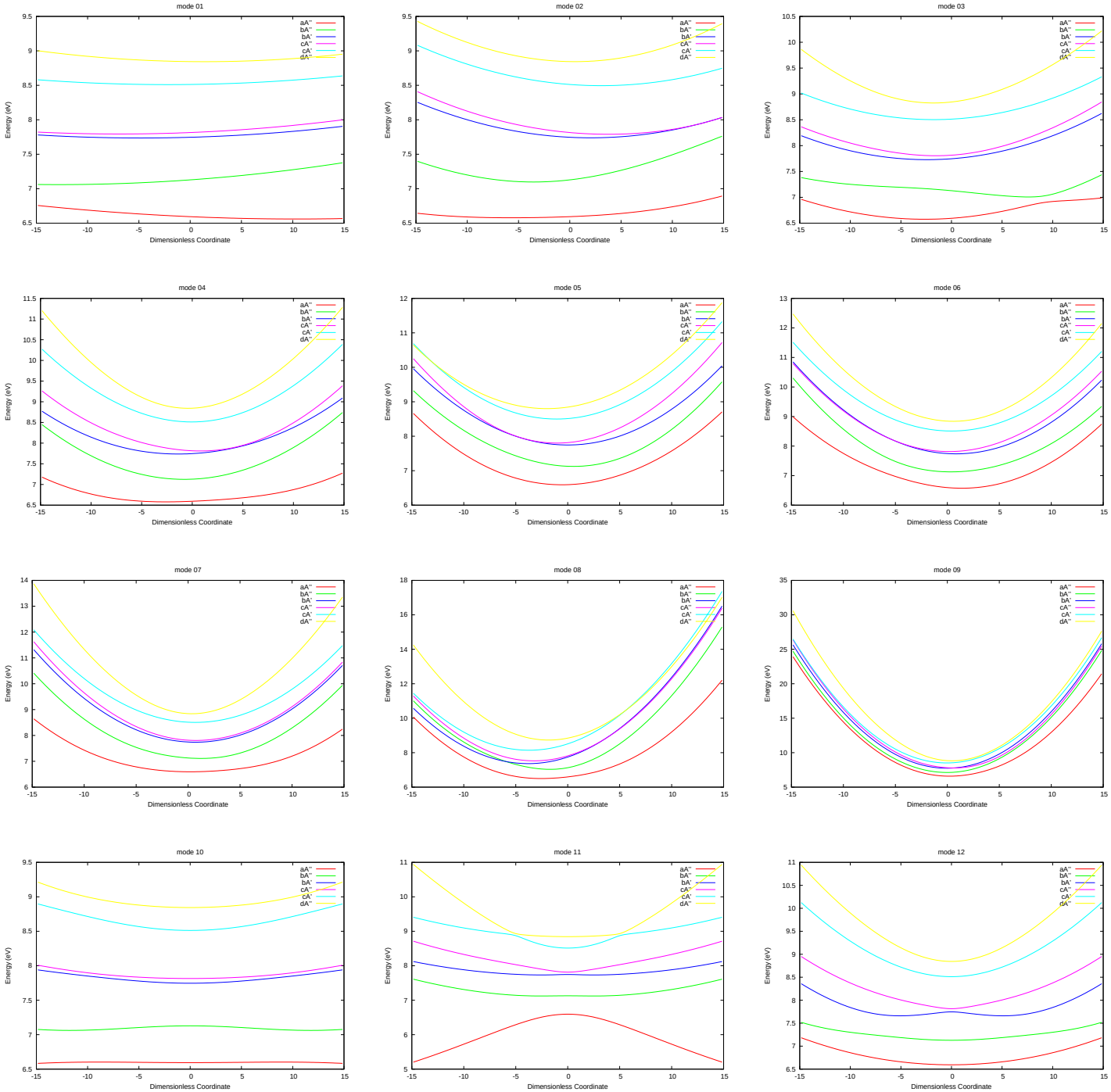

Figure 3.16: Potential energy curves of the excited states of trifluoroethylene along vibrational normal modes represented in figure 3.15 including linear couplings only.

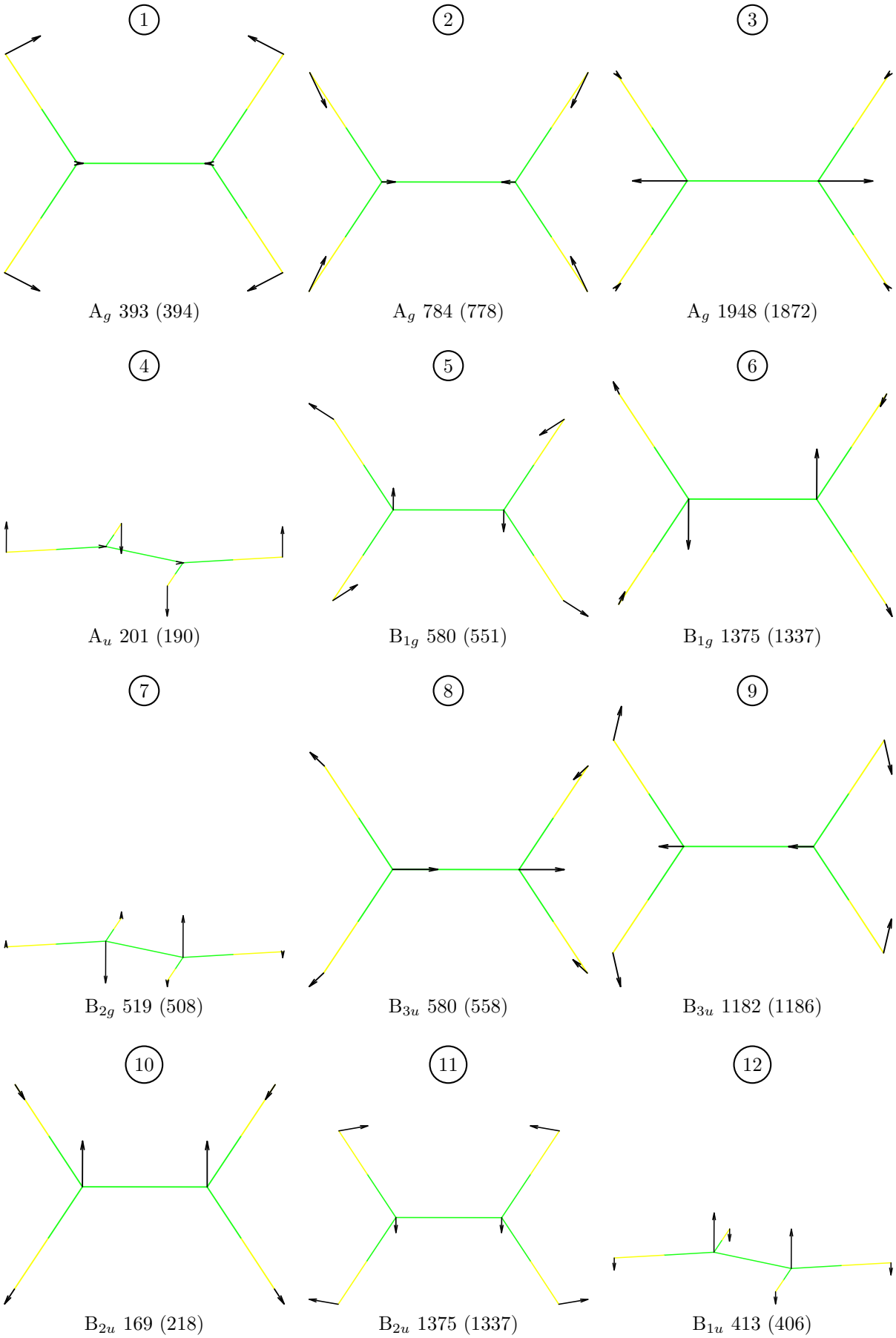

Figure 3.17: Calculated (and experimental [77] in parenthesis) frequencies for the vibrational normal modes of tetrafluoroethylene at CCSD level of theory.

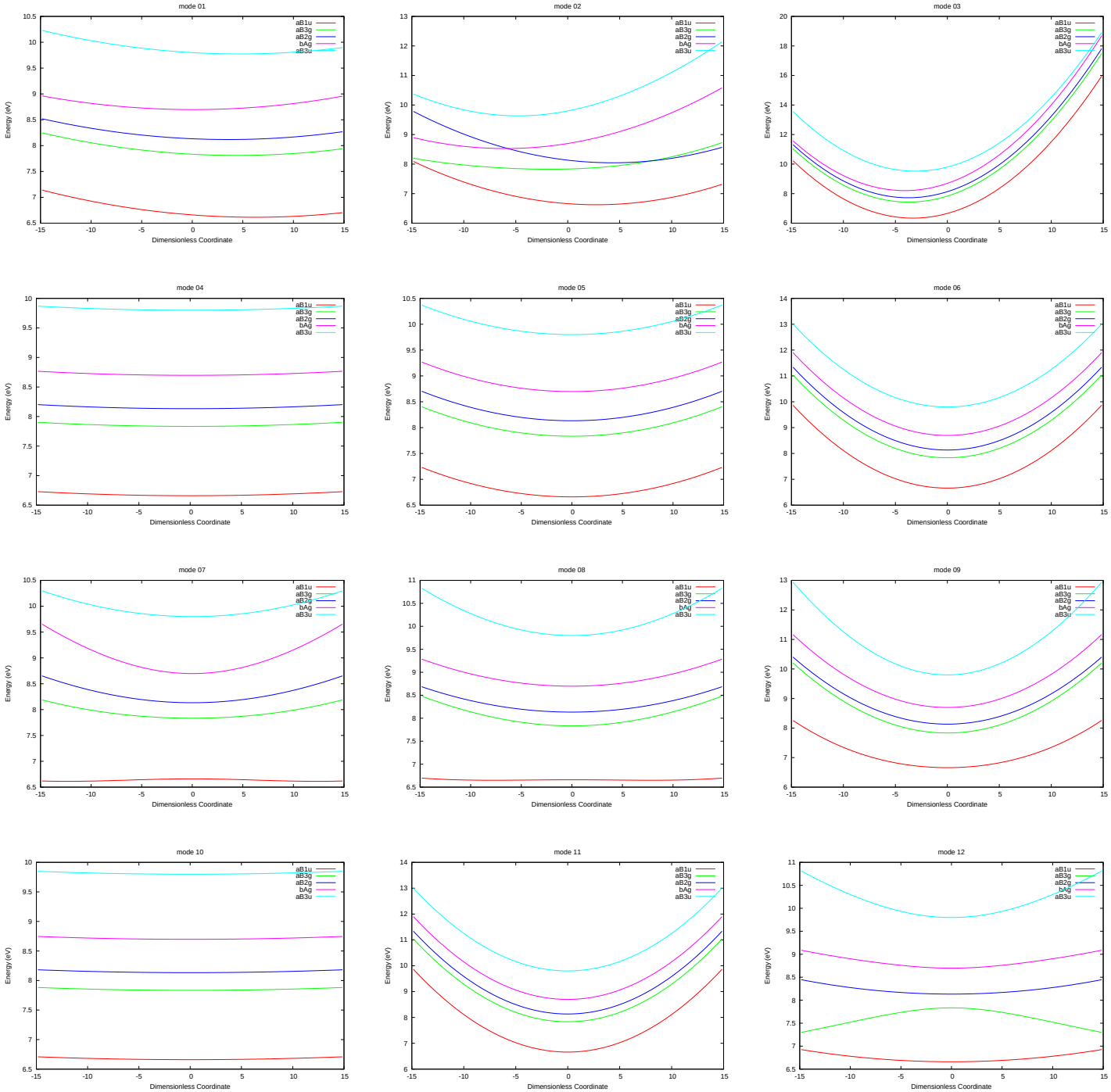

Figure 3.18: Potential energy curves of the excited states of tetrafluoroethylene along vibrational normal modes represented in figure 3.17 including linear couplings only.

Chapter 4

Spin-orbit effects on the spectroscopy of H_2X (X=O, Te, Po)

4.1 Introduction

The spectroscopic properties of water molecule still received much attention both from experimentalists [78, 79] and from theoreticians [80–83] even though they have been studied since long time ago [84,85]. Different levels of theory including CASPT2, coupled-cluster and other methods were applied to it. Particular attention has been devoted to answering wether the low-lying electronic excited states of water have a valence or a Rydberg character. Photodissociation of water also still receive much attention [86,87]. Meanwhile the spectroscopy of heavy hydrides (H_2Te, H_2Po) have been wildly investigated and spin-orbit effects are known to have key role in their photochemistry [88–90].

The aim of this work is to study the effect of spin-orbit coupling on the spectroscopy of H_2O, H_2Te and H_2Po and its evolution as the central atom changes, using the EPCISO method (chapter 1). EPCISO method has the advantage of treating the

so-called spin-orbit polarisation effects. To gauge the importance of these effects, results obtained with EPCISO are compared with SO-RASSI results.

4.2 Theoretical treatment of spin-orbit effects

The theoretical treatment of spin-orbit effects of H_2X (X=O, Te, Po) is summarised in the following article.

Electronic Absorption Spectroscopy of H2X (X = O, Te, Po) : Theoretical Treatment of Spin-Orbit Effects

Chérif A. A. NDOYE, Chantal DANIEL

Chinese Journal of Chemical Physics, 2009, vol. 22, numéro 2, pages 171-177

General summary

The goal of this work was to apply cluster expansion theory to transition metal complexes spectroscopy, validate the vibronic approach interfaced to ACESII quantum chemical software on small organic molecules and study the spin-orbit effects in the series H_2X (X=O, Te, Po).

The study of electronic structure and potential energy curves of MCH_2^+ (M=Fe, Co, Ni) by means of coupled-cluster and equation of motion coupled-cluster has characterized their ground states and identified the electronic states responsible of their photofragmentation. The lowest part of absorption spectra of $FeCH_2^+$, $CoCH_2^+$ and $NiCH_2^+$ is characterized by very low oscillator strengths and not expected to play a significant role in the electronic spectroscopy or in the photofragmentation of these molecules. Metal-$\pi^*_{MCH_2}$ charge transfer states with significant oscillator strengths in the visible/near-UV energy domain of the theoretical spectra of $FeCH_2^+$ and $CoCH_2^+$ are at the origin of the photofragmentation of these compounds observed after irradiation between 27800 and 32360 cm^{-1}. In contrast $NiCH_2^+$ does not show any significant absorption in this energy domain in agreement with the low cross section of photodissociation observed for this molecule.

All electronic states could not be represented all along the studied dissociation pathway. Some states present a strong mixing character resulting in an incoherent behavior. Further investigations will be necessary to study these states.

A simple model, including linear couplings only, shows that vibronic coupling effects can be significant and must be considered to correctly describe the absorption

spectroscopy of fluoroethylenes. Simulations do not reproduce perfectly the experimental spectra but reveal evidence of vibronic coupling effects. The absorption of Rydberg states of monofluoroethylene could be reproduced only with the inclusion of vibronic coupling effects. The long progression starting around 50000 cm^{-1} in the absorption spectrum of trans-difluoroethylene is another vibronic coupling effect. Vibronic coupling effects mitigate the intensity and the vibrational progression of the $\pi \rightarrow \pi^*$ (bA') valence state of trifluoroethylene. There is no major difference in FC and vibronic spectra of other fluoroethylenes. Nevertheless the calculation of vibronic coupling constants has to be improved to obtain higher order constants, that will allow us to reach high quality simulations and also have access to high order effects. After a good agreement with experiment is achieved, teasing the simulated spectra apart and identifying the root of spectroscopic contributions, whether it is from specific excited states, normal modes, or vibronic coupling effects, will give us great insight into the absorption spectroscopy of the studied molecules.

In the study of spin-orbit effects on the electronic spectroscopy of the group VI analogous H_2O, H_2Te, and H_2Po by means of scalar-relativistic and spin-orbit CASPT2 calculations the two approaches, EPCISO and RASSI, give very similar results. No effect on the calculated spectrum of H_2O which compares rather well with experimental data and available theoretical spectra from the literature. Whereas the SO effects induce significant splitting of the low-lying triplet states of H_2Po with large mixing between the SO-states they are unimportant for H_2Te. The absorption spectra of the heavy molecules are shifted to the red with respect to the one of water. Due to the theoretical difficulties at describing the scalar relativistic and spin-orbit effects in a balanced way a quantitative study is still a challenge. The results obtained in the present work for H_2Te and H_2Po will be confronted to further four and two-components relativistic calculations.

Bibliography

[1] J. Husband, F. Aguirre, C. J. Thompson, C. M. Laperle, R. B. Metz, *J. Phys. Chem. A* **104**, 2020 (2000).

[2] S. Arulmozhiraja, M. Ehara, H. Nakatsuji, *J. Chem. Phys.* **126** (2007).

[3] H. Koppel, W. Domcke, L. Cederbaum, *Adv. Chem. Phys.* **57**, 59 (1984).

[4] P.-A. Malmqvist, B. O. Roos, *Chem. Phys. Lett.* **155**, 189 (1989).

[5] J.-P. Flament, V. Vallet, L. Maron, C. Teichteil, EPCISO a spin-orbit CI program.

[6] J. F. Stanton, J. Gauss, J. D. Watts, M. Nooijen, N. Oliphant, S. A. Perera, P. G. Szalay, W. J. Lauderdale, S. R. Gwaltney, S. Beck, A. Balkova, D. E. Bernholdt, K.-K. Baeck, P. Rozyczko, H. Sekino, C. Huber and R. J. Bartlett, ACES II (Advanced Concepts in Electronic Structure II) - A program product of the Quantum Theory project, University of Florida. Integral packages included are VMOL (J. Almlof and P. R. Taylor), VPROPS (P.R. Taylor), ABACUS (T. Helgaker, H. J. Aa Jensen, P. Jorgensen and P. R. Taylor).

[7] S. Villaume, C. Daniel, A. Strich, S. A. Perera, R. J. Bartlett, *J. Chem. Phys.* **122**, 044313 (2005).

[8] S. Villaume, A. Strich, C. Daniel, S. A. Perera, R. J. Bartlett, *Phys. Chem. Chem. Phys.* **9**, 6115 (2007).

[9] M. Nooijen, A. Hazra, C. Leon, J. Neugebauer, VIBRON - A program for Vibronic Coupling and Franck-Condon calculations.

[10] V. Vallet, L. Maron, C. Teichteil, J.-P. Flament, *J. Chem. Phys.* **113**, 1391 (2000).

[11] G. D. Purvis III, R. J. Bartlett, *J. Chem. Phys.* **76**, 1910 (1982).

[12] A. Szabo, N. S. Ostlund, *Modern Quantum Chemistry: Introduction to Advanced Electronic Structure Theory* (Dover, 1996).

[13] S. A. Kusharski, R. J. Bartlett, *Adv. Quantum Chem.* **18**, 281 (1986).

[14] R. Bartlett, M. Musial, *Rev. Mod. Phys.* **79**, 291 (2007).

[15] Y. S. Lee, A. Kucharski, R. J. Bartlett, *J. Chem. Phys.* **81**, 5906 (1984).

[16] J. Noga, R. J. Bartlett, M. Urban, *Chem. Phys. Lett.* **134**, 126 (1987).

[17] K. Ragavachari, G. W. Trucks, J. A. Pople, M. Headgordon, *Chem. Phys. Lett.* **157**, 479 (1989).

[18] R. J. Bartlett, J. D. Watts, S. A. Kucharski, J. Noga, *Chem. Phys. Lett.* **165**, 513 (1990).

[19] M. Urban, J. Noga, S. J. Cole, R. J. Bartlett, *J. Chem. Phys.* **83**, 4041 (1985).

[20] M. Nooijen, R. J. Bartlett, *J. Chem. Phys.* **106**, 6441 (1997).

[21] M. Nooijen, R. J. Bartlett, *J. Chem. Phys.* **107**, 6812 (1997).

[22] M. Nooijen, *J. Chem. Phys.* **104**, 2638 (1996).

[23] E. Condon, *Phys. Rev.* **28**, 1182 (1926).

[24] J. Franck, E. G. Dymond, *Trans. Faraday Soc.* **21**, 536 (1926).

[25] M. Born, K. Huang, *Dynamical Theory of Crystal Latices* (Oxford University Press, Oxford, 1954).

[26] H. Hellmann, *Einführung in die Quantenchemie* (Franz Deuticke, Vienna and Leipzig, 1937).

[27] R. P. Feynman, *Phys. Rev.* **56**, 340 (1939).

[28] H. Bethe, E. Salpeter (Springer Verlag, Berlin, 1957).

[29] R. Samzow, B. A. Hess, *Chem. Phys. Lett.* **184**, 491 (1991).

[30] R. Samzow, B. A. Hess, G. Jansen, *J. Chem. Phys.* **96**, 1227 (1992).

[31] C. W. Bauschlicher, H. Partridge, J. A. Sheehy, S. R. Langhoff, M. Rosi, *J. Phys. Chem.* **96**, 6969 (1992).

[32] K. K. Irikura, W. A. Goddard III, *J. Am. Chem. Soc.* **116**, 8733 (1994).

[33] D. G. Musaev, N. K. K. Morokuma, *J. Chem. Phys.* **99**, 7859 (1993).

[34] F. Ogliaro, S. D. Loades, D. L. Cooper, P. B. Karadakov, *J. Phys. Chem. A* **104**, 7091 (2000).

[35] D. G. Musaev, *et al.*, *J. Phys. Chem.* **97**, 11435 (1993).

[36] R. R. Schrock **12**, 8 (1979).

[37] E. O. Fischer, K. H. Dotz, *Chem. Ber.* **103**, 1273 (1970).

[38] H. W. Turner, R. R. Schrock, *J. Am. Chem. Soc.* **104**, 2331 (1982).

[39] J. Levisalles, *et al.*, *J. Am. Chem. Soc. Commun.* **15**, 1981.

[40] E. O. Fischer, *Adv. Organomet. Chem.* **14**, 1 (1976).

[41] D. G. Musaev, K. Morokuma, N. Koga, *J. Chem. Phys.* **99**, 7859 (1993).

[42] D. G. Musaev, *et al.*, *J. Phys. Chem.* **97**, 11435 (1993).

[43] D. G. Musaev, K. Morokuma, *J. Chem. Phys.* **101**, 10697 (1994).

[44] J. S. Sears, C. D.Sherrill, A. I. Krylov, *J. Chem. Phys.* **118**, 9084 (2003).

[45] S. V. Levchenko, A. I. Krylov, *J. Chem. Phys.* **120**, 175 (2004).

[46] A. J. H. Wachters, *J. Chem. Phys.* **52**, 1033 (1970).

[47] T. H. Dunning Jr., R. J. Harrison, *J. Chem. Phys.* **96**, 6796 (1992).

[48] I. Lindgren, D. Mukherjee, *Physics Reports* **151**, 93 (1987).

[49] C. E. Moore, *Atomic Energy Levels* (National Bureau of Standards, 1952).

[50] G. Belanger, C. Sandorfy, *J. Chem. Phys.* **55**, 2055 (1971).

[51] P. Dauber, M. Brith, *Chem. Phys.* **11**, 43 (1975).

[52] M. J. Coggiola, W. M. Flicker, O. A. Mosher, A. Kuppermann, *J. Chem. Phys.* **65**, 2655 (1976).

[53] G. J. Verhaart, H. H. Brongersma, *Chem. Phys.* **52**, 431 (1980).

[54] S. Eden, *et al.*, *Chem. Phys.* **297**, 257 (2004).

[55] S. Arulmozhiraja, M. Ehara, H. Nakatsuji, *J. Chem. Phys.* **126**, 044306 (2007).

[56] B. Balko, J. Zhang, Y. Lee, *J. Phys. Chem. A* **101**, 6611 (1997).

[57] G. E. Hall, *et al.*, *J. Chem. Phys.* **101**, 3679 (1994).

[58] J. J. Lin, S. M. Wu, D. W. Hwang, Y. T. Lee, X. Yang, *J. Chem. Phys.* **109**, 10838 (1998).

[59] S.-R. Lin, Y.-P. Lee, *J. Chem. Phys.* **111**, 9233 (1999).

[60] W. A. Guillory, G. H. Andrews, *J. Chem. Phys.* **62**, 3208 (1975).

[61] S.-R. Lin, *et al.*, *J. Chem. Phys.* **114**, 7396 (2001).

[62] J. J. Lin, T. C. Hsu, D. W. Hwang, Y. T. Lee, X. Yang, *J. Chem. Phys.* **109**, 10719 (1998).

[63] T. K. Minton, P. Felder, R. C. Scales, J. R. Huber, *Chem. Phys. Lett.* **164**, 113 (1989).

[64] K. Sato, S. Tsunashima, T. Takayanagi, G. Fijisawa, A. Yokoyama, *Chem. Phys. Lett.* **242**, 401 (1995).

[65] S. A. Trushin, S. Sorgues, W. Fuss, W. E. Schmid, *ChemPhysChem* **5**, 1389 (2004).

[66] M. Barbatti, A. J. A. Aquino, H. Lischka, *J. Phys. Chem. A* **109**, 5168 (2005).

[67] A. J. Sadlej, *Theor. Chim. Acta.* **79**, 123 (1991).

[68] M. Wladyslawski, M. Nooijen, *Adv. Quant. Chem.* **49** (2005).

[69] H. Nakatsuji, *Chem. Phys. Lett.* **67** (329).

[70] B. J. Smith, D. Coffey Jr., L. Radom, *J. Chem. Phys.* **97**, 6113 (1992).

[71] M. D. Harmony, *et al.*, *J. Phys. Chem. Ref. D.* **8**, 619 (1979).

[72] N. Craig, *et al.*, *J. Phys. Chem.* **100**, 5310 (1996).

[73] F. C. Mijlhoff, G. H. Renes, K. Kohata, K. Oyanagi, K. Kuchitsu, *J. Mol. Struc.* **39**, 241 (1977).

[74] F. Duschinsky, *Acta Physicochim. URSS* **7**, 551 (1937).

[75] G. J. Small, *J. Chem. Phys.* **54**, 3300 (1971).

[76] T. Shimanouchi, *Tables of Molecular Vibrational Frequencies Consolidated*, vol. 2 (National Bureau of Standards, 1972).

[77] T. Shimanouchi, *Tables of Molecular Vibrational Frequencies Consolidated*, vol. 1 (National Bureau of Standards, 1972).

[78] P. Maksyutenko, *et al.*, *J. Chem. Phys.* **126**, 241101 (2007).

[79] R. Mota, *et al.*, *Chem. Phys. Lett.* **416**, 152 (2005).

[80] M. Rubio, L. Serrano-Andres, M. Merchan, *J. Chem. Phys.* **128**, 104305 (2008).

[81] X. Li, J. Paldus, *Molecular Phys.* **104**, 661 (2006).

[82] I. Borges Jr., *J. Phys. B: Atomic, Molecular and Optical Physics* **39**, 641 (2006).

[83] I. Borges, Jr., *Chem. Phys.* **328**, 284 (2006).

[84] W. C. Price, *J. Chem. Phys.* **4**, 147 (1936).

[85] R. S. Mulliken, *J. Chem. Phys.* **3**, 506 (1935).

[86] P. A. Thorn, *et al.*, *J. Chem. Phys.* **126**, 064306 (2007).

[87] R. van Harrevelt, M. C. van Hemert, *J. Chem. Phys.* **112**, 5777 (2000).

[88] A. B. Alekseyev, H.-P. Liebermann, C. Wittig, *J. Chem. Phys.* **121**, 9389 (2004).

[89] K. Sumathi, K. Balasubramanian, *J. Chem. Phys.* **92**, 6604 (1990).

[90] J. Underwood, D. Chastaing, S. Lee, C. Wittig, *J. Chem. Phys.* **123**, 084312 (2005).

Spectroscopie électronique de petites molécules organiques et organométalliques: corrélation électronique, couplages vibronique et spin-orbite

La prédiction de propriétés spectroscopiques moléculaires et l'interprétation de spectres expérimentaux nécessitent de faire appel à la théorie. Une première étape consiste à se limiter à la spectroscopie électronique dans l'approximation de Born-Oppenheimer ce qui consiste à considérer les noyaux de la molécule comme étant fixes et les états électroniques indépendants les uns des autres. L'objectif de cette thèse est d'étudier la structure électronique de petites molécules organiques et organométalliques dans l'approximation de Born-Oppenheimer dans un premier temps avant d'aller au delà en prenant en compte des effets tels que le couplage vibronique ou le couplage spin-orbite entre les états électroniques. Le premier chapitre est consacré aux méthodes *ab initio* utilisées pour obtenir les résultats présentés dans les chapitres ultérieurs. Une première partie est consacrée aux méthodes de structure électronique dans l'approximation de Born-Oppenheimer, elle est suivie d'une partie qui traite des effets de couplage vibronique et spin-orbite. Le second chapitre présente une étude de la structure électronique et des courbes d'énergie potentielle des carbènes de métaux de transition MCH_2^+ (M=Fe, Co, Ni). Le troisième chapitre rapporte les spectres vibroniques des fluoroéthylènes obtenus par simulation et comparés aux spectres expérimentaux afin d'identifier l'origine de différentes contributions spectroscopiques. Enfin le dernier chapitre traite des effets spin-orbite dans l'eau et ses homologues lourds (H_2X avec X=O, Te, Po).

Electronic spectroscopy of small organic and organometallic molecules: electronic correlation, vibronic and spin-orbit couplings

Theory is sometime necessary to predict molecular spectroscopic properties and interpret experimental spectra. A first step study can be limited to the electronic spectroscopy in Born-Oppenheimer approximation which consists in considering nuclei fixed and electronic states independent from each other. The scope of this thesis is to first study the electronic structure of small organic and orgnometallic molecules in the Born-Oppenheimer approximation and ultimatly go beyond by taking into account effects such as vibronic or spin-orbit couplings between electronic states. The first chapter is dedicated to the *ab initio* methods used to obtain the results presented in the following chapters. Electronic structure methods in the Born-Oppenheimer approximation are first presented followed by the methods that treat vibronic and spin-orbit couplings. The second chapter is a study of the electronic structure and potential energy curves of MCH_2^+ (M=Fe, Co, Ni) transition metal carbenes. Chapter three reports simulated vibronic spectra of fluoroethylenes, they are compared to experimental spectra to indentify the origin of the different spectroscopic contributions. A last chapter deals with the spin-orbit effects in water and its heavy homologous (H_2X with X=O, Te, Po).